POLITECNICO DI MILANO

School of Civil, Environmental and Land Management Engineering

Master of Science in
Environmental and Land Planning Engineering

Impacts of land cover change on hydrological regime patterns over the Red River basin, Vietnam: a model based analysis

Supervisor:

Prof. Andrea Castelletti

Co-Supervisor:

Prof. Paolo Burlando

Dr. Daniela Anghileri

Master Graduation Thesis by:

Alessia Goffi

Id. number: 803947

Academic Year 2013/2014

Acknowledgments

I would like to express my gratitude to all the people who made possible this thesis.

I begin by saying thank you to prof. Andrea Castelletti who gave me the chance to work on a very interesting topic and to develop my experience at Institute of Environmental Engineering of ETH in Zurich. For the welcome, the dedicated time and the possibility to work in a young, international and active team in Switzerland, I thank prof. Paolo Burlando. Beside my curriculum vitae and the awareness of train punctuality, my character has also benefited from this experience. Surely, it will be useful for my future. All this has been also possible thanks to the thesis abroad scholarship of Politecnico di Milano.

A huge thanks goes to my co-supervisor Daniela for her availability and constancy in following the advancing of my thesis for an entire year. She is my advisor.
Moreover, I want to thank Daniele, Rafael, Pietro and PhD students at ETH.

It was a pleasure to work with you all.

In this special moment for me, my gratitude goes to the people I care most.
I wish to warmly thank my parents and my entire family for the support given to me and the expectations (and anxiety) put on me. In particular Silvia, thank you a lot for everything.
To Adriano a special thanks for always staying close to me.
Finally I wish to thank you my friends and class mates.

And now enjoy reading my thesis.

CONTENTS

List of Figures

List of Tables

Abstract

As known, land cover can influence significantly the hydrological cycle of catchments. Land cover change is usually a slow phenomenon, spanning on decades, but it can be greatly accelerated by the economic and population growth, typical of developing countries. The objective of the thesis is to analyse the relationship between land cover change and its effect on precipitation and streamflow patterns in the Red River Basin (China, Vietnam, and Laos). Vietnam is one of the fastest growing economies in the world and natural resources have been considerably exploited to support post-war development. The specific objectives of the thesis are to characterize the changes in the hydrological regime of the Vietnamese part of the Red River basin occurred in the last five decades and to verify if the observed changes are compatible with land cover changes through the use of a hydrological model. In the first part of the thesis, time series analysis techniques and trend detection tools (e.g., Mann-Kendall test, Pettitt homogeneity test, and Moving Average over Shifting Horizon) are applied to several observed time series of evaporation, temperature, precipitation and streamflow. For some stations, results show a decrease of precipitation volume and an increase of the streamflow volume. This counterintuitive behavior, which however can be justified by a change in the land cover, e.g., through deforestation, is further explored focusing on a particular sub-basin, Nam Muc. We use a spatially distributed and physically based model, Topkapi-ETH to understand the role of land cover change on streamflow patterns and to verify if the observed changes can be attributed to a shift from a mainly forested landscape to a mainly agricultural one, which is actually what happened in the basin starting from the sixties. We defined different land cover scenarios to test the model sensitivity to parameters related to soil and vegetation cover. Results show that land cover change can significantly contribute to modify the annual streamflow pattern in the transition from an afforested to a deforested basin.

Riassunto

Come noto, la copertura del suolo è in grado di influenzare significativamente il ciclo idrologico di un bacino imbrifero. Il cambiamento di copertura di suolo non è un fenomeno rapido, bensì un percorso graduale nel tempo generalmente su scala decennale, ma che può essere però fortemente accelerato dallo sviluppo economico e dall'incremento della popolazione, caratteristiche tipiche dei Paesi in crescita. La tesi si occupa di analizzare il legame tra il cambiamento di copertura di suolo e i suoi effetti sulle variabili di precipitazione e portata nel bacino del fiume Rosso (in Cina, Vietnam e Laos). Il Vietnam è un paese che ha vissuto una forte crescita economica dopo la guerra, parallelamente ad un intenso sfruttamento delle risorse naturali. Nello specifico, gli obiettivi della tesi consistono nello studio dei cambiamenti del regime idrologico avvenuti nel corso dell'ultimo cinquantennio nella parte vietnamita del bacino del fiume Rosso, ed in particolare degli effetti dovuti al cambiamento di copertura di suolo, con focus sul legame che sussiste con la portata mediante un modello idrologico. Nella prima parte del lavoro, l'individuazione dei cambiamenti riscontrati nelle variabili considerate (evaporazione, temperatura, precipitazione e portata) è stata resa possibile dall'uso di strumenti di analisi delle serie temporali (test di Pettitt), di comuni metodi statistici (test di Mann-Kendall) e di nuove tecniche (MASH). Essi hanno messo in risalto come, per certe stazioni, ad una diminuzione del volume di precipitazione corrisponda invece un aumento della portata. Questo fenomeno potrebbe essere dovuto al cambio di copertura di suolo ed un'analisi più approfondita è stata effettuata sul sottobacino di Nam Muc. Quest'area, come la maggior parte del bacino, è stata sottoposta a una forte deforestazione a partire dagli anni '60. Per capire gli effetti del cambio di copertura di suolo sulla portata e per verificare se i cambiamenti osservati possano essere dovuti al passaggio da foreste a campi coltivati, è stato impiegato un modello spazialmente distribuito e fisicamente basato, Topkapi-ETH. Delineando diversi scenari di copertura di suolo, è stata studiata la sensitività del modello ai parametri legati all'uso di suolo e alla copertura vegetale. I risultati mostrano come il cambio di copertura del suolo abbia un contributo rilevante sulla portata lungo tutto il corso dell'anno, nel passaggio del bacino da uno scenario afforestato a uno deforestato.

Chapter 1

Introduction

1.1 Background

With the economic and population growth, world outlook has really changed and nowadays it is still evolving, in particular in developing countries, and it has resulted in an extensive land cover and land use change at the expense of forests. Obviously, this transition has not only a strong visual impact, but it has consequences, for example, on the hydrological regime of river basins affecting evapotranspiration, precipitation, temperature, and streamflow.

Vietnam is one of the fastest growing economies in the world and natural resources have been considerably exploited to support post-war development. Vietnam War destroyed much of the country's agrarian system, leading the post-war government to implement a planned economy to revitalize agriculture and industrialize the nation. As a side effect of this policy, Vietnam holds the second highest rate of deforestation of primary forests in the world, second only to Nigeria (FAO, 2005), with consequent problems like abrupt change in run-off, erosion, sediment transport, and flash floods. Each year, extreme floods kill and displace hundreds of thousands of people and result in billion dollars of damages, especially in developing countries with rural and agrarian economy (FAO & CIFOR, 2005; Jonkman, 2005). Moreover, it is important to consider that some land cover change effects are not immediate, but can gradually change during a time period, like influence on soil properties.

In this thesis we analyse the Red River basin, an international river basin which spans among Vietnam, China and Laos (*figure 1.1*). The basin has an area of about 169,000 km^2 and it is located in a monsoon dominated region. For its climate, there are two completely different seasons during the year, dry and wet, that make the study of hydro-climatic changes particularly challenging. We focus on Vietnamese portion of the basin, which represents the second largest basin of the country, after Mekong.

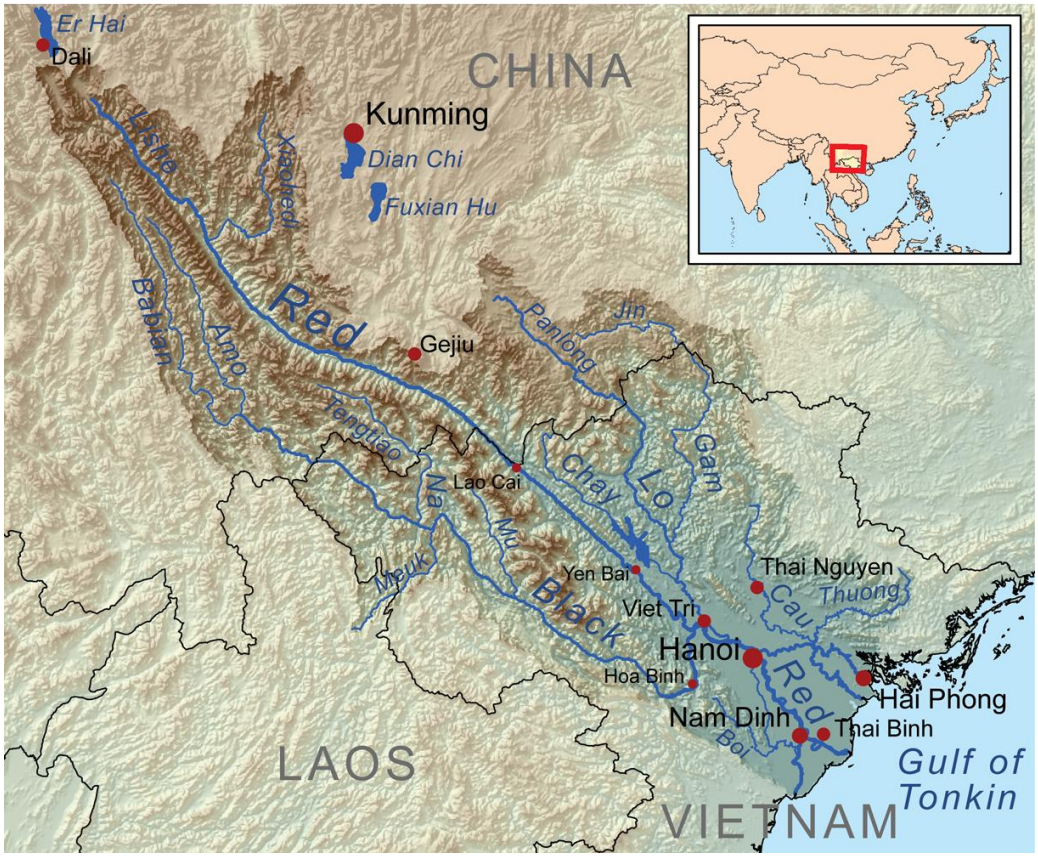

Figure 1.1: Location of the Red River basin.

1.2 Objectives of the thesis

The research question we want to address in this thesis is the following: is it possible to tie the trends of precipitation and streamflow data to land cover change in South-East Asia?

To find an answer to this matter, we fix three objectives, studying the basin of the Red River. The first one is to analyse the evolution of the hydrological regime in the examined area in the second half of the last century and to quantify the intensity of occurred changes. In these fifty years, the entire Red River basin was subjected to a deep land cover change. First, before nineties, a strong deforestation occurred and after nineties some areas were afforested. Therefore this is a suitable scenario to reach the second aim of this thesis, that is a model based study to understand the role of land cover change on streamflow patterns. At last, the third objective of the thesis consists in studying the sensitivity with respect to the model parameters representing soil properties and land cover.

Previous preliminary studies (Casali and Rota, 2012) showed that the hydrological regime of the Da River, the most important Red River affluent, has changed in the last fifty years. More precisely, it seems that a decrease of precipitation volume corresponds to an increase of the flow rate and to a shift of the flow peak all over the watershed. In this thesis we want to analyse the streamflow and precipitation patterns, studying the entire Red River basin. Detecting, analysing and modelling hydro-climatic regime changes are essential steps to understand the occurring processes to eventually apply mitigation strategies and adaptation plans, balancing economic development and ecosystem protection. Trend detection methods are usually adopted to identify and characterize changes in time series and/or spatially distributed data (Kundzewicz and Robson 2004, Sonali and Kumar 2013). In hydrological studies, trend detection techniques and various plotting tools (see, among others, Brunetti et al. (2001), Longobardi 2009, Fleming 2012, Anghileri 2013) can be used to find out changes in the magnitude or in temporal and spatial distribution of hydro-climatic variables, such as precipitation, temperature and streamflow.
First of all, we perform a trend detection analysis of precipitation, evaporation, temperature and streamflow time series of gauge stations distributed over the Vietnamese part of the Red River basin, using graphical methods (e.g., MASH) combined with traditional trend detection techniques (e.g., Mann-Kendall test). Moreover, we adopt methods to identify when significant changes have occurred in time series (e.g., Pettitt's test).

Drivers of the potential detected flow-rate changes in the case study are: regulation of upstream reservoirs in the upper Chinese part of the basin and construction of new ones, climate change and land cover change. Since we want to focus on the last driver only, we select on Nam Muc, a sub-basin of Red River, which is entirely located in Vietnam, has no streamflow coming from China and is characterized by land cover change. Using a spatially distributed and physically based model, Topkapi-ETH, we analyse the selected area and the effects due to land cover change. In fact, mathematical simulation models can play an important role in the basin analysis, since they improve the understanding of the most important physical processes. To investigate the model sensitivity to soil and land cover parameter changes, we compare the behavior of deforestation and afforestation scenarios to a fixed and homogeneous land cover on the considered basin.

The key instrument used to answer to the research question is the model. In this type of analysis, the power of the model and also the results we obtain, depend on its sensitivity with respect to the parameters on which it acts, in this case the parameters related to soil properties and land cover. Our analysis does not use satellite images for several reasons. First, satellite images do not go back far

enough in time and the temporal distribution among the available images is fragmented and uneven. NASA was the first to launch a satellite in space in 1972 (Landsat 1), but Thematic Mapper instruments were available only ten years later. It is also important to have images with a good resolution, without cloud cover and which belong to a close period to avoid seasonality problems. Moreover, another issue is that from satellite images it is difficult to extract information about soil cover. In fact, heterogeneous changes of soil cover may occur sometimes in a basin and it becomes complicated to assign the results to the changes experienced by station data. For example, it can often happen that a basin is affected partially by deforestation and partially by afforestation.

1.3 Outline of the thesis

The thesis is organized as follows:

- Chapter 1, introduction;
- Chapter 2, presentation of the impacts of land cover change on the hydrological cycle;
- Chapter 3, details about the study area;
- Chapter 4, description of the methods and tools used in the work for the trend detection and model based analysis;
- Chapter 5, results of time series analysis;
- Chapter 6, explanation of the model characteristics and parameters/scenarios experiments;
- Chapter 7, discussion of the obtained results.

Chapter 2

Literature review of land cover change consequences on water cycle

In this chapter we analyse how land cover change affects all hydrological cycle variables.

World's forests influence climate through physical, chemical, and biological processes that affect the planetary energy, the hydrologic cycle, and the atmospheric composition. In fact, the main effects of land cover change involve temperature, evapotranspiration, precipitation, streamflow, and soil properties.

Figure 2.1 summarizes the interdependence among geographical, meteorological and hydrological variables. Direct proportional effects are represented with α, while inverse proportional effects with α^{-1}. As an example of the land cover change, the graph shows the effects of deforestation; proportional signs would be opposite if we considered afforestation.

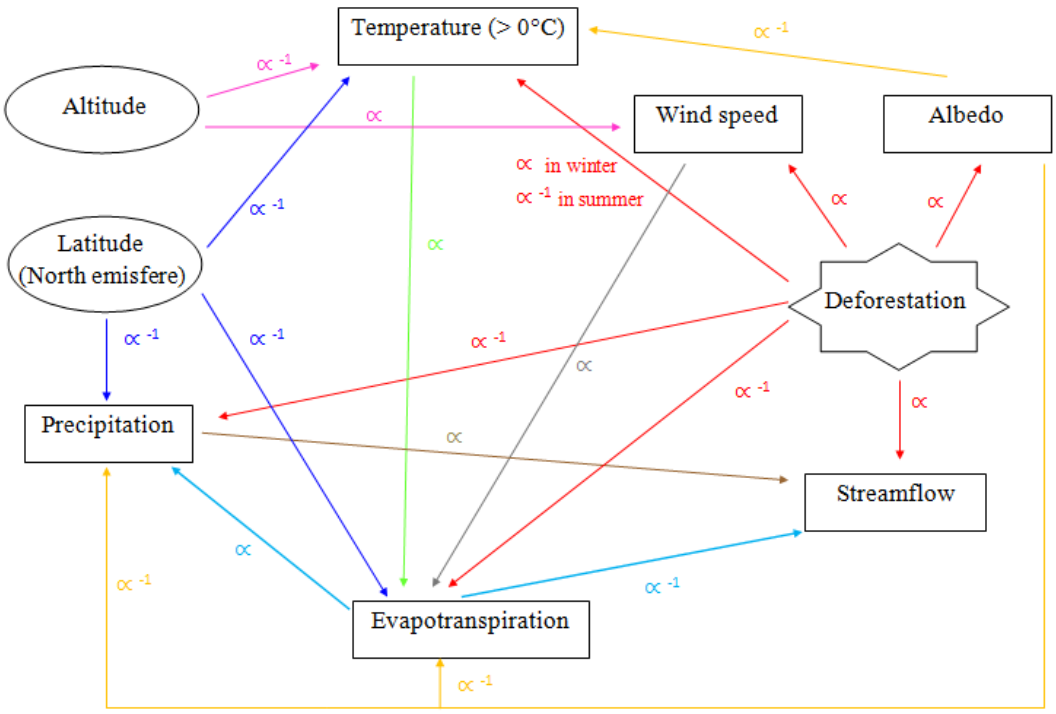

Figure 2.1: Relationships among variables influenced (directly or indirectly) by deforestation. Land cover change consequences on soil structure are complex and for this reason they are not included.

2.1 Impact on temperature

Deforestation and afforestation have more than one effect on temperature, conditioning albedo surface and trees evapotranspiration.

Albedo is the ratio between reflected radiation from the surface and incident radiation upon it and depends on cloud occurrence and surface type. In fact, the vegetation albedo feedback mechanism suggests that the vegetation cover increases, the surface albedo decreases, the absorbed solar radiation at the surface increases, and surface temperature rises (Charney, 1975). Therefore, surface temperature is lower in open land than in nearby forested land. However, this effect is greater northward 45°N; on the other side, below 35°N there is weak evidence that deforestation leads to warming (Lee, 2010).

Evapotranspiration (ET) is the sum of evaporation and plant transpiration processes from the Earth' surface to the atmosphere. On the one hand, evaporation represents the movement of water to the air from different sources, such as the soil, canopy interception, and water bodies. On the other hand, transpiration is the measure of water movement in a plant and the subsequent loss of water as vapour through stomata in its leaves.
Evapotranspiration is higher in forest land than bare soils. Temperature increase, due to vegetation cover rise, affects ET primarily by increasing the capacity of air to hold water vapour (Goyal, 2004). Water vapour is the most important contributor to the natural greenhouse effect, and its amount in the atmosphere is expected to increase under conditions of greenhouse-gas induced warming, leading to a significant feedback on anthropogenic climate change and, therefore, on temperature too.

What we can notice in response to afforestation is that the local surface air temperature significantly decreases in summer and increases in winter (Liang et al., 2009). The summer cooling is attributed to enhanced evapotranspiration from increased tree cover.

Moreover, the daily variation in ground temperature is much higher in denuded areas compared to forested zones (Meher-Homji, 1991).

2.2 Impact on evapotranspiration

Although the net change in global vapour flows is close to zero, deforestation has decreased global vapour flows from land by 4% (3000 km3/yr), a decrease that is quantitatively as large as the increased vapour flow caused by irrigation (2600 km3/yr) (Gordon et al., 2005).
The main areas that have experienced decreases of vapour flows in the second half of the last century due to deforestation are Southeast Asia (particularly the Philippine Islands, Sumatra and Borneo), southwestern and central Africa, the arc of deforested areas around the edge of the Amazon basin, northern South America, and the temperate forest regions of the eastern United States and centraland western Europe (Gordon et al., 2005).

Surface specific humidity and relative humidity regulate evaporation and transpiration processes.
Specific humidity is the concentration, by mass, of water vapour in a moist air sample. Therefore, it is the ratio of water vapour mass to the total mass in the same sample moist air, including both dry air and water vapour.
Relative humidity is a measure of the actual amount of water vapour in the air compared to the total amount of vapour that can exist in the air at its current temperature. Warm air can possess more water vapour (moisture) than cold air. So with the same amount of absolute/specific humidity, air will have a higher relative humidity if the air is cooler, and a lower relative humidity if the air is warmer.
Through evapotranspiration, forests bear the hydrologic cycle, which cools climate through feedbacks on clouds and precipitation. The ratio of evapotranspiration to available energy is generally low in forests than in crops and lower in conifer forests than in deciduous broadleaf ones.
Changes on atmospheric humidity may have important implications, because it is a key variable in determining the geographical distribution, maximum intensity of precipitation and human heat stress.

As we said, evapotranspiration depends on temperature. The deforestation effects on temperature are opposite. On the one hand deforestation leads to an albedo increase and hence to a temperature decrease; on the other hand it brings to an evapotranspiration decrease and a temperature rise.

Moreover, saturation pressure increases exponentially with increasing temperature. All the other factors remaining unchanged, warming should cause drier air and hence more ET. In fact, low humidity increases the atmospheric demand for moisture and causes partial to full stomatal closure

in plants, resulting in reduced transpiration, photosynthesis and plant productivity (Komer and Bannister, 1985; Choudhury and Monteith, 1986). However, actual vapour pressure may also change in response to increased ET.

Besides, we have to consider that atmosphere is not a static compartment, but is subjected to a continuous movement of air masses and consequently of the amount of vapour present inside it. Moisture quantity can be changed by circulation movements. In fact, not only the amount of moisture in a particular location is important, but also the one delivered to the area from advection and convergence processes.
The process of vapour removal depends, to a large extent, on wind and air turbulence, which transfer large quantities of air over the evaporating surface. Higher wind speed can increase or decrease ET, depending on the other climatic factors, in particular humidity and the plant/crop characteristics, such as stomatal resistance. Increase in wind velocity could also result in higher dust content in the atmosphere, which in turn leads to lower incoming solar radiations (Goyal, 2004).

Beside humidity, evapotranspiration depends also on other variables, as cloud cover, and albedo. With a decreasing cloudiness and increase of solar radiation would increase ET. As well an increase in cloudiness, caused by increased ET, would have the opposite effects (Goyal, 2004).

2.3 Impact on precipitation

For precipitation formation, the air must reach at a sufficient rate to enhance condensation of water vapour into liquid water droplets or ice crystals (depending on air temperature) and to promote growth of water droplets, supercooled droplets, and/or ice crystals in clouds. Droplets grow through a process called "collision-coalescence" whereby droplets of varying sizes collide and fuse together (coalesce). Ice crystal processes (including deposition and aggregation) are also important for particle growth.

Studies on effects of deforestation generally result in a decrease of precipitation over the deforested areas (Zhang, 1986). In particular, after land cover change, main variations in precipitation can be due to change in evapotranspiration, albedo and roughness. These variables depend on geographical region, season and climate variability. Generally albedo mechanisms dominate at high latitudes with trees masking of snow for boreal forest, instead evapotranspiration dominates at low latitudes in tropical forest, where it has high rates (Chen et al., 2012).

Spracklen et al. (2012) have demonstrated an increase of moisture in the air that passes above a forested area than a not forested one. They verify that for more than 60% of the tropical land surface (latitudes 30 degrees south to 30 degrees north) air, which has passed over extensive vegetation in the previous few days, produces at least twice as much rain as air that has passed over little vegetation (Spracklen et al., 2012). The evapotranspiration mechanism indicates that increase vegetation cover results in enhanced plant transpiration, leading to an increase in water vapour availability and greater precipitation through local moisture recycling (Shukla and Mintz, 1982). Schnell (1975) has emphasized that the organic nuclei deflated from the surface litter aid in seeding the cumuliform clouds. Litter is the most superficial soil layer, which is composed by not yet decomposed organic material, such as leaves, twigs and seeds.

Pollen grain, debris and other parts of the plants serve as condensation nuclei during precipitation formation. Their role as seeds of crystallization is more effective than the inorganic debris like dust because the ice is formed on them at a much lower temperature (Glantz, 1987). Therefore the loss of litter due to deforestation causes rainfall reduction at short time-scale.

So, changing the land use from forest to bare soil, for instance, could create a decrease in precipitation because of the reduced numbers of pollen grains in the air.

The greater is the deforested area around a station, the stronger is the declining trend of rainfall/rainy days. Exception to this rule are the coastal stations where evaporation from the sea maintains sufficient humidity in the atmosphere (Meher-Homji, 1980).

Generally, rainy days are more prone to decline than rainfall volume (Meher-Homji, 1980). Sometimes there is even shrinkage of the rainy season duration (Padmavalli, 1976). Often in the areas where rainfall season is characterized by monsoon blowing, the decreases are noticed in the pre-monsoon period (Warren, 1974) or after its peak (Kanae, 2001). For what concerns these zones, there are evidences which show that when monsoon is weaker, and so convectional rainfall are dominant, anthropogenic land cover changes can influence regional precipitation and a significant decrease in rainfall can occur.

Moreover, forests reduce wind speed through their aerodynamically rough, undulating canopy. Roughness is a function of canopy height. High roughness length of vegetation results in an increase of turbulent fluxes, thus reducing surface air temperature. On the other hand, it results in more mass of air convergence associated with anomalous lower pressure, increasing upward moisture transport and convective cloud cover, thus increasing precipitation (Sud et al., 1988). With the decrease of wind speed caused by forests, air masses are forced to stack and so they are able to

rise; hence mechanical friction effect of forests is important in lifting the moist-air and enhancing the rainfall (Sud and Smith, 1985).
With deforestation, the soil is also less protected. It has been estimated that a decrease in roughness length can produce a reduce in evaporation through a decrease in the surface drag coefficient (Kanae, 2001). Anyway, the change in precipitation due to this mechanism is complex and can vary from region to region.

Friction effect of forests is important also for what concerns the formation of orographic rainfall. In fact, forests act as an obstacle and increase the effective height of the land surface in providing an obstruction to air movement (Meher-Homji, 1991). This means that if the air that is "climbing" the mountain passes over forest, it will bring likely more precipitation than if it was passing over the same side without forest cover.

Among the mechanisms that take place in interaction between forest and precipitation, the role of albedo is really important. As we said in paragraph 2.1, deforestation increases albedo, in fact the albedo of bare soils is considerably greater than vegetated surfaces. It means that forest absorbs more energy than bare soils.
This energy brings to either increasing temperature and evaporation in forested area (maintaining humidity in the air) or to heats up the air, causing locally drier climate in bare zones.
So the decreases in net radiation and evaporation may cause a decline in rainfall (Charney et al., 1977). As albedo changes bring to energy balance changes, in case of a large scale afforestation or deforestation they can affect general atmospheric circulation and even alter the tropical atmospheric circulation of Hadley (Swann, 2011).

Concerning afforestation, the experimentations are less than deforestation, but they commonly estimate an increase in precipitation over the afforested zones. Moreover some effects on adjacent afforested regions have been noticed: an increase in temperature during winter period and a decrease of precipitation during summer (Chen et al., 2012).

In conclusion, it is generally recognised that deforestation, including both albedo and roughness changes, can produce a decrease in evaporation and complex changes in moisture convergence and consequently a precipitation decrease. Furthermore, for the case study taken into consideration in this thesis, it is important to highlight the deforestation effects observed in monsoon climate regions; as we said, rainfall decrease occurs in pre-monsoon or post-monsoon period.

2.4 Impact on streamflow

Streamflow depends on amount and distribution of precipitation, evapotranspiration mechanisms and soil characteristics, like water storage capacity and hydraulic conductivity.
Trees are the interface between soil and atmosphere. With their roots, they take water from the ground, use it for their life functions (photosynthesis and respiration), and then transpire water vapour through their leaves.
Over longer temporal scales, humidity may have effects on plant evolutionary adaptations such as leaf area and cuticle thickness (Grantz, 1990). These factors condition soil moisture and run-off at local scales and may influence precipitation and atmospheric circulation patterns at regional to global scales (Hansen et al., 1984).
Trees play a role also in interception of precipitation with their canopies. In fact, soil behaviour after precipitation event is related to land cover. With a forested area, precipitation does not directly turn in run-off, like it occurs on a bare soil for instance. Therefore, forests act as temporary storage for water.

There are not many studies about the quantitative assessment of the change, because it depends on a different catchment, climatic factors and different forest practice. However, they provide important qualitative indications about the contribute of forests on streamflow and particularly on low-flows: deforestation increases the streamflow volume especially in low flows, while afforestation decreases it.

In particular, on the one hand, studies that relate changes in land cover with changes in river discharge at the small scale (<1 km^2) are abundant. They generally indicate that deforestation causes an increase in the annual mean discharge (Costa et al., 2003). On the other hand, observational studies are not suitable to explore the impacts of large-scale deforestation, without using any specific model (Spracklen et al., 2012).

Moreover, hilly regions are often vulnerable to water and wind erosion, for example in China, some studies have documented that forests can reduce soil erosion and sediment transport (Wei et al., 2005), and enhance carbon sequestration (Fang et al., 2001).

Although there is a large variability due to differences in climate, soils, and vegetations, studies agree that deforestation generally increases water yield and base-flow, and afforestation reduces the two variables for most watersheds. There is more uncertainty on the effect of afforestation on peak-

flows than that on annual water yield and base-flows (Jones and Grant, 1996; Thomas and Megahan, 1998; Bruijnzeel, 2004; Andreassian, 2004).

2.5 Impact on soil structure and properties

2.5.1 Change in soil characteristics

As we said, deforestation influences also soil structure.
After deforestation, land cover of many parts of the world has become more fragmented and highly complex, as it happened in the tropics. Secondary forest has emerged as the dominant forest type, alternated with remains of old-growth forest and other intermediate land covers (Giambelluca, 2002; Drigo, 2004; Holscher et al., 2004; Cuo et al., 2008). For example within South and Southeast Asia, it was estimated that about 45% of the total land area has been affected by human-induced soil degradation (Eswaran et al., 2001; Scott et al., 2004).

When forest changes, the drainage of the soil also changes, in fact deforestation causes a long term decrease in the water storage capacity of the soils and an increased movement of sub-surface water (Johnson, 1998).

Properties of special interest affecting water transport of soils are soil texture, soil structure, pore volume, pore size distribution, bulk density and organic matter. Parameters like soil texture can be expected not to vary over time. Soil structure and geometry and volume of pores can be influenced by soil tillage and soil biological activity (e.g., of earth worms) instead. Those characteristics can vary with season and weather. Frost, for example, can reduce the bulk density by alternation of freezing and thawing of the soil (Unger, 1991). As well, swelling and shrinkage of clay minerals and organic matter also have an impact on soil water flow (Hartge and Horn, 1991). Intense rainfalls can change the soil structure. Cameira et al. (2003) found that the pore size distribution established by soil tillage is partly degraded by intense rainfalls. Only the growth of plant roots can re-establish a continuous pore system. Similarly, soil compaction by soil tillage must not be constant from year to year.

Drastic and fast changes in soil properties are caused by traditional soil tillage, influencing bulk density, infiltration rate, aggregate size distribution and earthworm population (Logan et al., 1991). In particular, soil structure is affected by crop production activities and mechanic exposures. Moreover, while conventional soil tillage temporarily increases porosity and the portion of large

pores in the topsoil, bulk density decreases in the subsoil (Hermawan and Cameron, 1993). In contrast, forest soils are aerated by wind stress, which is transmitted into the soil via plant roots (Hintikka, 1972) inducing a decrease in bulk density.

In addition, macropores can have a major impact on water and nutrient transport into soils. In the topsoil, specially, secondary macropores caused by soil structure prevail over primary ones caused by soil texture. The secondary macropores govern the infiltration process. They mostly depend on plant roots (Tippkötter, 1983) and the presence of soil fauna (Léonard et al. 2004; Chan 2004; Bastardie et al., 2005). Presence and density of the root system are related to vegetation and land use, while mechanic stresses can reduce the pore volume and destroy the pore continuity (Larink and Schrader, 2003).

Forest soils show a higher soil biological activity compared to cultivated land (Parker and Chartres, 1983) and a reduced bulk density (e.g. Murty et al., 2002). Martinez and Zinck (2004) found that soils under pasture showed a bulk density by 42% higher than for forest soils. They also detected a reduced infiltration capacity for pasture.
Schwartz et al. (2003) state that land use practices have a greater impact on the water flow in soils compared to soil genetic processes. The secondary macropore system is primarily developed by the macrofauna. During ploughing, the vertical distribution of organisms in the soil is altered or destroyed, and about 60% of the earthworm population is killed (Larink and Schrader, 2003). Hence, the portion of biologically induced macropores is much higher for alternative soil tillage methods (Logan et al., 1991).

2.5.2 Change in hydraulic conductivity

There are not many studies investigating how soil hydraulic properties are influenced by vegetation cover and land use, even if lately this topic is becoming of great interest.

Soil hydraulic properties govern the transport of water and nutrients in soils. The intensity of forest use and effects of monoculture plantations on soil ecology (relative to native, mixed forests) is likely to be the critical factor in affecting surface hydraulic conductivity over time (Bonell et al., 2010).

Bormann et al. (2008) state that land use influences considerably soil hydraulic and soil hydrological properties. They have identified statistically significant systematic impacts on bulk density, saturated hydraulic conductivity, infiltration capacity and field capacity.

Land cover change causes a substantial reduction in soil infiltrability (Hillel, 1980) and permeability (e.g. Scott et al., 2004). A common cause for enhancing the occurrence of infiltration-excess overland flow is surface soil compaction arising from various trampling pressures, such as intensive over-grazing, human pathways and roads (Ziegler et al., 2004; Hamza and Anderson, 2005; Cuo et al., 2008; Zimmermann and Elsenbeer, 2008, 2009). Moreover selected soils in the tropics are particularly vulnerable to significant changes in structure as an effect of human disturbance (e.g. Gilmour, 1977; Schaak-Kirchener et al., 2007). Additional causes are the exposure of unprotected soils to high rainfall intensities, which can bring to raindrop compaction and sealing (Sandstrom, 1998; Grip et al., 2004; Scott et al., 2004). Thus the overall reduction in surface permeability and infiltration results in a change of the flow pathways from sub-surface to infiltration-excess overland flow. It will also affect the vertical percolation flux in the uppermost soil layers (Bonell et al., 2010).

Degraded forest has been prone to a loss of macro-porosity due to enhanced compaction and a reduction in soil fauna from multi-decadal disturbance, as reported elsewhere in the humid tropics. Further, there is a progressive decline in saturated hydraulic conductivity down the soil profiles.
Intense agricultural use or intensive pasture increase bulk density and reduce hydraulic conductivity (saturated and unsaturated) and plant available water (reduced field capacity). This is mainly caused by soil compaction due to heavy machines and a reduction in macrofaunal activity, for example after ploughing, resulting in a loss of macropores. In contrast, forest soils show the highest hydraulic conductivities and the highest amounts of stored water, while soils under grassland behave in-between forest soils and cropland soils (Bormann et al., 2008).

In addition, it is important to consider the seasonal variability while investigating soil hydrological properties and characteristics. An increase in macropores and soil aggregation leads to a decreasing bulk density in late spring and summer, saturated hydraulic conductivity (partly doubled conductivities) and also infiltration capacity increase noticeably. In contrast, field capacity slightly decreases and brings to a reduced soil storage capacity.

Seasonal variability was statistically significant only for the minority of the soil property variables. Nevertheless, soil hydraulic and soil hydrological properties were not constant over time, as assumed in most hydrological models (Bormann et al., 2008).

In conclusion, it is well known that many physical and chemical soil properties are variable in space and time. Soil hydraulic and soil hydrological properties also vary (Bormann et al., 2008). Possible reasons are soil biological activity, frost related processes, impact of wind via the plant roots, soil tillage and others.

Chapter 3

Study area

The Red River basin is the second largest of Vietnam, with a total area of approximately 169,000 km^2. Its average length is about 875 km and its width is about 467 km. It is an international river which flows for 48% in China, for 51% in Vietnam, and the rest in Laos. In this thesis, we consider only the Vietnamese part of the basin, because of the lack of information about China, which covers 26% of the entire country territory. From an administration point of view, the basin covers an area of 26 provinces and cities in the Northern region of Vietnam, with a total population of about 30 million in 2009 (Quach, 2011).

The basin is undergoing rapid development in terms of population and economic growth. This brings, for example, to the common tendency to move from rural areas to the main cities, which are sprawling uncontrolled, and to energy demand increase.

There is ongoing development also in terms of natural resources exploitation, including water. In particular, increased population stress on the basin has effects on water quantity and creates quality problems: in the last years the basin has suffered large interannual variations between severe floods and droughts, as well as problems related to water pollution. Furthermore, the construction of massive water infrastructures, such as dams and reservoirs, is booming, often inducing problems like river bed change and erosion (Castelletti et al., 2012; Quach, 2011).

In this new heterogeneous context, water resources development and management need to be reconsidered to foster economy, society and environment systems in the entire Northern region of Vietnam (Castelletti et al., 2012).

3.1 Basin description

The Red River basin is located in Southeast Asia, in a northwest-southeast direction (from 20° 00 to

25°30 N; from 100° 00 to 107° 10 E). Its structure is designed by the confluence of three main tributaries which all rise in China: Lo, Thao and Da River (see figure 3.1). Lo River is 470 km long and it has an area of about 39,000 km^2. The basin starts being mountainous at China border and becomes flat further downstream. Thao River is 843 km long and its catchment is 51,800 km^2. It rises in a mountainous region of the Yunnan province in China, and its course is very straight. Da River, also called Black River, is 900 km long and its area is about 52,900 km^2. It flows in China too, in the South-Western part of the Yunnan province, at 2,400 m a.s.l. height. First the Da flows into the Thao, then Thao and Lo pour into the Red River at VietTri. The Red River name is used from the confluence of the Thao and Lo Rivers at VietTri, a little downstream from the location where the Da throws into the Thao. This denomination comes from the red color due to the large quantity of silt, rich of iron oxide, that the river carries along its path.

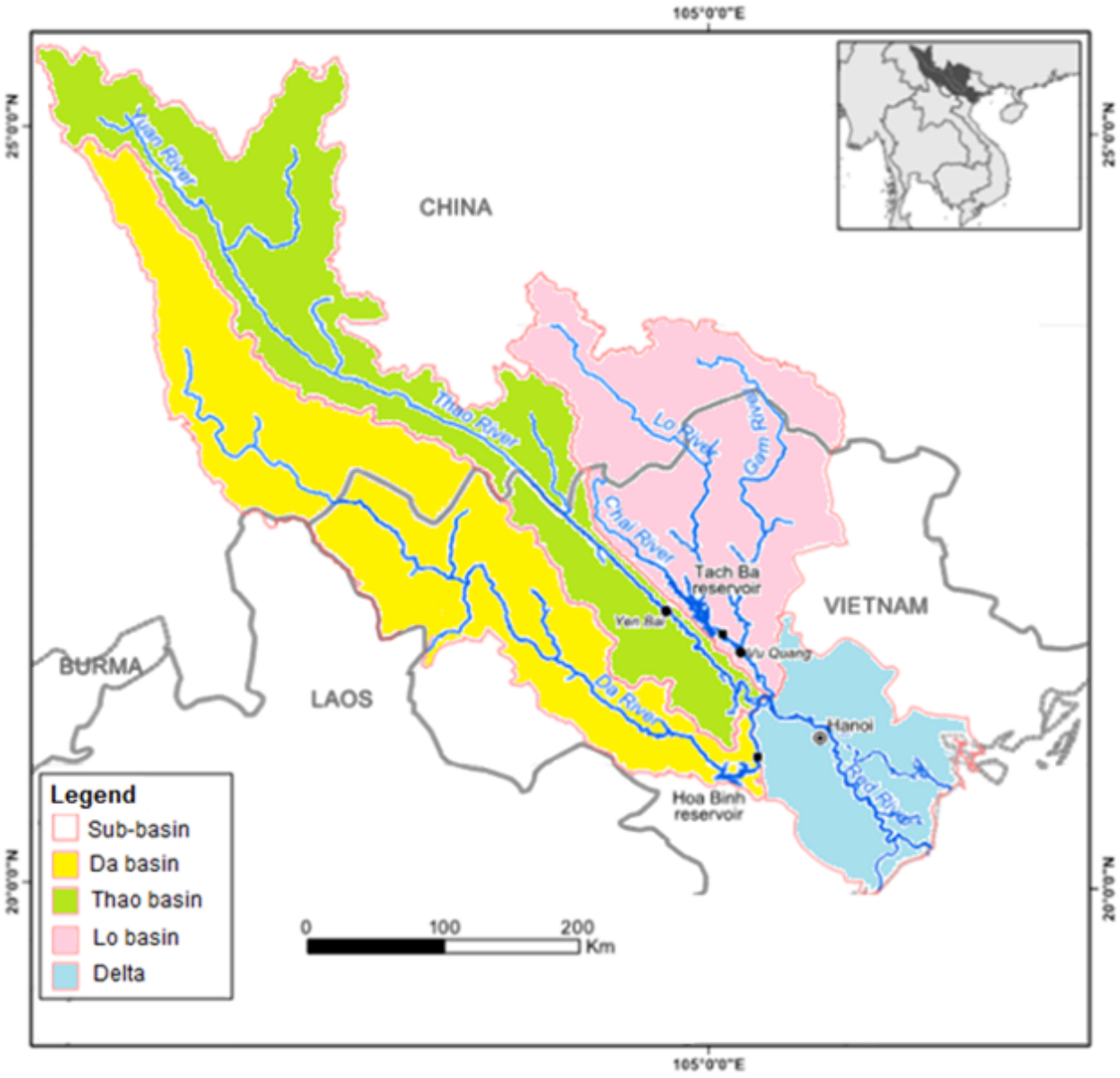

Figure 3.1: Map of the Red River basin structure. It is composed by the Da, Thao, Lo sub-basins and the delta.

The Da is the largest among the Red River three tributaries and it is the most important water source, contributing for about 40% of the total streamflow at Son Tay, approximately 50 km north of Hanoi, the capital city of Vietnam.

Basin topography is composed by the central delta lowlands, the midlands, and the mountainous areas, which present a maximum elevation of about 3,200 m. Figure 3.2 shows the digital terrain model of the entire basin: it is mountainous and the slope direction is Northwest-Southeast.

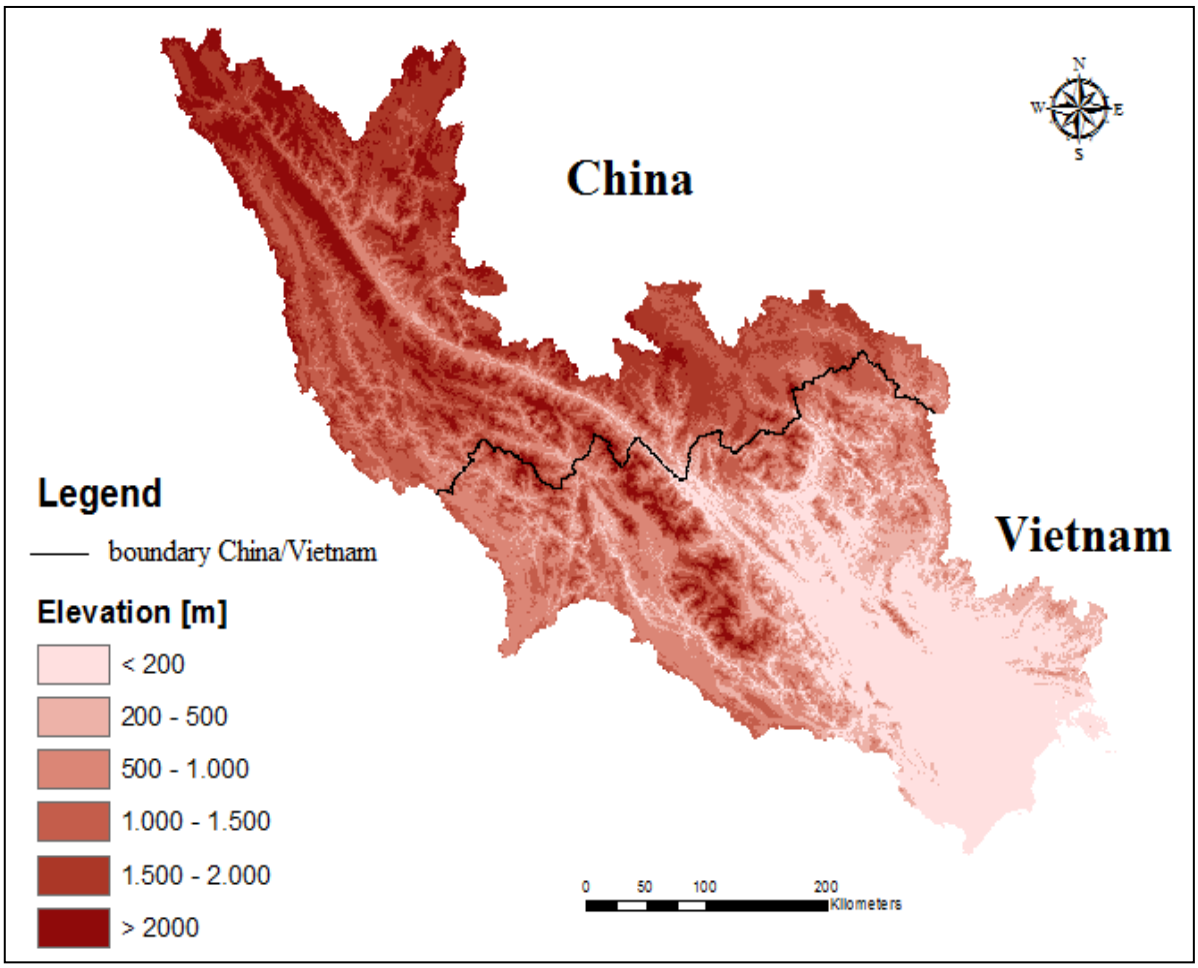

Figure 3.2: Digital elevation model of Red River basin.

3.2 Climate

The basin is situated in a tropical monsoon region which is characterized by two well distinguished seasons: wet (from May to October) and dry (from November to April). During the wet season, winds blow from South-South East, bringing humid air masses to the basin resulting in high temperatures and abundant rainfall; during the dry one, air circulation reverses to North-East carrying dry air masses to the basin, inducing cooler weather and little rain, instead. There are also

some local winds such as very hot and dry winds in Thanh Uyen and whirlwinds in Lai Chau province of the Da basin. Average temperatures range from 16 °C to 21 °C in winter season. During the wet season, temperatures are constantly high throughout the area, especially from May to September, ranging from 27 °C to 29 °C with the peak in July-August (Li et al., 2006), as shown in figure 3.3.

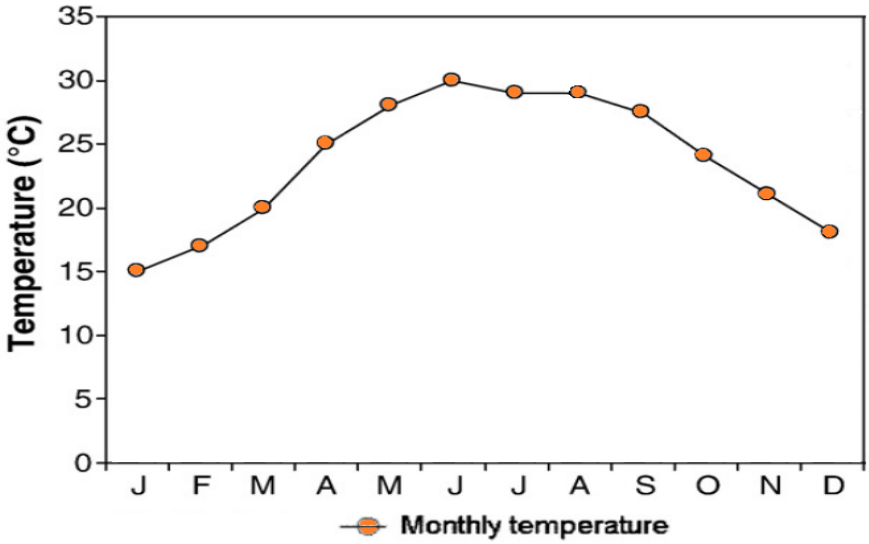

Figure 3.3: Mean monthly temperature at Son Tay station (data from 1960 to 2008).

Moreover, solar radiation and sunshine regime are copious in the region, whereas cloud cover is quite slight. The three months with the maximum sunny hours are March, April and May, when it varies from 170 to 210 hours/month.

Annual average evaporation ranges from about 1,000 mm, in the Southern part of the basin, to about 700 mm, in the Northern part. The behaviour of evaporation does not follow the temperature annual trend. Generally, high temperatures are expected to cause high values of evaporation; however, in this area high temperatures are associated with the wet monsoon season, when heavy rainfall saturates the air with moisture and cloudiness prevents solar irradiation. As a result, the highest values of evaporation occur in early spring (March) just as the temperature growth rate is maximum, rather than during summer.

Rainfall distributes unevenly on the basin both in time and space. This depends on a lots of factors, but the most important ones are topography elevation and mountains orientation. Annual rainfall varies from 1,200 to 2,800 mm/year, moving from the downstream part of the basin towards the mountainous region, with the highest values being recorded at the border between Vietnam and China. Figure 3.4 represents the rainfall distribution in the whole basin and table 3.1 shows precipitation and temperature data measured at Ha Noi.

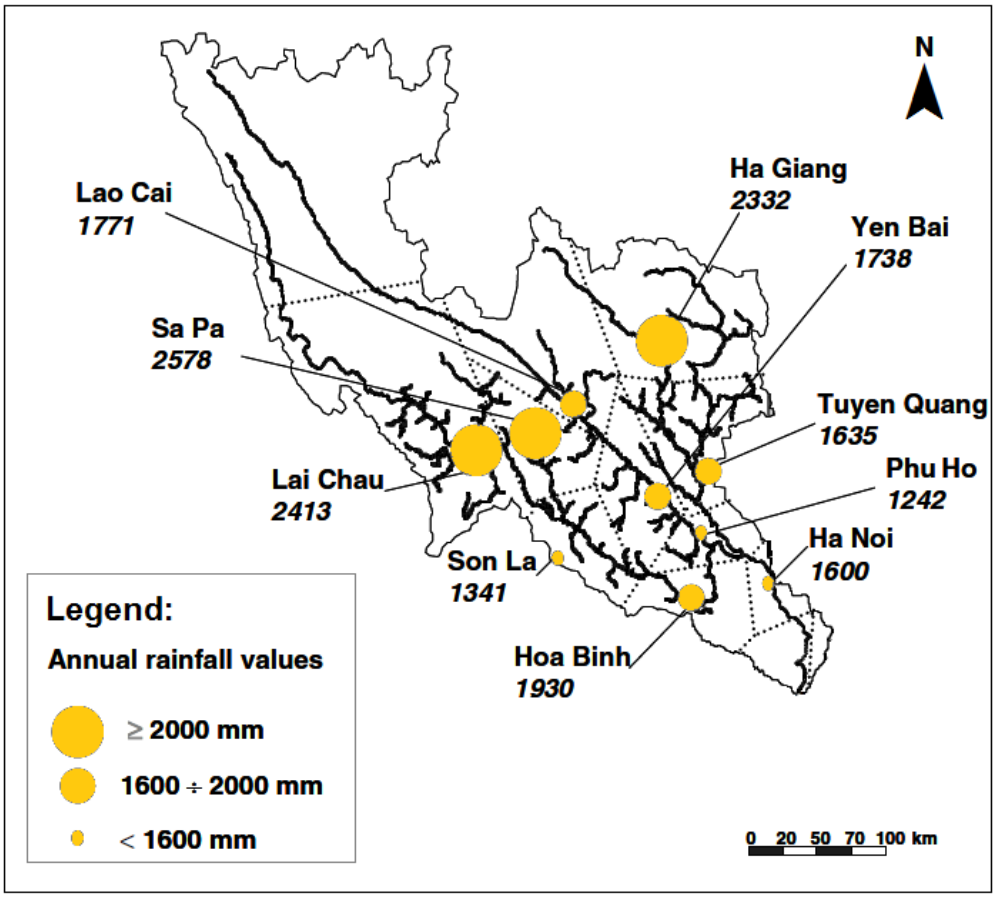

Figure 3.4: Annual rainfall distribution in the Red River basin for the period 1997-2003.

Hanoi						
Month	Rainfall (mm)		Temperature (Celsius)			
	Average monthly	Ave no of days with 1mm	Average daily		Lowest recorded	Highest recorded
			min	max		
Jan	19	8	12	20	6	33
Feb	27	13	13	21	7	35
Mar	39	14	18	24	11	37
Apr	80	15	21	29	10	38
May	198	16	22	32	15	42
Jun	240	14	25	33	20	39
Jul	322	16	26	32	23	40
Aug	345	17	25	32	21	39
Sep	250	13	24	31	18	37
Oct	99	9	23	28	14	37
Nov	44	8	19	25	8	36
Dec	21	7	16	21	7	37

Table 3.1: Historical precipitation and temperature data at Ha Noi.

The seasonal pattern of rainfall follows the monsoon driven seasonality (see figure 3.5) with about 80% of rainfall occurs during the wet season, peaking in July, while the lowest rainfall is in December-February.

3.3 Streamflow

Wet and dry seasons can be well recognized also in the flow regime (see figure 3.5). Flood (high flow) season goes from June to October, with the highest streamflow usually occurring in July-August; low flow season is longer and goes from December to May, instead. Because of this irregular distribution of rainfall, flows throughout the basin are unevenly distributed in time, causing floods and water-logging in the rainy season and water shortages in the dry season (Quach, 2011). Also Ha Noi suffers from flood problems.

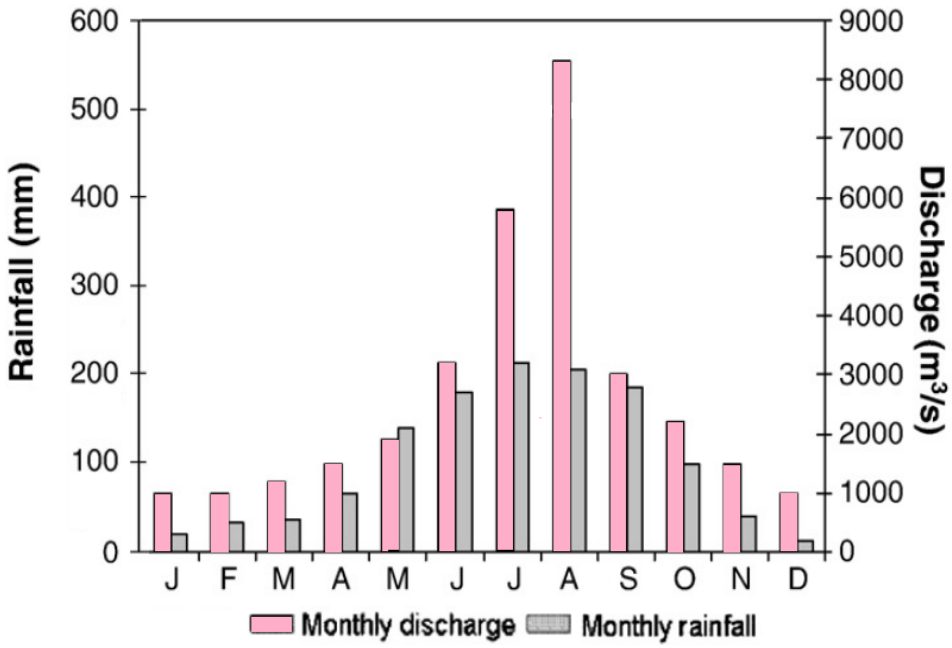

Figure 3.5: Mean monthly rainfall and discharge at Son Tay station (data from 1960 to 2008).

The mean annual water discharge of the Thao River is 3,500 m^3/s, corresponding to a specific run-off of 20.5 $l/s/km^2$ (for the period 1960-2008). For the same period, the mean annual water discharges of the Da and the Lo Rivers are respectively 1,700 m^3/s and 1,050 m^3/s (Tran et al., 2007).

In the last 100 years, the highest daily discharge, 37,800 m^3/s, was observed in August 1971, and the lowest, 368 m^3/s, in May 1960. Figure 3.6 shows the seasonal variations of discharge at the outlets of the four sub-basins in 2003.

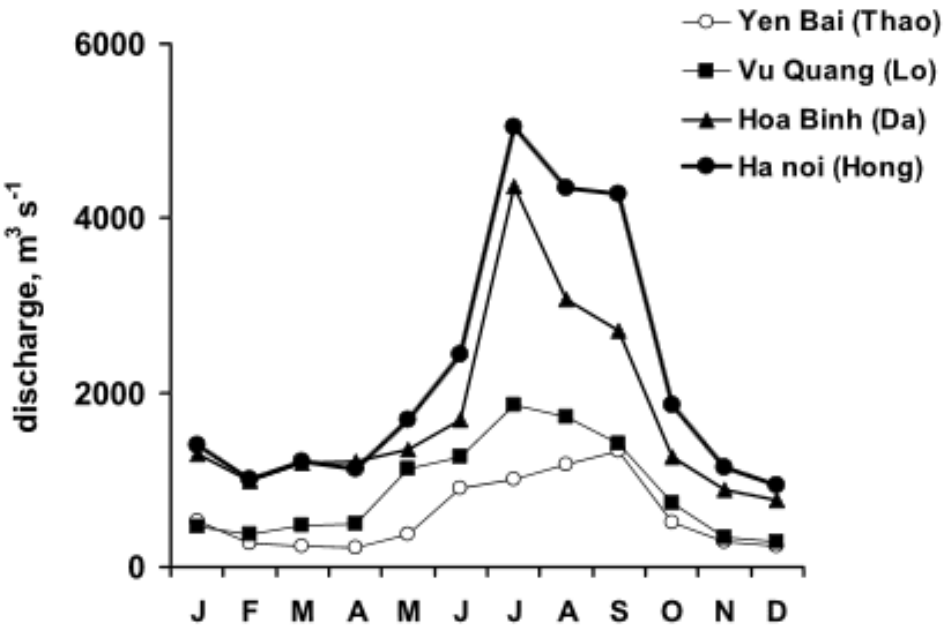

Figure 3.6: Run-off at the three outlets of the Red River upstream sub-basins, and in the delta area at Ha Noi station, in 2003.

3.4 Economy

Despite the considerably increasing importance of the industrial and service branches, wet-rice agriculture is still the most important economic driver and a primary food source. The Red River Delta is the second largest rice production area in the country, after the Mekong Delta, with 850,000 ha of irrigated agriculture (Turral and Chien, 2002). Beside rice, other crops are coffee, tobacco, soybean, corn, sugar cane, cotton and potato plantations, and are mostly grown during the dry season.

3.5 Land use

Land use changes significantly among the three upstream sub-basins and the delta of the Red River (see table 3.2). Overall, in 1997 forest was the largest land use of the upstream Red River (54%), while cultivated land represented 33% (12% for the rice culture, 20% for industrial crops). The Lo sub-basin differs from the other two sub-basins by a greater acreage of industrial crops (58.1%) than the Da (2.6%) and Thao (12.8%) areas. Forest dominates the Da sub-basin (74.4%), while urban areas represent a very small proportion (1%) of the upstream Red River basin. In the delta, however, cultivated land (mainly rice fields) holds the largest share of land use (63%), far above forest (18%); urbanized areas represent a much larger surface (6.8%) than in the upstream basins.

Sub-Basin	Rice	Industrial Culture	Dry Cereals	Grassland	Fruits	Forest	Rocks	Urban Areas
Da	12.5	2.6	0.4	3.6	0	74.4	6.2	0.3
Thao	18.7	12.8	0.7	7.2	0.9	54.2	4.1	1.4
Lo	8.1	58.1	0.4	3.9	0.1	22.4	6.4	0.6
Hong delta at Hanoi	66.3	7.6	0.7	2.2	0.6	14.9	1.0	6.7
Total Hong delta	63.0	3.7	0	2.6	0.2	17.8	5.9	6.8

Table 3.2: Percentage of land uses of the Red River basin in 1997.

The deforestation, due to economic growth, was rapid in the second half of the last century until mid 1990's, not only in the basin but also in the whole country. Furthermore, from nineties, consistent investments in forestry branch were promoted leading to a reforestation process. Figure 3.7 shows the percentage of land uses from 1960, divided in the three tributaries areas and the delta. Urban land cover is negligible in the three upstream basins, because they have a very low density of population which has not grown much in last decades, and towns are small and far away from each other. Population density differs greatly among the sub-basins, from 101, 132, and 150 inhabitants/km^2 in the Da, Lo, and Thao area, respectively, to 1,173 inhabitants/km^2 in the delta. Moreover, apart from the delta, in all the Red River basin, forest strongly decreased from 1960 to 1990 in favour of bare soil and agriculture land use, while this data seems almost stable since 1990. Forest vegetation mostly consists of woodland, cork, bamboo and mixed forests. It can be separated into three different zones, corresponding to the elevation. The low zone (< 600 m) is mainly tropical forest and the trees seldom get over 20 m high. The middle zone (700-1,700m) is a mountainous jungle where trees height is about 25-30 m. Finally, the high zone (> 1,700 m) is a mountainous tropical forest which includes trees with 50 meters high and trunk diameter up to 2 m.

In all parts of the basin, baresoil areas decreased from 1990 in favour to mainly agriculture land use and, a little part, to forests (not in the delta).

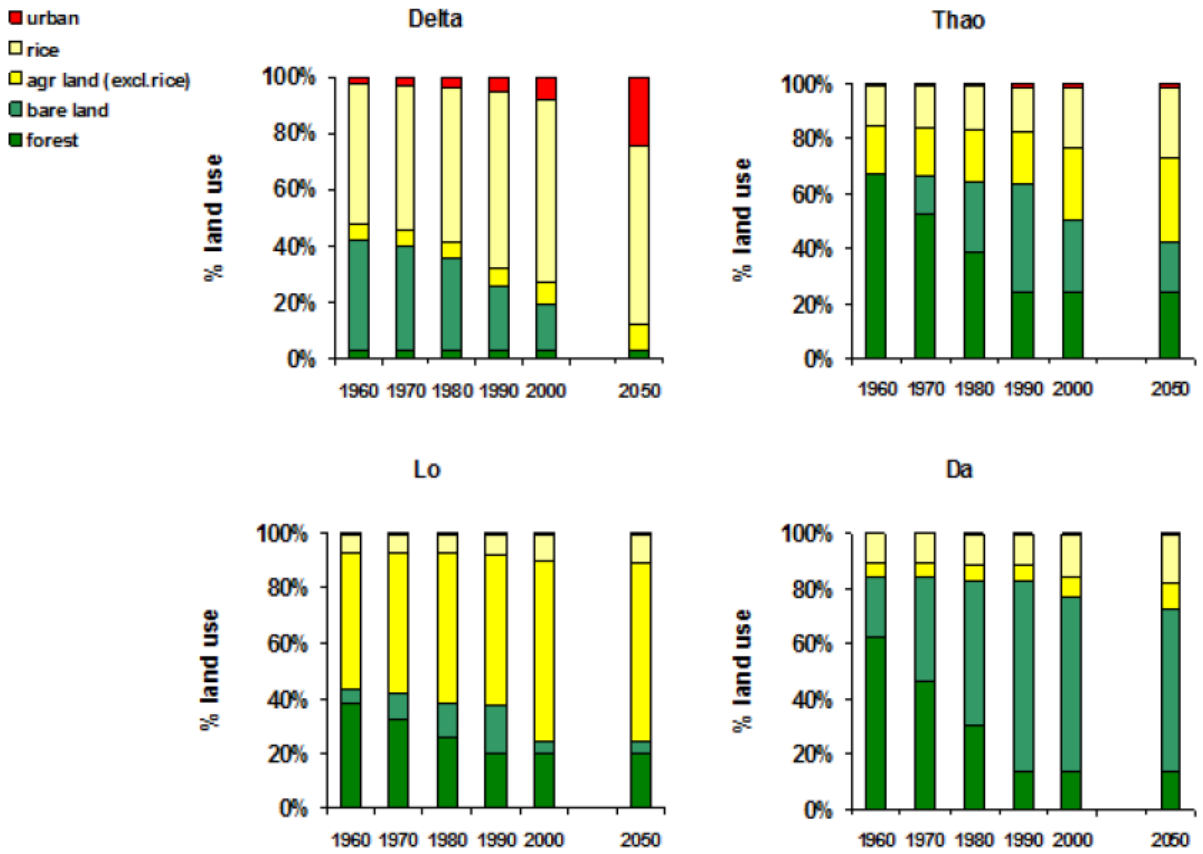

Figure 3.7: Land use in the Red River basin, documented by the Research Centre for Forest Ecology and Environment (RCFEE).

Chapter 4

Methods and tools of hydro-meteorological analysis

4.1 Introduction

In a long time series of hydrological data, change detection is a determinant and difficult issue of increasing interest. Data are the backbone of any effort to detect trend or other change in hydrological records, so it is really important to properly prepare the data before use them, and it is necessary to work with high quality data. Missing values and gaps in dataset can often cause many difficulties. It is required to decide whether or not to fill them, and in which way. The problem is quite delicate and needs particular care when the gaps are non-random, e.g. following equipment damage from a flood event of exceptional magnitude (Kundzewicz, 2004). If we have a great availability of stations, an unbiased selection between them is also very crucial.

A comprehensive trend detection study usually includes formal mathematical methods combined with the application of EDA, Exploratory Data Analysis (Kundzewicz, 2004). The latter represents all data analysis approaches besides formal statistical ones, including, for instance, graphical tools like time series plots and scatter plots. EDA aim is a better understanding of the available time series and the underlying processes. Mathematical methods include statistical tests for detecting the presence of a trend like, for example, the Mann-Kendall test and regression methods, to quantify its magnitude (Sonali, 2013). A well-conducted EDA is a powerful tool and statistical tests become a way of confirming whether an observed pattern is significant, rather than a means of searching through data.

Generally, EDA and statistical tests complete each other. EDA can support the selection of appropriate statistical tools and techniques, while statistical tests can quantify and prove the significance of the trends detected by visual inspection.

In this chapter we introduce the methodology used in this work to analyse the Red River basin hydro-meteorological variables (precipitation, evaporation, streamflow, and temperature) and to investigate land cover change effects on discharge.

4.2 Moving Average over Shifting Horizon

In this work, among exploratory data analysis techniques, we use the method called "MASH" (Anghileri et al., 2013). MASH is the acronym for Moving Average over Shifting Horizon and represents a novel visual method to detect flow-rate trends.

Dealing with hydrological variables time series, trend detection is complicated by the seasonality and the interannual variability which is typical of all natural systems.

Seasonality denotes the cyclical, usually yearly, natural processes behaviour. For instance, in the Red River basin, variables patterns are influenced by monsoon climate that presents two different seasons, wet and dry (see chapter 3). On the contrary, interannual variability is the normal variability that is recognizable from one year to another in every natural system. It can cause apparent trends, which can be avoided only using long time series data and a robust trend detection method.

MASH allows to simultaneously investigate the seasonality in the data and filter out the effects of interannual variability, thus facilitating trend detection (Anghileri et al., 2013). In this thesis, we use MASH to assess changes in variables seasonal pattern, which is represented by the 365 values of average daily volume over the year.

MASH considers two moving windows: the first averages the data over consecutive days in the same year, while the second over the same days in consecutive years. The horizon of consecutive years is progressively shifted ahead to allow trends to emerge. This detecting method has been implemented as a MATLAB function that needs as input the number of consecutive years and the number of consecutive days to be averaged. Hence, MASH result is a matrix of 365 days length as rows and number of columns depends on the considered time horizon.

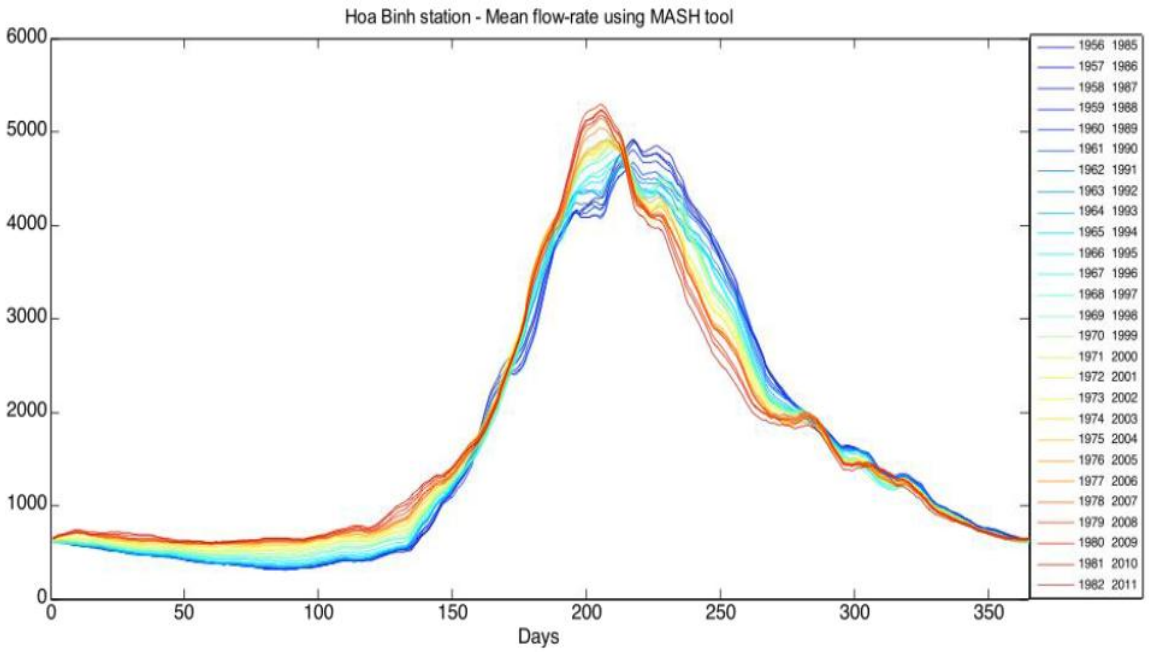

Figure 4.1: Example of MASH plot of flow-rate as annual series.

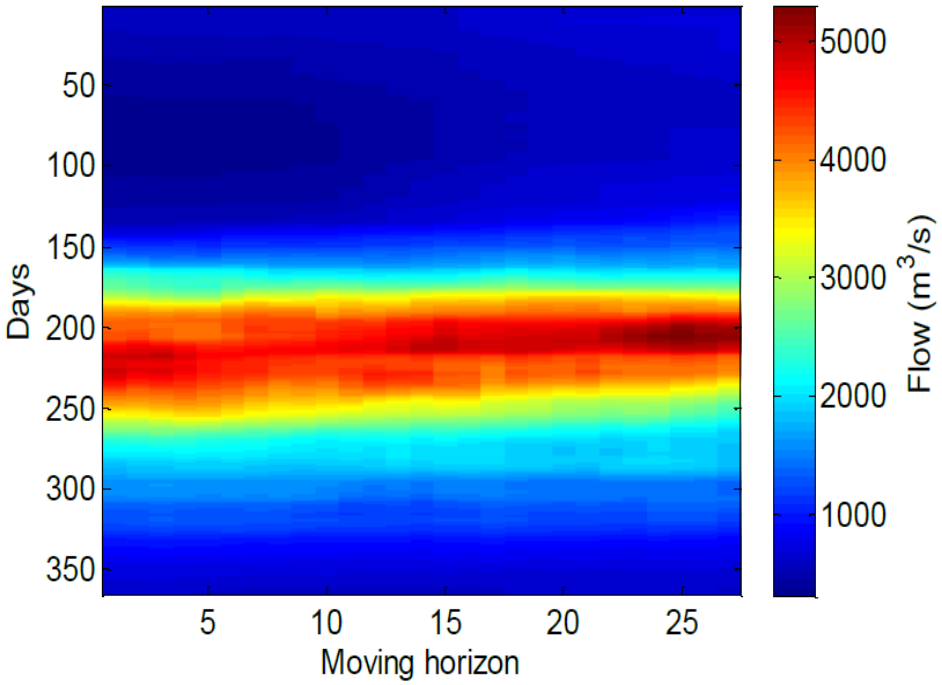

Figure 4.2: Example of MASH plot of flow-rate as a matrix.

MASH allows two types of visualizations. The first one uses blue colours for the average of first years in the time series and red colours for the last years; the second one uses colours to underline the changes in magnitude of variable volume. Hence looking at the colours of the two plots, it is immediately possible to recognize qualitatively the presence of a trend and its direction. Figures 4.1

and 4.2 illustrate in two different ways the same trend detection analysis of flow-rate measured in the period 1956-2011 at the outlet of the Da river.

Using MASH, we analysed all the hydrological available data for Vietnamese part of Red River basin, including precipitation, flow-rate, temperature and evaporation time series.

This tool has two tuning parameters: the half number of consecutive days to be averaged (f) and the number of consecutive years to be averaged (H). They can vary a lot the resulting plot and the consequent considerations about the trend existence. On the one hand, moving H, the interannual variability is changed letting the trends come out; on the other hand, moving f, the variability among the days is smoothed. In figure 4.3, we report an example of how the change of these two parameters can influence the plot moving.

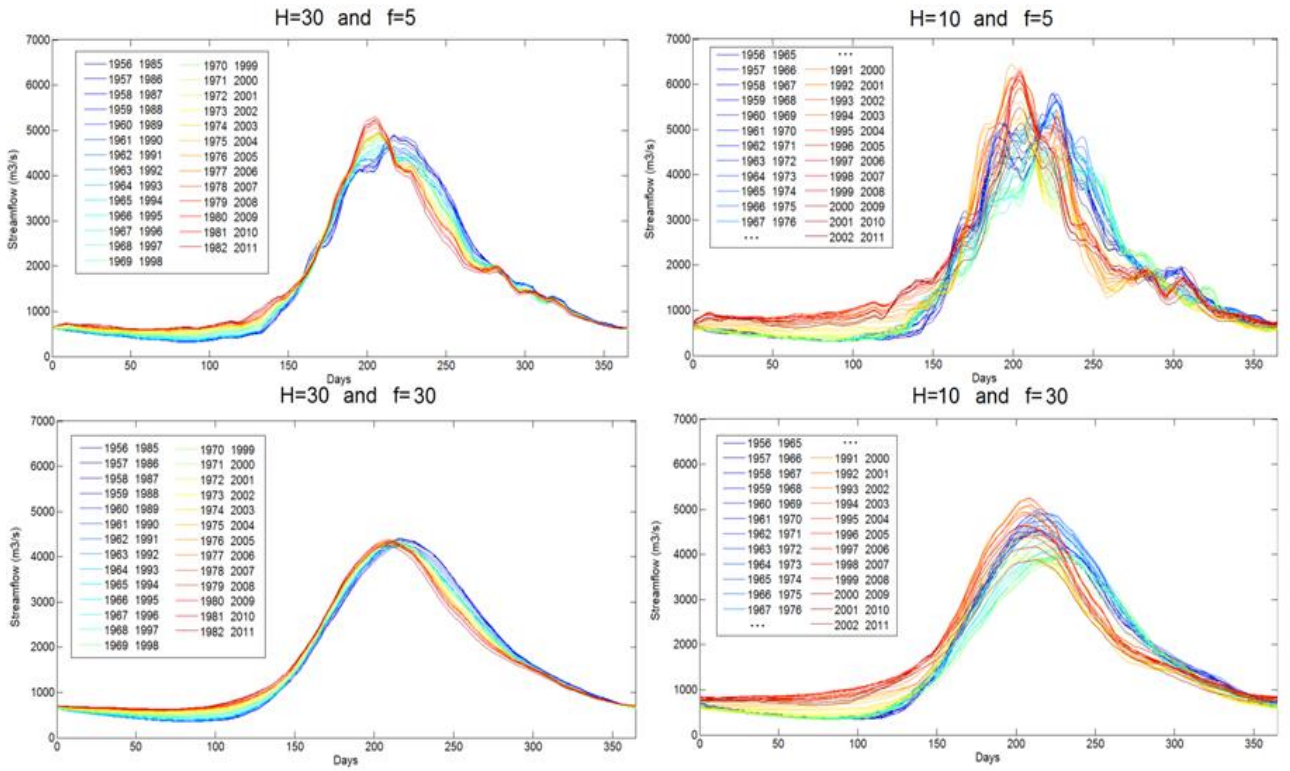

Figure 4.3: Effects of the tuning parameters f and H in MASH tool plot on precipitation data. Figures on the left side (H=30) show that using bigger H, the interannual variability is reduced respect to the right side ones (H=10). Instead figures on the top (f=5) respect to the plots on the bottom (f=30) show the smoothing effect given by a higher f value.

Therefore when using this tool, we have to pay attention to the number of years and months to average, and a sort of sensitivity analysis is suggested to understand their effect on data.

4.3 Trend detection test

MASH provides a qualitative assessment of trends based on visualization. To quantify trends, we use statistical tests.

In order to carry out a statistical test, it is necessary to define the null and alternative hypotheses; these are statements that describe what the test is investigating. For example, to test for trend in the mean of a series, the null hypothesis (H0) would be that there is no change in the mean of a series, and the alternative hypothesis (H1) would be that the mean is either increasing or decreasing over time. In carrying out a statistical test, one starts by assuming that the null hypothesis is true, and then checks whether the observed data are consistent with this hypothesis. The null hypothesis is rejected if the data are not consistent.

In this work, among the most used techniques in trend detection, we have applied the Mann-Kendall test. We cannot employ linear regression method to analyse all variables. In fact, with Kolmogorov's test, we verify that time series are not normally distributed, which is a necessary condition to implement the method. Both Mann-Kendall test and linear regression are used for finding out monotonic trends in time data series.

The Mann-Kendall test is a rank based method, i.e. a non-parametric one. To use this test, time series need to satisfy only the independency assumptions, but normal distribution is not required.

Mann (1945) presented a nonparametric test for randomness against time which constitutes a particular application of Kendall's test for correlation (Kendall, 1975) commonly known as the *Mann-Kendall* test.

Let y_1, y_2, ..., y_n be a sequence of measurements over time, Mann proposed to test the null hypothesis, *H0*, that the data come from a population where the random variables are independent and identically distributed. The alternative hypothesis, *H1*, is that the data follow a monotonic trend over time. Under *H0*, the *Mann-Kendall test statistic* is

$$S = \sum_{k=1}^{n-1} \sum_{j=k+1}^{n} sign(y_j - y_k)$$

where

$$sign(y) = \begin{cases} +1, & y > 0 \\ 0, & y = 0 \\ -1, & y < 0 \end{cases}$$

So the data values are evaluated as an ordered time series. Each data value is compared with all subsequent data values. If a data value from a later time period is higher than a data value from an earlier time period, the statistic S is incremented by 1. On the other hand, if the data value from a later time period is lower than a data value sampled earlier, S is decremented by 1. The net result of all such increments and decrements yields the final value of S.

In 1975, Kendall showed that S is asymptotically normally distributed and gave the mean and variance of S, for the situation where there may be ties in the *x* values, as

$$E[S] = 0$$

$$var(S) = \left\{ n(n-1)(2n+5) - \sum_{j=1}^{r} (t_j - 1) t_j (2t_j + 5) \right\} / 18$$

where r is the number of tied groups in the data set and t_j is the number of data points in the j_{th} tied group. A positive value of S indicates that there is an upward trend in which the observations increase with time. On the contrary, a negative value of S means that there is a downward trend. Because it is known that S is asymptotically normally distributed and has a mean of zero, it is possible to check whether an upward or downward trend is significantly different from zero or not. If the S is significantly different from zero, based upon the available information, H0 can be rejected at a chosen significance level (α) and the presence of a monotonic trend, H1, can be accepted.

The statistical significance of the trend is assessed by computing the standard normal statistic Z

$$Z = \begin{cases} \dfrac{S-1}{var} & if\ S > 0 \\ 0 & if\ S = 0 \\ \dfrac{S+1}{var} & if\ S < 0 \end{cases}$$

and the associated p-value

$$p = \frac{1}{\sqrt{2\pi}}\, e^{\left(\frac{z^2}{var^2}\right)}$$

The null hypothesis of trend absence is rejected at significance level if the p-value is less than or equal to α. It expresses the probability that the null hypothesis is incorrectly rejected; incorrect rejection of the null hypothesis is known as type I error. The range of p-values can be seen as a

measure of statistical confidence: the lower the p-value, the higher the confidence in rejecting the null hypothesis and vice versa. The significance level chosen for our analyses is 5%.

The principal advantage of Mann-Kendall test if compared to other tests is that it is not affected by outliers because its statistic is based on the sign of differences, not directly on the values of the random variable. Mann-Kendall test power depends on the pre-assigned significance level, magnitude of trend, sample size, and the amount of variation within a time series. The test is more powerful with bigger absolute magnitude of trend, longer data series and less variations in it. Moreover, when H0 is rejected, that is to say there is a monotonic trend, test power is also dependent on the distribution type and skewness of the time series (Sheng et al., 2001).

Mann-Kendall test uses the p-value as confidence parameter. The magnitude of the trend is quantified by the Sen' slope "s" (Sen's method: Sen, 1968). It is estimated as the median slope between all possible pairs y_i and y_j:

$$s = \text{median}\left(\frac{y_i - y_j}{i - j}\right) \quad \text{for all } i>j \quad i=2,...., N \quad j=1,....,N-1$$

where y_i and y_j are data at time points i and j, respectively and N is total number of data points in the series. Positive and negative signs of test statistics indicate increasing and decreasing trends respectively.

4.4 Pettitt's homogeneity test

Homogeneity tests are statistical tools to verify the possibility to reject or accept the null hypothesis of homogeneity of a time series. Hence the null hypothesis H0, that says that the series is homogeneous, can be rejected if the p-value of the test is less or equal to the selected confidence level α. If H0 is rejected, Ha (alternative hypothesis) will be accepted.

Among a quite rich presence of homogeneity tests, in this work we apply Pettitt's one. The Pettitt's test is a homogeneity non-parametric test that requires no assumption about the distribution of data. It is a rank-based method and it is an adaptation of Mann-Whitney test that allows identifying the time at which a shift in the mean of a time series occurs. The test is considered to be robust to changes in distributional form and relatively powerful (Kundzewicz et al., 2013).

In his article of 1979, Pettitt describes the null hypothesis as being that the T variables follow the same distribution F, and the alternative hypothesis as being that at a time t there is a change of distribution. Nevertheless, the Pettitt's test does not detect a change in distribution if there is no change of location. For example, if before the time t, the variables follow a normal N(0,1)

distribution and from time t a N (0,3) distribution, the Pettitt's test will not detect the change. The null hypothesis is formulated as: the T variables follow one or more distributions that have the same location parameter (same mean). The alternative one is instead formulated as: there exists a time t from which the variables change of location parameter (change the mean).
The test is based on the rank of the X and it ignores the normality of the series.

$$D_{ij} = sign\ (x_i - x_j)$$

The bi-direction test statistic is:

$$K_T = \max_{1 \le t < T} |U_{t,T}|$$

$$U_{t,T} = \sum_{i=1}^{t} \sum_{j=t+1}^{T} D_{ij} \qquad \text{where } 1 \le t < T$$

P value expression is:

$$p = 2\sum_{r=1}^{\infty} (-1)^{r+1}\, exp\{-6kr^2/(T^3 + T^2)\} \cong 2exp\{-6k^2/(T^3 + T^2)\}.$$

If the null hypothesis H0 is rejected ($p < \alpha/2$), the test gives as output the year at which the change point in the mean of the time series occurs (see figure 4.4).

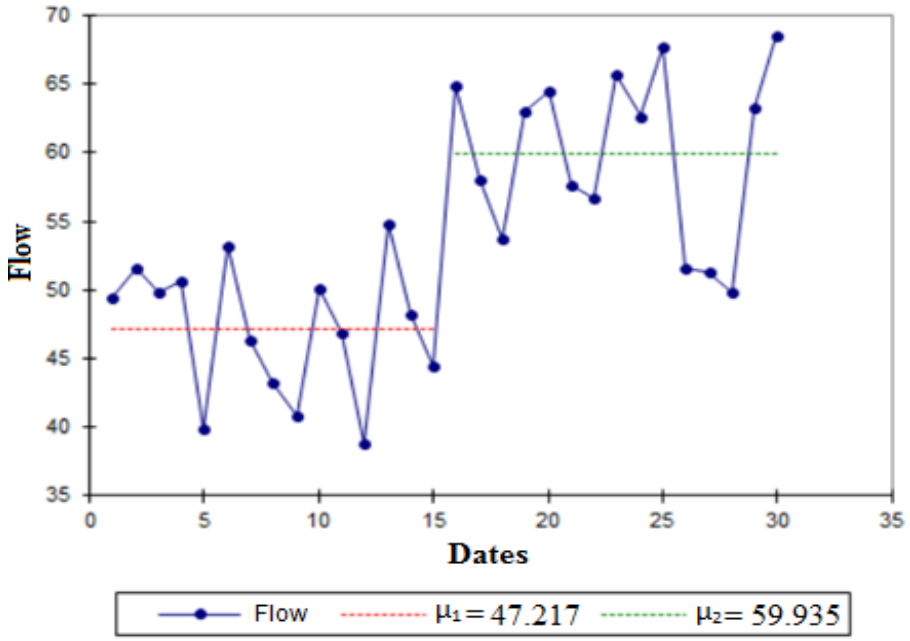

Figure 4.4: An example of Pettitt's test in case of null hypothesis rejection. The break point is on 15th year.

4.5 A hydrological model: Topkapi-ETH

4.5.1 Introduction

Hydrological models are key tools in modelling the Earth system. They allow a better understanding of the hydrologic phenomena operating in a catchment and how changes in the catchment may affect these phenomena. Hydrology models are also providing valuable information for studying the potential impacts of changes in land use or climate (Xu, 2002).
In this thesis, after analysing trends in the available data, we use a hydrological model to understand the contribute of land cover change in streamflow patterns. We choose the physically based rainfall-runoff model called Topkapi-ETH (TE) to examine land cover change impacts on hydrological regime of Nam Muc, a Red River sub-basin. This model is not the only one which describes relations between land cover and hydrological regime, but it offers additional advantages. In fact it can be used also with a 'lower' resolution and it does not require a lot of data as inputs (that we have not for this case study).
The name "Topkapi" is an acronym of "TOPopographic Kinematic wave Approximation and Integration"; it was originally developed by Todini and others (Ciarapica and Todini, 2002; Todini and Ciarapica, 2002; Liu and Todini, 2002; Liu et al., 2005) as well as the spin-off company PROGEA2. It has become "Topkapi-ETH" after enhancements at Chair of Hydrology and Water Resource Management (HWRM), Institute of Environmental Engineering (IfU), of the Federal Institute of Technology Zurich, Switzerland.

4.5.2 Main characteristics of the model and its structure

Topkapi-ETH (TE) is suitable for continuous simulation over long periods and for mountainous regions, considering snow dynamics and glaciers. It includes the operation of anthropogenic structures (such as reservoirs and river diversions) and components of model geomorphologic processes (like bed-load transport, erosion and land-slide occurrence).
TE works with a regular grid whose resolution depends upon data availability and computational consideration. The larger the basin, the lower, obviously, the resolution.

The smallest computational element within TE operates is the grid cell (GC), just like a pixel in an image. Flow directions are defined in the 2x2 neighbourhood with a single outflow direction, called D4 single flow as well (see figure 4.5). Each GC can have a maximum of three upstream GCs and one downstream GC.

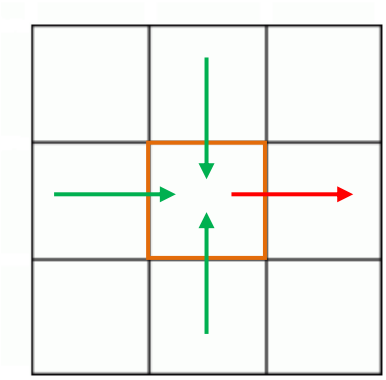

Figure 4.5: Potential flow direction in the D4 system. The downstream grid cell is indicated with red arrow.

Numerically, each GC is processed sequentially for increasing flow accumulation area, known as tree cascade. This information is derived from cell elevation. Within a GC, the processes are accounted for in a fixed numerical order. First, precipitation (P) is separated into frozen (snow, PS) and liquid (rain & drizzle, PR) parts by a strict threshold air temperature. PS will turn in the snow pack while PR will add directly to the surface streamflow. Then, the model computes evapotranspiration, with Priestly-Taylor's method beside others. Land cover type differences are accounted for by the application of crop factors. Evapotranspiration sources can be either the storages of interception, the surface, the upper most sub-surface layer, or lakes/reservoirs. The remaining surface water is available for infiltration. The updated water volumes as subjected to percolation and again updated. There are two soil layers and, starting with the lowest sub-surface one, the horizontal fluxes are shaped and the excess water of each layer is transferred upwards as an ex-filtration flux. Upper most sub-surface layer ex-filtration adds again to the surface storage. Eventually, the horizontal fluxes at the surface and in the channel network are computed.

4.5.3 Inputs and Outputs

The input data required to run a simulation are the spatial properties and the initial hydrological state of the catchments (if available), and the parameters to define both processes and specify the simulation itself. In the case study, reservoirs are not considered.
Furthermore, the model requires at least one time series each for air temperature, precipitation, and cloud cover transmissivity. Moreover it needs maps of soil and land cover, and the digital terrain model (DTM) of the area.

The model outputs could be the following:

- Water volume in soil layers,

- Water volume in groundwater aquifer,
- Infiltration/exfiltration balance at the surface,
- Channel discharge,
- Lateral flow in soil layers,
- Lateral groundwater flow,
- Snow pack height,
- Total actual evapotranspiration.

Main simulation output for this work is the channel run-off, that will be compared to the observed one. This is a trial-and-error iterative process of parameters manually moving to find their best combination which will be the baseline for the next land cover experiments.

4.5.4 Indicators

To assess the predictive power of hydrological model and to validate the used parameterization, we use different indicators.

The *coefficient of determination* (R^2) describes the proportion of the variance in measured data explained by the model. R^2 can assume a value between 0 and 1, with higher values indicating less error variance, and therefore a better fitting of observed variable. Typically, values greater than 0.5 are considered acceptable (Santhi et al., 2001; Van Liew et al., 2003). Although R^2 has been widely used for model evaluation, it is over-sensitive to high extreme values (outliers) and not sensitive to additive and proportional differences between model predictions and measured data (Legates and McCabe, 1999). Its expression is:

$$R^2 = 1 - \frac{var(y_{sim} - y_{obs})}{var(y_{obs})}$$

where y_{sim} is the simulated variable and y_{obs} is the observed one.

The *Nash-Sutcliffe efficiency* (NSE) is a normalized statistic that represents the relative magnitude of the residual variance (called "noise") compared to the measured data variance (called "information") (Nash and Sutcliffe, 1970). NSE is calculated as:

$$NSE = 1 - \frac{\sum_{i=1}^{n}(y_i^{obs} - y_i^{sim})^2}{\sum_{i=1}^{n}(y_i^{obs} - y^{mean})^2}$$

where y_i^{obs} is the i^{th} observation of the series and y_i^{sim} is its corresponding i^{th} simulated value; y^{mean} is the mean of observed data, and *n* is the length of the series.

NSE ranges between $-\infty$ and 1, where NSE =1 being the optimal value. Positive values are generally considered as acceptable levels of performance; whereas negative ones indicate that the mean observed value is a better predictor than the simulated value, so this is an unacceptable performance. Sevat and Dezetter (1991) found that NSE is the best objective function for reflecting the overall fit of a hydrograph.

Another frequently used indicator is the *Root Mean Square Error* (RMSE), also called the root mean square deviation. This indicator represents the sample standard deviation measure of the differences among predicted values and observed ones. These individual differences are called residuals when the calculations are performed over the data sample that was used for estimation, while are called prediction errors when computed out-of-sample. The RMSE deals to aggregate the magnitudes of the errors in predictions for various times into a single measure of predictive power.

The RMSE of a model prediction is defined as the square root of the mean squared error:

$$RMSE = \sqrt{\frac{\sum_{t=1}^{n}(y_{obs,t} - y_{model,t})^2}{n}}$$

where y_{obs} is observed values and y_{model} is modelled values at time *t*. The calculated RMSE value has the same unit of the variable X.

Beside these three indicators, we use also the maxima error, the mean absolute error (on the same day of the year) and the percentage of error.

Chapter 5

Time series analysis

To answer to the research question at the base of this thesis, the first objective to reach is to investigate the hydrological regime changes in the Red River basin. In this chapter, we describe how to reach the purpose, analysing hydrological variable time series with the techniques explained in the previous chapter (paragraphs *4.1-4.4*).

5.1 Data description

The hydro-meteorological data available for the Red River basin are streamflow, precipitation, evaporation and temperature recorded in different stations starting from the 50's. In order to cover the longest common possible observational time horizon with the largest reasonable number of stations and the highest reliability, we consider the period 1974-2002.
The Red River basin hydro-meteorological conditions are monitored on a daily basis through a relatively dense network of stations. The complete list of available data is the following:

- 23 streamflow stations,
- 48 rainfall stations,
- 18 temperature stations, and
- 19 evaporation stations.

Among all stations, we select only the ones that have a high data quality and overlap the chosen time horizon (1974-2002). The available stations are located in the Vietnamese part of the basin and are reported in table 5.1: the selected stations are the ones with a higher colour intensity, while the others are not considered. For rainfall we have the greatest number of available stations, more than twice as much for other hydrological variables. The common period of streamflow time series is 1968-2011, but here we report the analysis on the period 1974-2002 that is the same used for the other hydrological variables.

Stations	Evaporation	Temperature	Precipitation	Streamflow
Bac Ha				*n.a.*
Bac Me	*n.a.*	*n.a.*		
Bac Quang	*n.a.*	*n.a.*		*n.a.*
Bac Yen				*n.a.*
Ban Cung	*n.a.*	*n.a.*		
Bao Lac	*n.a.*	*n.a.*		*n.a.*
Bao Yen	*n.a.*	*n.a.*	*n.a.*	
Chiem Hoa	*n.a.*	*n.a.*		
Chora	*n.a.*	*n.a.*		*n.a.*
Co Noi				*n.a.*
Dien Bien	*n.a.*	*n.a.*		*n.a.*
Dinh Hoa	*n.a.*	*n.a.*		*n.a.*
Ghenh Ga	*n.a.*	*n.a.*	*n.a.*	
Ha Giang	*n.a.*	*n.a.*		*n.a.*
Ha Noi	*n.a.*	*n.a.*	*n.a.*	
Ham Yen	*n.a.*	*n.a.*		
Hoa Binh				
Hoang Su Phi	*n.a.*	*n.a.*		*n.a.*
Kim Boi				*n.a.*
Lai Chau				
Lao Cai	*n.a.*	*n.a.*	*n.a.*	
Luc Yen	*n.a.*	*n.a.*		
Mai Chau				*n.a.*
Mc Chai	*n.a.*	*n.a.*	*n.a.*	
Minh Dai	*n.a.*	*n.a.*		*n.a.*
Moc Chau				*n.a.*
Mu Cang Chai				
Muong Cha	*n.a.*	*n.a.*		*n.a.*
Muong Nhe	*n.a.*	*n.a.*		*n.a.*
Muong Te				*n.a.*
Na Hu	*n.a.*	*n.a.*	*n.a.*	
Nam Giang	*n.a.*	*n.a.*		
Nam Muc	*n.a.*	*n.a.*		
Nguyen Binh	*n.a.*	*n.a.*		*n.a.*
Phu Ho	*n.a.*	*n.a.*		*n.a.*
Phu Yen				*n.a.*
Quynh Nhai				*n.a.*
Sa Pa	*n.a.*	*n.a.*		*n.a.*
Sin Ho		*n.a.*		*n.a.*
Son La				*n.a.*
Son Tay				
Ta Bu	*n.a.*	*n.a.*	*n.a.*	
Tam Dao	*n.a.*	*n.a.*		*n.a.*
Tam Duong				*n.a.*

Thac Ba	*n.a.*	*n.a.*	*n.a.*	
Than Uyen				*n.a.*
Thanh Son	*n.a.*	*n.a.*		*n.a.*
Thuan Chau	*n.a.*	*n.a.*		*n.a.*
Thuong Cat	*n.a.*	*n.a.*	*n.a.*	
Tuan Giao				*n.a.*
Tuyen Quang	*n.a.*	*n.a.*		
Van Chan	*n.a.*	*n.a.*		*n.a.*
Viet Tri	*n.a.*	*n.a.*		*n.a.*
Vinh Yen	*n.a.*	*n.a.*		*n.a.*
Vu Quang	*n.a.*	*n.a.*	*n.a.*	
Yen Bai	*n.a.*	*n.a.*		
Yen Chau				*n.a.*

Table 5.1: All available stations of evaporation, temperature, precipitation and streamflow in the basin area have a coloured cell. The other ones have n.a. (not available) in their cells. We consider only the stations with higher colour intensity cells for each variable.

Figure 5.1 shows the location of stations in the basin. In particular, we can note that temperature stations distribution is not homogenous, in fact the stations are only located in the Da river area.

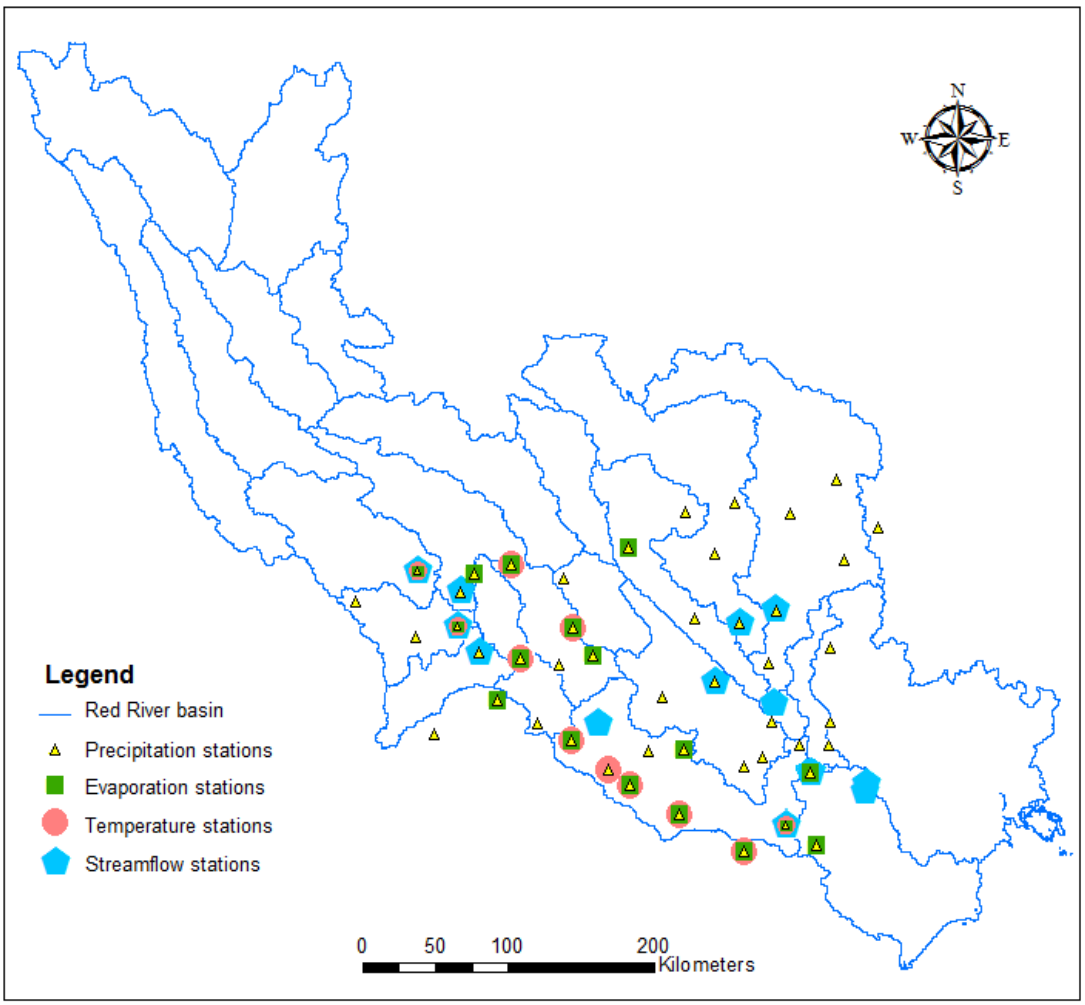

Figure 5.1: Location of considered stations in the Red River basin.

5.2 Evaporation results

After station selection, we have analysed evaporation time series using the Mann-Kendall's test and MASH, to detect monthly and annual trends.

Using the Mann-Kendall's test with a significance level of 5%, we have obtained the results schematized in table 5.2 for the period 1974-2002, where:

- grey cells represent the trend absence (H0 accepted),
- green ones correspond to an increasing trend (H0 rejected),
- orange cells symbolize a decreasing one (H0 rejected).

Each column from January to December represents the applied test answer on monthly evaporation volume, while the last one on annual volume.

Evaporation stations	January	February	March	April	May	June	July	August	September	October	November	December	year
Bac Ha													
Hoa Binh													
Kim Boi													
Lai Chau													
Mai Chau													
Moc Chau													
Muong Te													
Phu Yen													
Quynh Nhai													
Sin Ho													
Son La													
Son Tay													
Tam Duong													
Than Uyen													
Tuan Giao													
Yen Chau													

Table 5.2: Scheme of Mann-Kendall's test outputs for evaporation stations. Annual and monthly volumes are tested; each column corresponds to monthly results, except the last one which is relative to annual volume. Increasing trend, decreasing trend and no trend are represented respectively with green, orange and grey cells.

As we can see, a lots of stations have a decreasing trend in July and an increasing one in January and November. Instead, annually all stations have no trend, except one.

It is also important to combine these considerations with the magnitude of the trend, through Sen' slope. The analysis show that, for all detected trend, Sen' slope is next to the zero (for example see figure 5.2); it means that changes in evaporation volumes are not so quantity relevant.

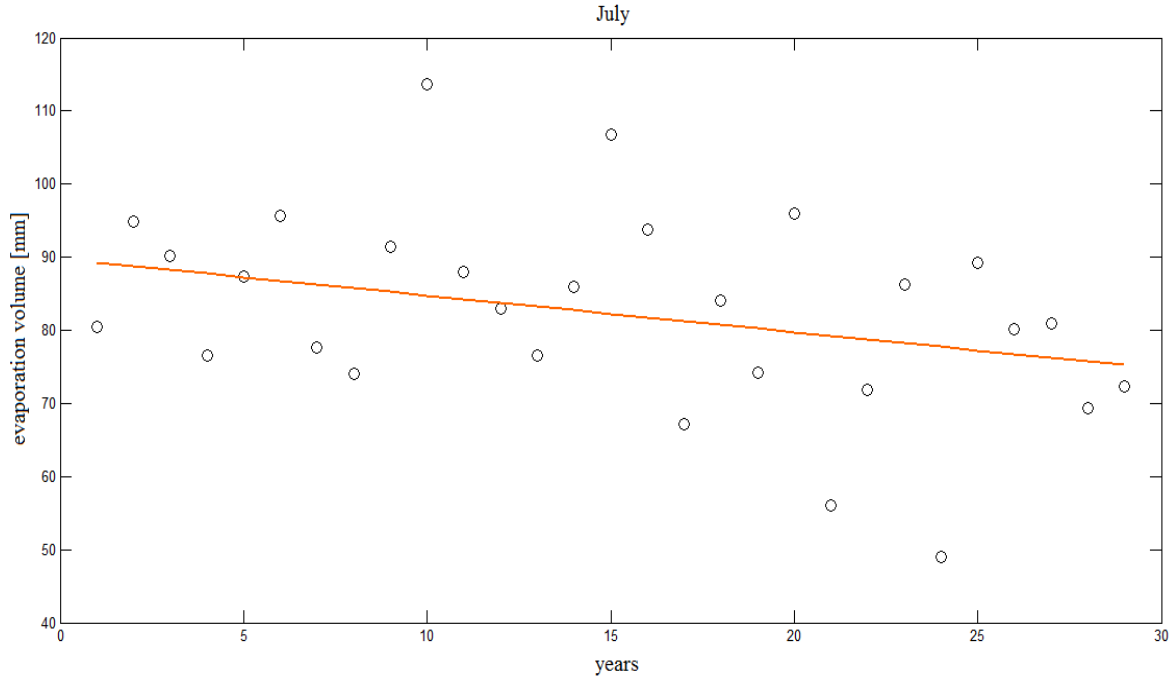

Figure 5.2: Monthly volume of July at Mai Chau station, where there is a decreasing trend (p-value = 0.0489) with a Sen' slope of -0.50 mm/month. The line represents the Sen' slope.

Moreover, the Pettitt's test did not find any break point testing the annual and monthly evaporation volume of considered stations, except for November and July, where two stations show a distinctive change between 1987 and 1989. Finally, MASH confirmed the above results. For example, the maximum evaporation change at Hoa Binh station is about 0.2 mm (see figure 5.3).

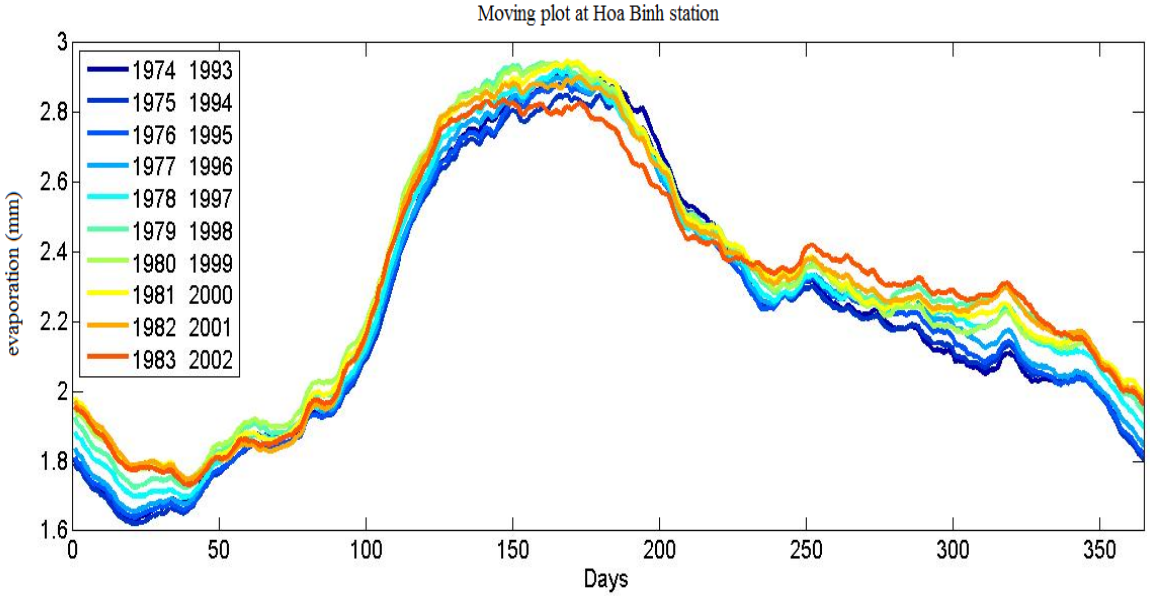

Figure 5.3: Evaporation volume moving plot at Hoa Binh station, with H=20 and f=20, in the period 1974-2002.

Similarly, very small changes can be noticed between October and February in figure 5.4. Both horizontally and vertically.

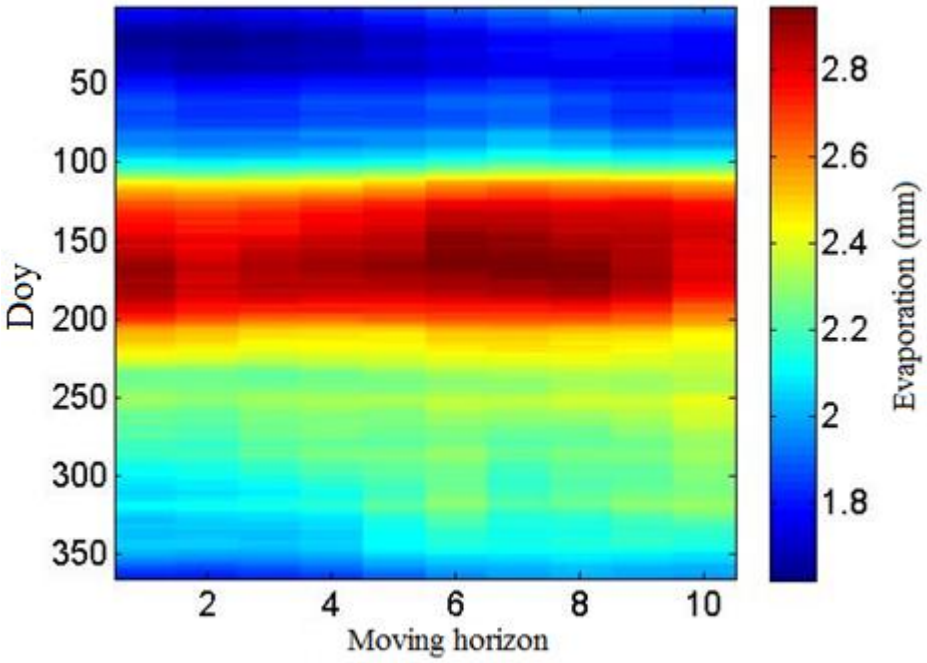

Figure 5.4: Moving plot effects on evaporation volume at Hoa Binh station between 1974-2002.

In conclusion, evaporation time series do not show any evidence of trend and because of the lack of accurate information on how evaporation data are measured, we discarded them.

5.3 Temperature results

As done for evaporation, we use the Mann-Kendall's test to detect both annual and monthly trend with a significance level of 5%, but with temperature series we operate on monthly/annual mean and not on the sum, because it cannot treated like a volume. The test results evidence an increasing annual trend in more than half of the considered stations (see figure 5.5 and table 5.3), which meanly present a Sen' slope of 0.0301 °C/year. The Pettitt's test detects a break point in annual mean temperature between 1985-86 for many stations.

Temperature stations	January	February	March	April	May	June	July	August	September	October	November	December	year
Co Noi													
Hoa Binh													
Lai Chau													
Mai Chau													
Moc Chau													
Muong Te													
Quynh Nhai													
Son La													
Tam Duong													
Than Uyen													
Yen Chau													

Table 5.3: Scheme of Mann-Kendall's test outputs for temperature stations. Annual and monthly averages are tested; each column corresponds to monthly results, except the last one which is relative to annual average. Increasing trend, decreasing trend and no trend are represented respectively with green, orange and grey cells.

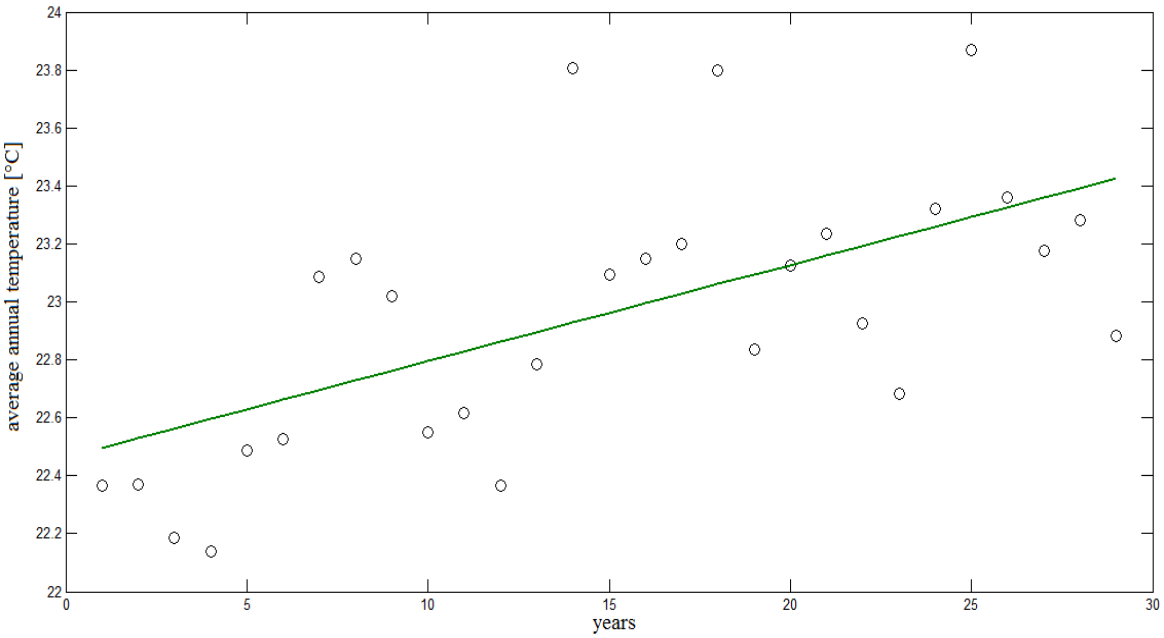

Figure 5.5: Average annual temperature at Yen Chau station in the period 1974-2002. The line represents the Sen' slope.

Looking at monthly Mann-Kendall's test outputs, we can also recognize an increasing trend in January, April and December, with a Sen' slope of 0.0750, 0.0573, and 0.0644 °C/month, respectively. In addition, few stations show a rising tendency in the wet season period, but this phenomenon looks like a local one.

Using MASH, it is possible to look at an increase of average temperature, in particular in January and December, also at stations which do not reject H0 in the Mann-Kendall's test. We consider Yen Chau station as example: even if it does not present a rising trend in December (see table 5.3), it has increased its average temperature also in the last part of the year during the period 1974-2002. In fact, in figure 5.6, we can observe a rising progression from blue to red lines between day 1 and day 30, from day 80 to day 120, and from day 320 to the end of the year.

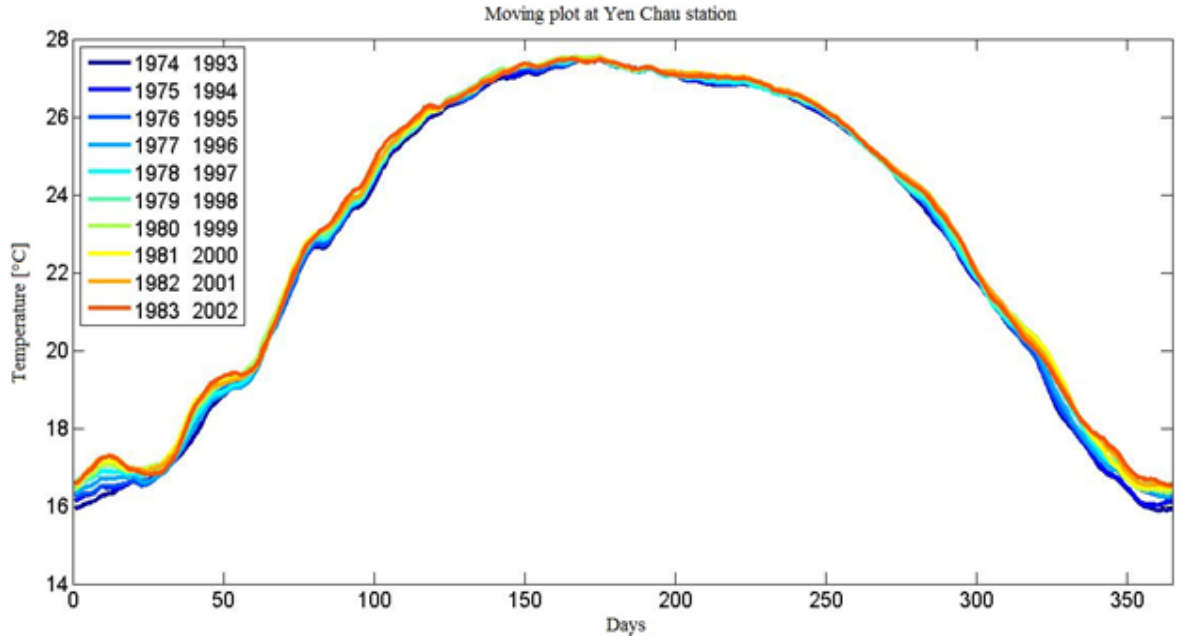

Figure 5.6: Average temperature moving plot at Yen Chau station, with H=20 and f=10, in the period 1974-2002.

This evidence is also confirmed by figure 5.7 where a horizontal evolution from dark to lighter blue in the top and in the bottom of the heat map can be noticed, and a darker red development in the middle of the year.

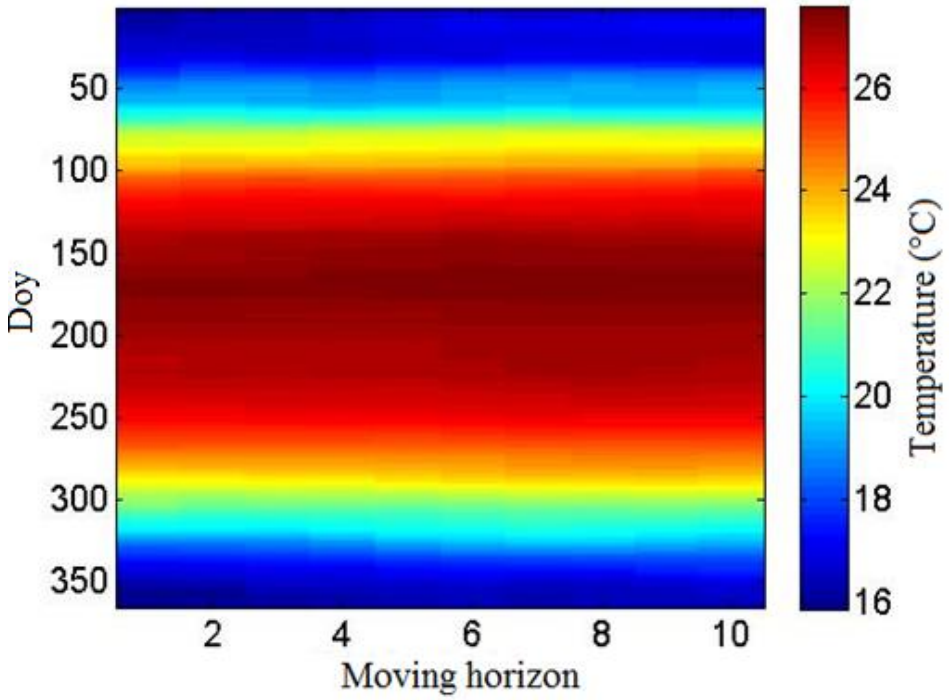

Figure 5.7: Moving plot effects on average temperature at Yen Chau station between 1974-2002.

5.4 Precipitation results

Using the Mann-Kendall's test (α=0.05) on annual and monthly precipitation volume series on period 1974-2002, we find out a widespread behaviour, which is schematized in table 5.4.

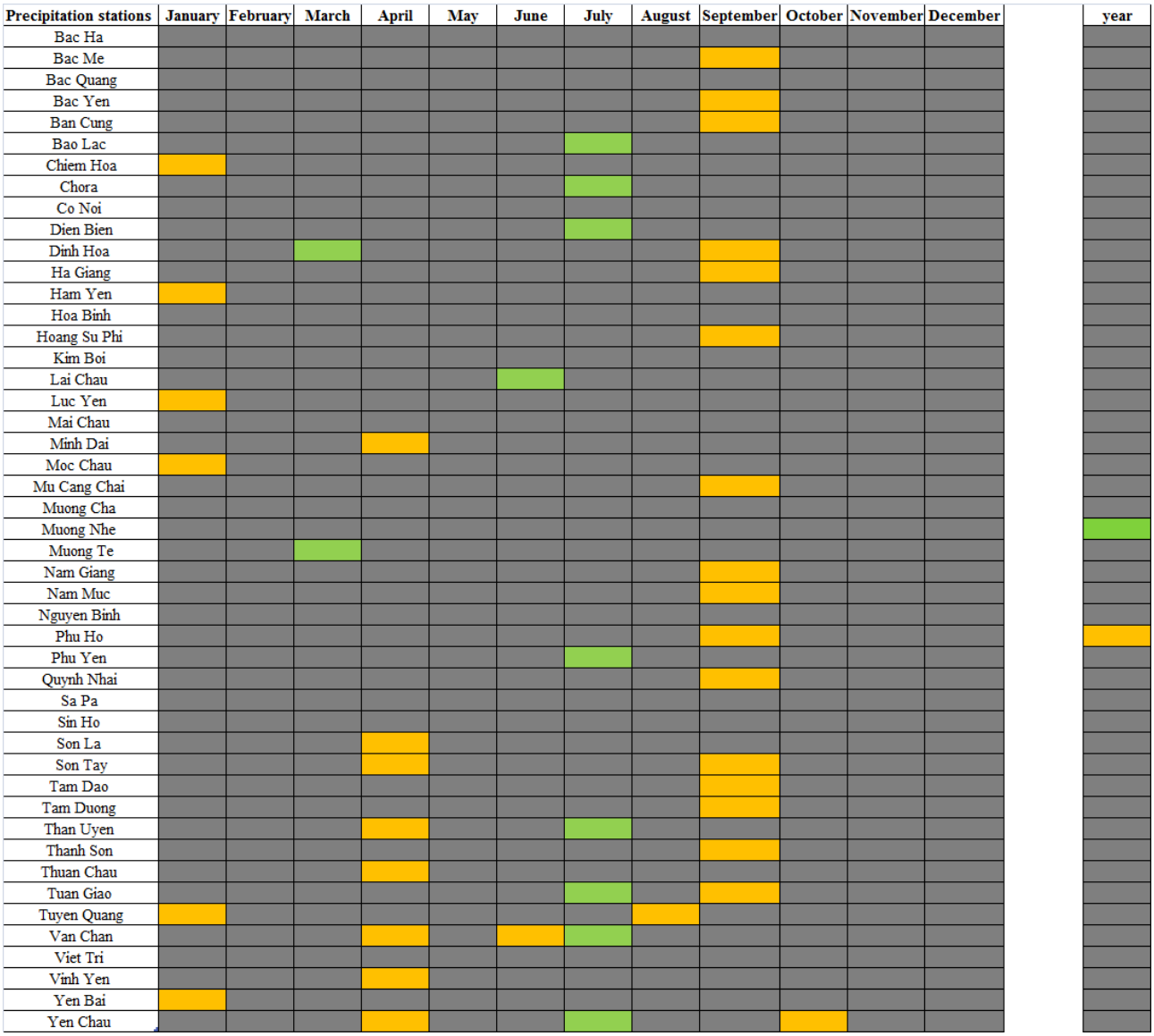

Table 5.4: Scheme of Mann-Kendall's test outputs for precipitation stations. Annual and monthly volumes are tested; each column corresponds to monthly results, except the last one which is relative to annual volume. Increasing trend, decreasing trend and no trend are represented respectively with green, orange and grey cells.

Annually, apart from two stations, the others do not present any trend.

Monthly, we observe an increasing trend on rainfall volume in July and a decreasing trend in January and April, but in particular in September. To understand the magnitude of these changes, we look at Sen' slope. Medially, it is weaker in January and April, respectively -0.8145 and -2.8330 mm/month, whereas it is stronger in July and September, respectively +5.4538 and -4.7062 mm/month. Among all, the ninth of the twelve months presents the highest number of stations

where H0 of Mann-Kendall's test is rejected; figure 5.8 shows the evolution of the precipitation volume in September at Son Tay station.

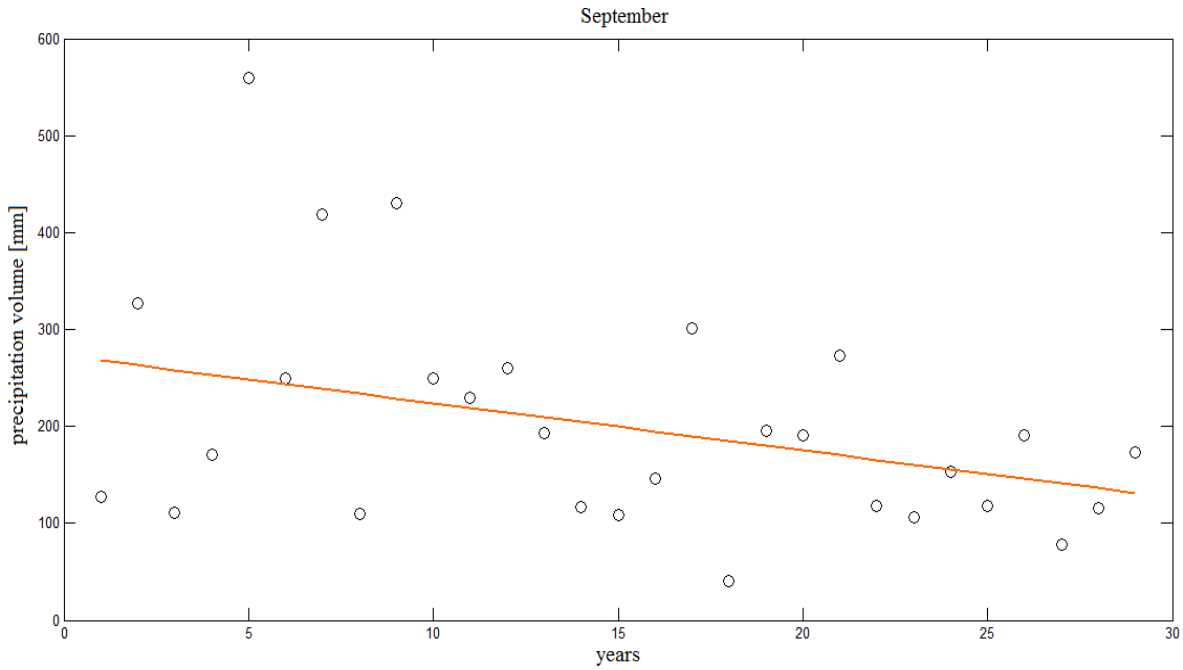

Figure 5.8: September precipitation volume in the period between 1974-2002 at Son Tay station. The line represents the Sen' slope.

The Pettitt's test underlines the presence of break point in the mean of monthly precipitation volume during April (see figure 5.9), June, July and September in the second half of 1980s for a number of stations.

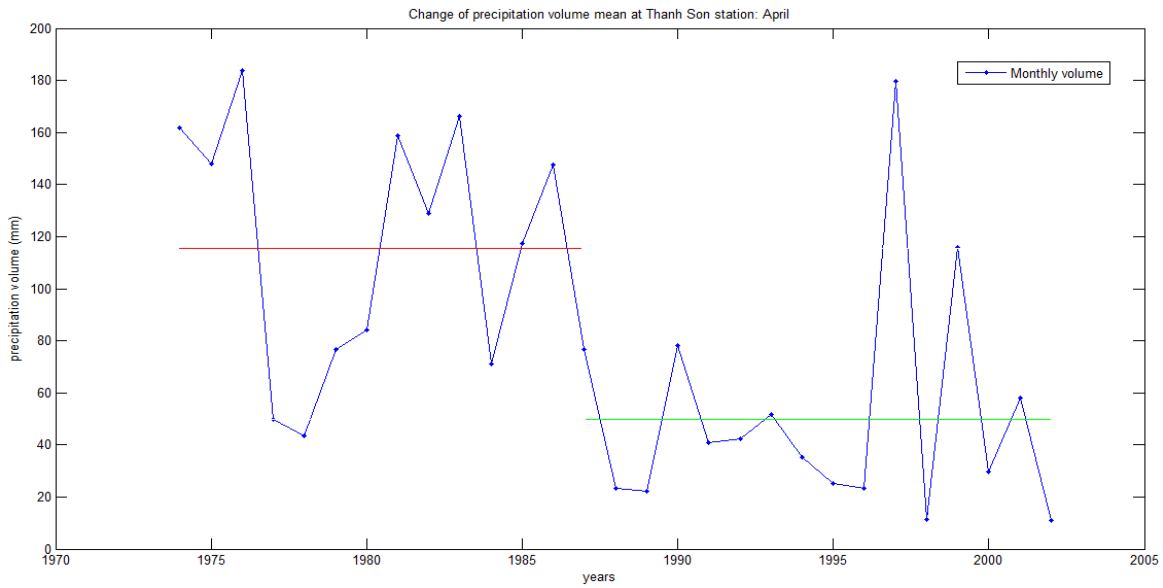

Figure 5.9: Break point in 1987 in the monthly mean rainfall volume of April using Pettitt's test with α=0.05 at Thanh Son station during the period 1974-2002.

Employing MASH, we can overall observe the volume changes during the year in the period of 1974-2002 and a visual point of view can help to interpret the rainfall evolution in this period in the basin. In fact, on the one hand, looking at figures 5.10 and 5.11, we can note the decreasing rainfall volume between August and October at Thanh Son station, but also in the first part of the year until May, except March. On the other hand, an increasing precipitation volume can be observed between June and July.

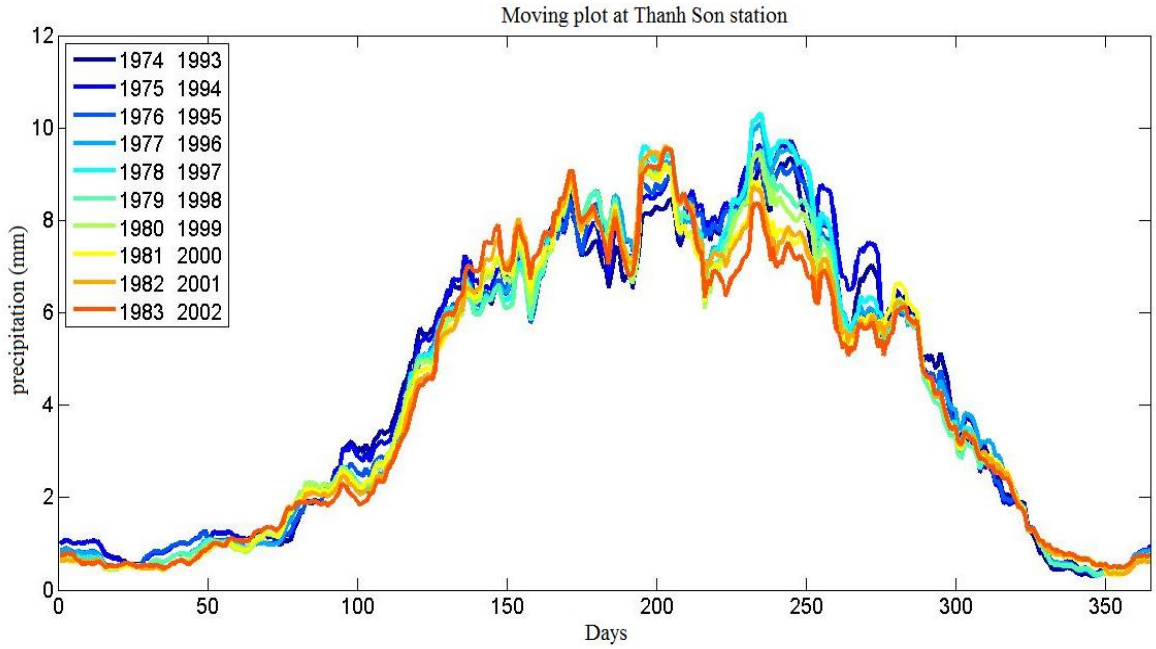

Figure 5.10: Precipitation moving plot at Thanh Son station, with H=20 and f=10, in the period 1974-2002.

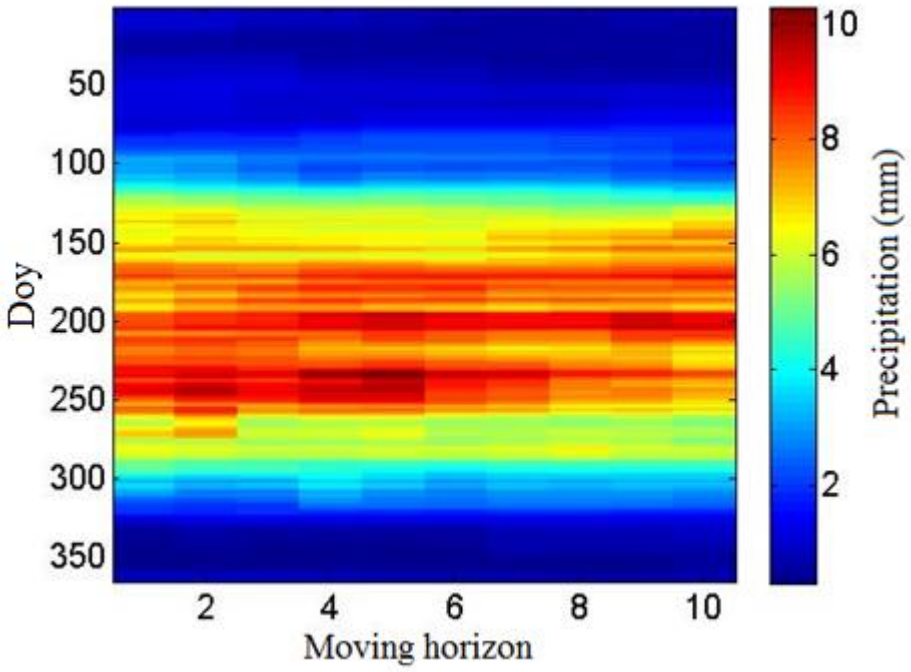

Figure 5.11: Moving plot effects on precipitation volume at Thanh Son station between 1974-2002.

Moreover, it is important to investigate if the stations which show trends are closed to each other, in a particular region of the basin, to understand if the driver/s of hydrological regime changes is/are local and geographically limited. For this reason, we conduct a spatial analysis. We divide the Red River basin through Thiessen's polygons, assuming to extend the punctual data (precipitation stations information) to a spatial one. In this way, every station is surrounded by a polygon which represents its area of influence; hence, any location inside the polygon is closer to the included precipitation station than any others. In the next four figures (5.12-5.15), we can see the position of the areas which have trend in the main months where we check a rainfall volume change: January, April, July and September. In these plots, we report not only the direction of the trend, but also the corresponding Sen' slope and p-value. If time series of the station has no trend for the Mann-Kendall's test (p-value>α), its polygon is white and contains the symbol "x". On the contrary, if it has trend, its polygon is coloured: green represents an increasing trend, whereas orange a decreasing one, such as in the previous tables. Another information derives from the intensity of the colour which depends on the magnitude of trend (darker colour, higher absolute Sen' slope value). Moreover, each coloured polygon includes a filled circle: the bigger is the symbol diameter, the lower is p-value (and the probability of type I error).

During these four months, looking at moving plot figures in almost all precipitation stations, we recognize the same volume behaviour explained above, but now we concentrate only on the stations where H0 of Mann-Kendall's test has been rejected.

The stations which present trend in January, have no trend in any of the other three months. These stations are concentrated in the middle of the basin. In April, the area characterized by decreasing trend is located in the Southern part of the Red River catchment, instead. In July the green polygons, which represent the increasing trend areas, are more scattered than other months. As we said, in September a number of stations have trends, but the ones which have lower p-value are in the North and in the East of the Vietnamese part of the basin. It is noteworthy that only one station has a trend both in July and in September.

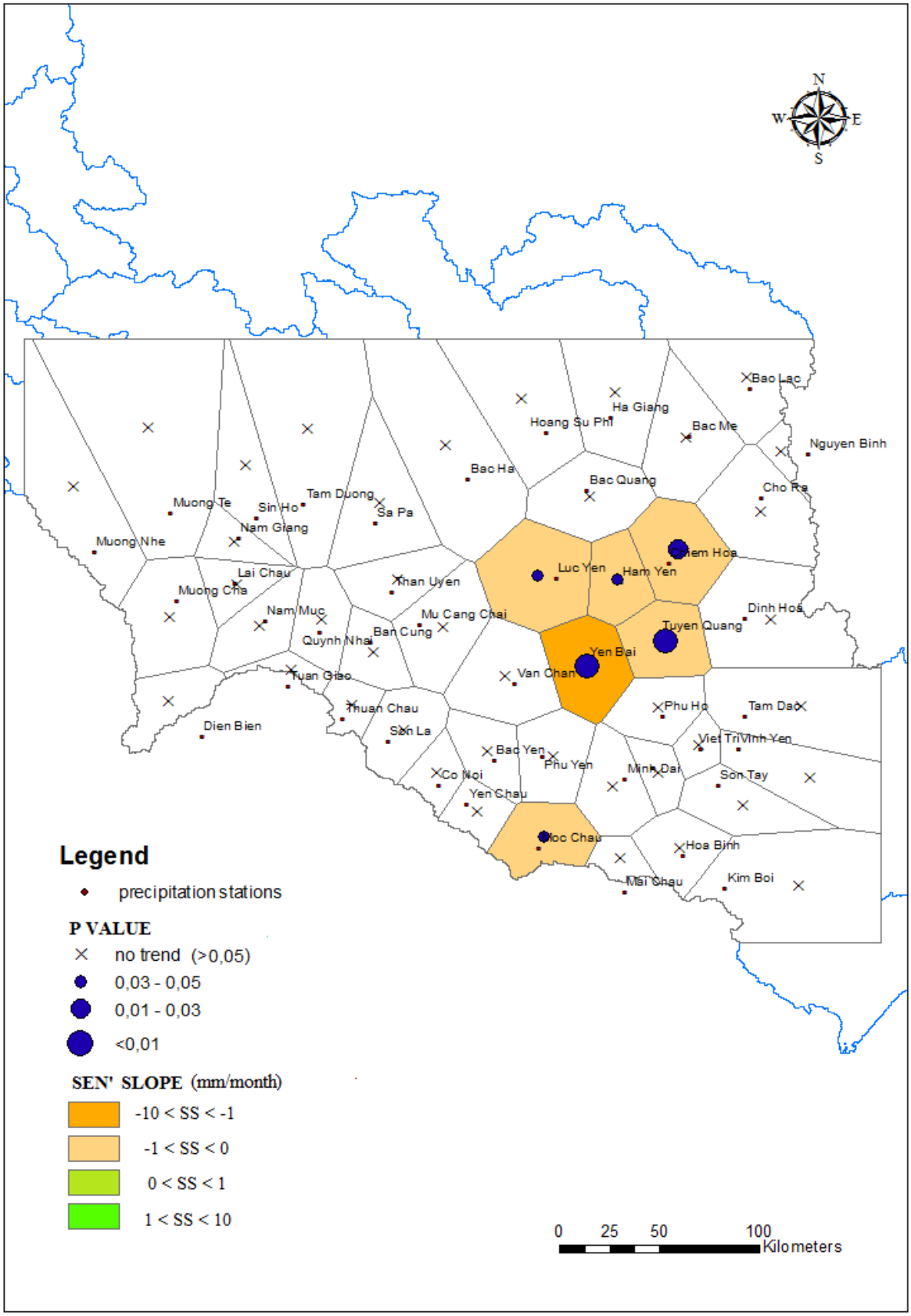

Figure 5.12:Spatial analyis of precipitation station with trend in January. Map of p-value and Sen' slope considering the period 1974-2002.

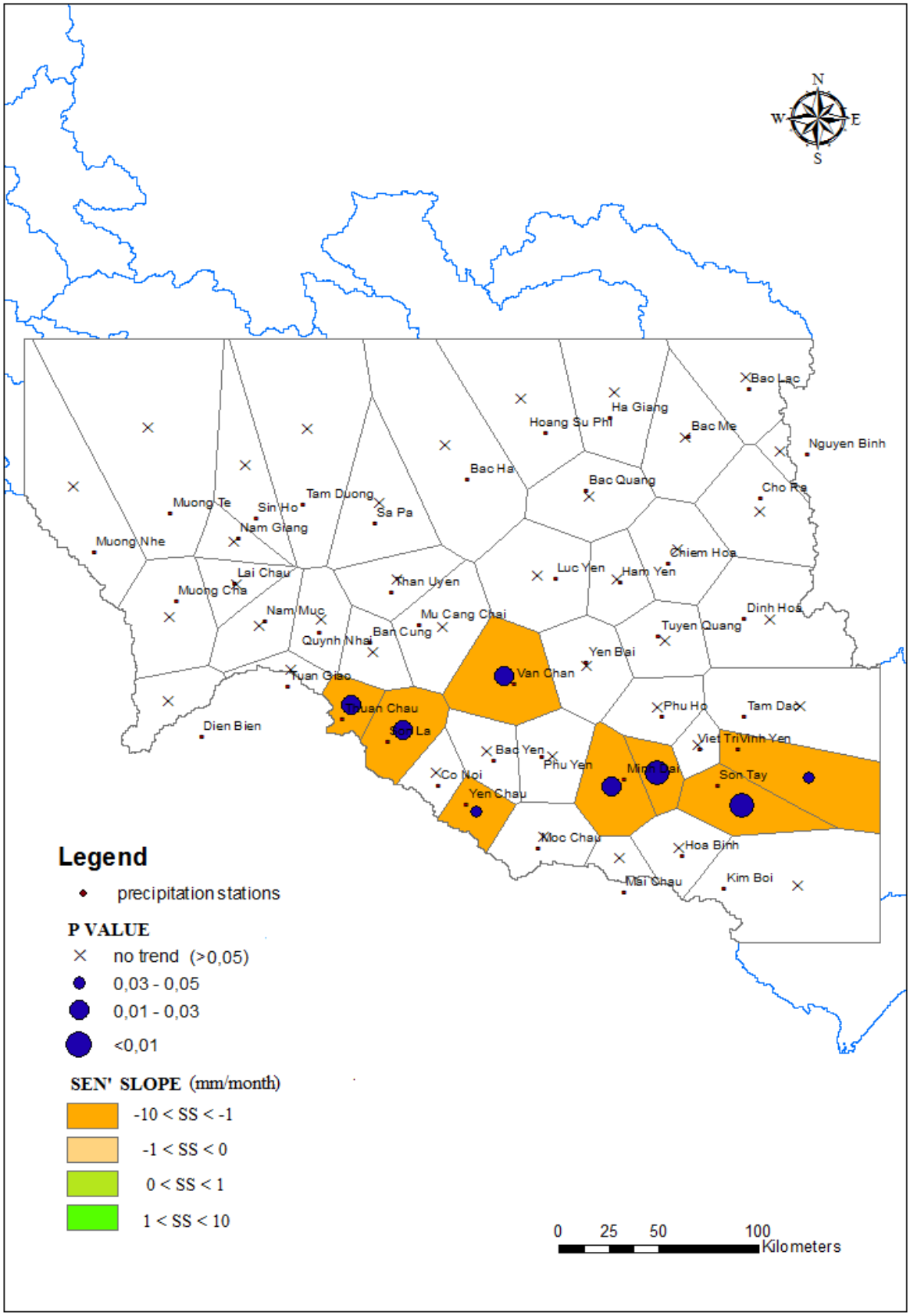

Figure 5.13: Spatial analyis of precipitation station with trend in April. Map of p-value and Sen' slope considering the period 1974-2002.

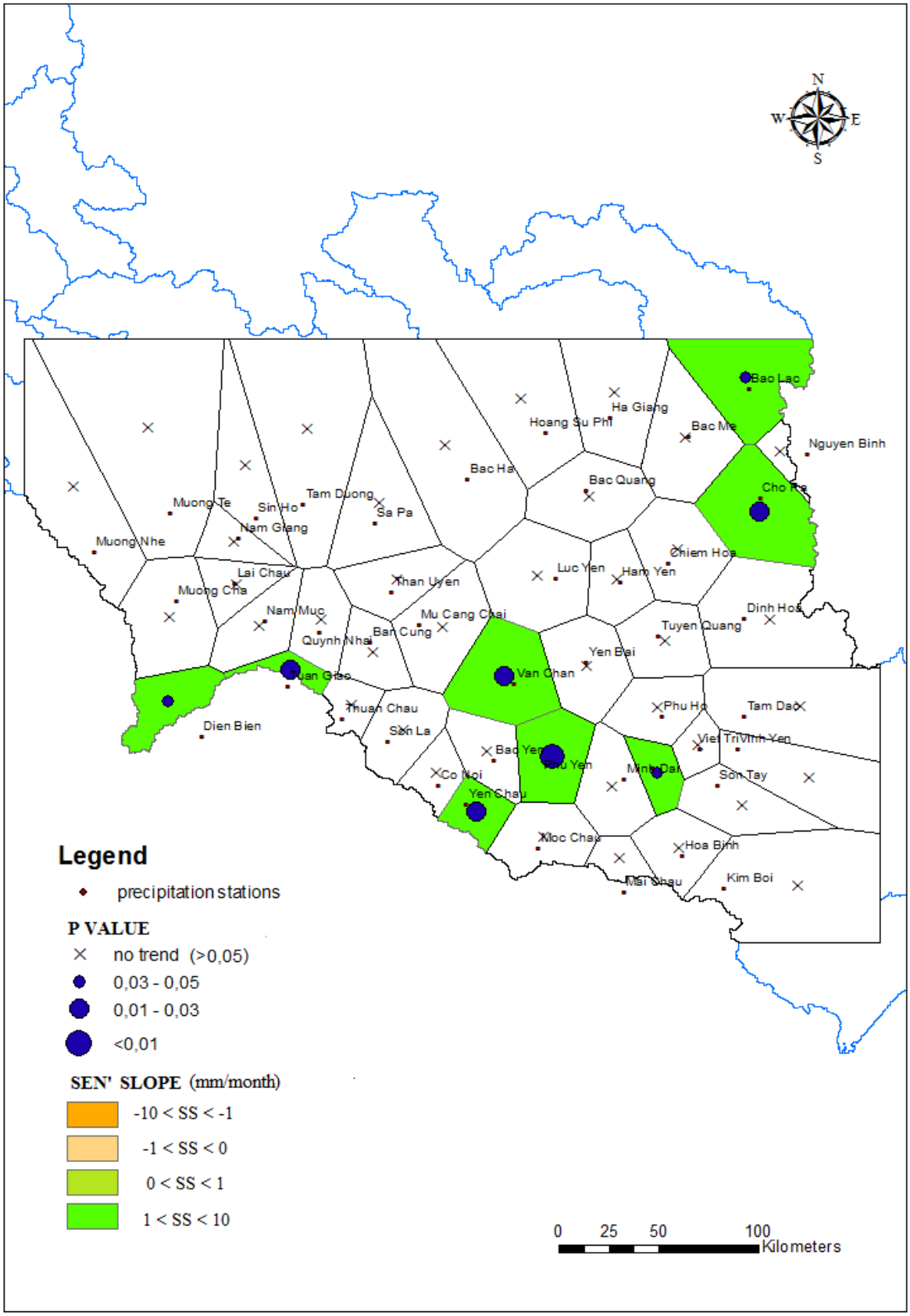

Figure 5.14: Spatial analyis of precipitation station with trend in July. Map of p-value and Sen' slope considering the period 1974-2002.

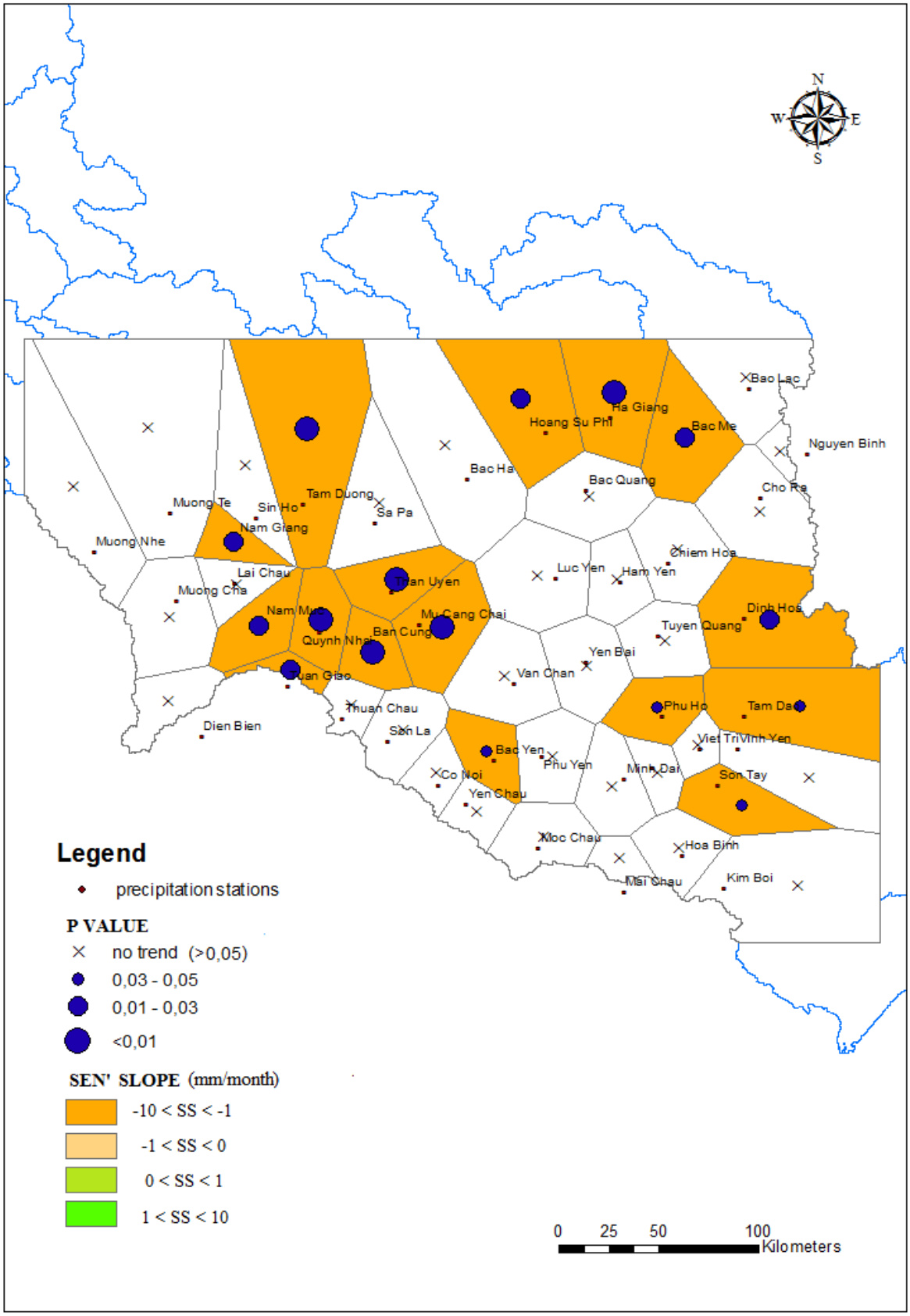

Figure 5.15: Spatial analyis of precipitation station with trend in September. Map of p-value and Sen' slope considering the period 1974-2002.

5.5 Streamflow results

Figure 5.16 illustrates the position in the basin of each run-off stations used in this work and its influence area. Starting from the DEM of the Red River basin, we implement flow direction and accumulation algorithms to find each station sub-basin, with the software Arcgis. Stations are the outlets of the corresponding sub-basins.

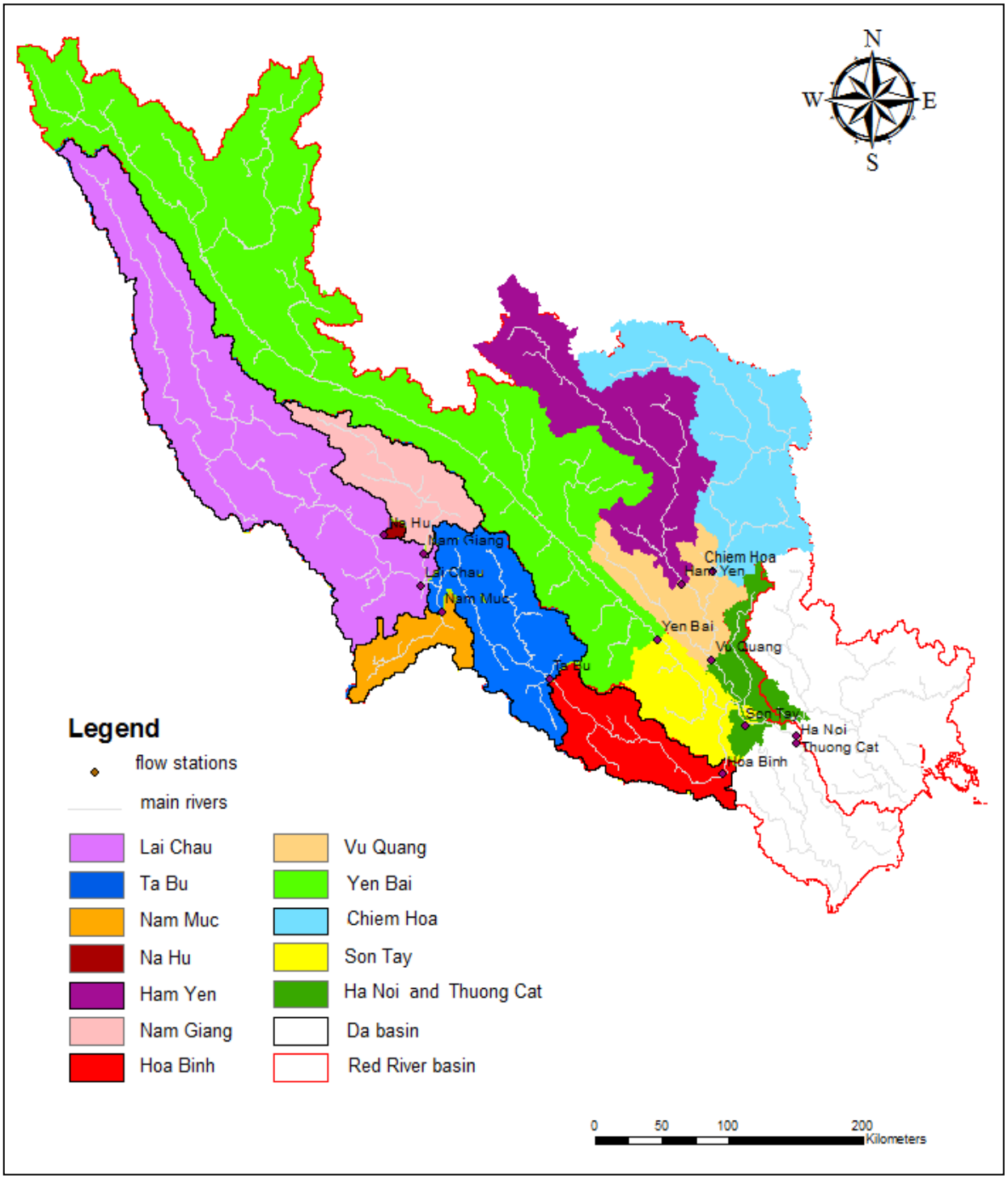

Figure 5.16: Area of influence of each considered streamflow station in the Red River basin.

In figure 5.16, any overlapping area can be seen. Hoa Binh is the outlet of the Da basin, so its influence area includes Ta Bu one, which is not only composed of the blue area, but also of Lai Chau, Na Hu, Nam Muc and Nam Giang ones. Moreover, Yen Bai area is contained in Son Tay one, and Vu Quang includes also Chiem Hoa and Ham Yen areas. Finally, the Red River basin outlet is Ha Noi, so its drained area is the whole basin (except the delta).

The results of the Mann-Kendall's test (α=0.05) on the period 1974-2002 are outlined in table 5.5. A number of stations present annual rising trend (green cells in the last column), with an average Sen' slope value of 3,550 (m^3/s)/year. Monthly, a decreasing trend leaps out in many stations during September and also an increasing one in the first half of the year, in particular between March and July. The most widespread tendency is just in July.

Streamflow stations	January	February	March	April	May	June	July	August	September	October	November	December	year
Chiem Hoa													
Ham Yen													
Ha Noi													
Hoa Binh													
Lai Chau													
Na Hu													
Nam Giang													
Nam Muc													
Son Tay													
Ta Bu													
Thuong Cat													
Vu Quang													
Yen Bai													

Table 5.5: Scheme of Mann-Kendall's test outputs for streamflow stations. Annual and monthly volumes are tested; each column corresponds to monthly results, except the last one which is relative to annual volume. Increasing trend, decreasing trend and no trend are represented respectively with green, orange and grey cells.

The mean Sen' slope in September is -1,936.54 (m^3/s)/month, whereas from January to July it is respectively of 187.80, 238.93, 297.58, 349.12, 392.39, 603.52 and 1,506.43 (m^3/s)/month. Moreover, analysing the entire time period, many stations present a break point in January, February, March, July and September using Pettitt's test with a significance level of 0.05 between 1980 and 1993, but, in particular, in the second part of '80s.

Confirmed by statistical test, we can observe a lot of changes in the discharge distribution of many stations using moving plot (see figures 5.17 and 5.18). In fact, from day 1 to about day 230 of the year, a rising movement of the curve occurs, (look at transition from blue to red line in figure 5.17, from dark to light blue in the top and from light to dark red in the middle of 5.18 one).

This change is composed by:

- a higher baseflow from January to April,
- a steeper of curve ascending branch,
- an increase of the peak in July and August.

In the second part of the year, from about day 230 to day 280, a streamflow volume decrease occurs, instead.

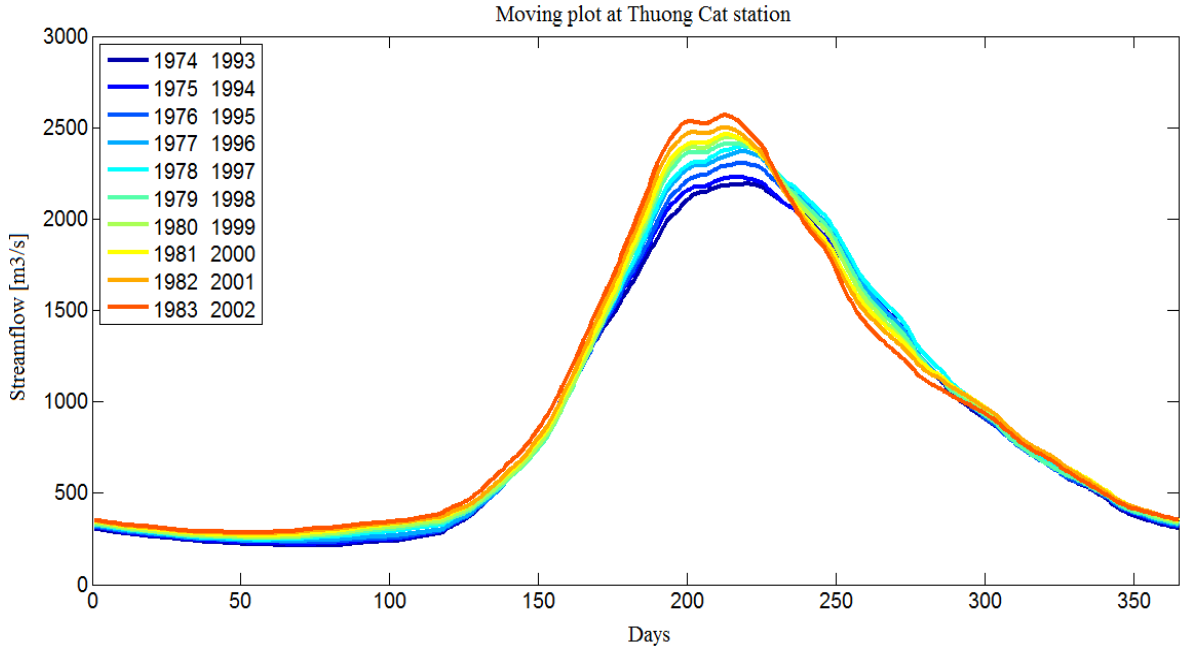

Figure 5.17: Streamflow moving plot at Thuong Cat station, with H=20 and f=20, in the period 1974-2002.

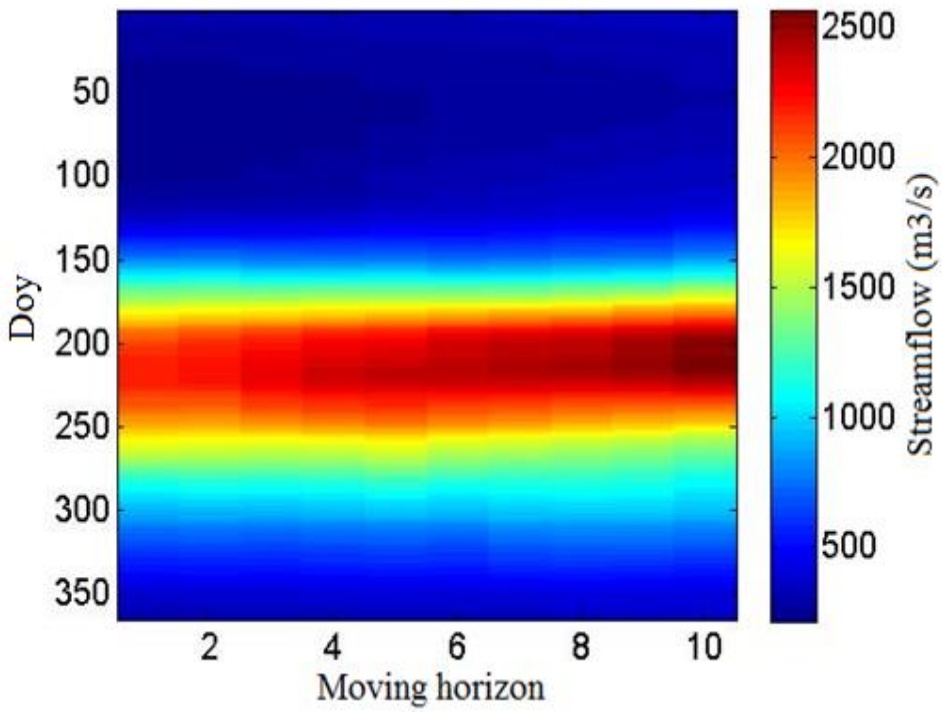

Figure 5.18: Moving plot effects on streamflow volume at Thuong Cat station between 1974-2002.

As done for the precipitation data, we conduct a spatial analysis to understand if streamflow volume changes involve all the basins or for example only some tributaries. In this case, we do not need to use Thiessen's polygons, but drained area of each station. In figure 5.19, we report the moving plot

of the main available stations to describe the streamflow changes of the entire basin. Moreover, in figure 5.20, we can observe the results of the Mann-Kendall's test of these stations (with p-value and Sen' slope values); if the bars are green, p-value is lower than significance level, so those months have trend. Sen' slope positive values represent an increasing tendency, while negative ones a decreasing tendency.

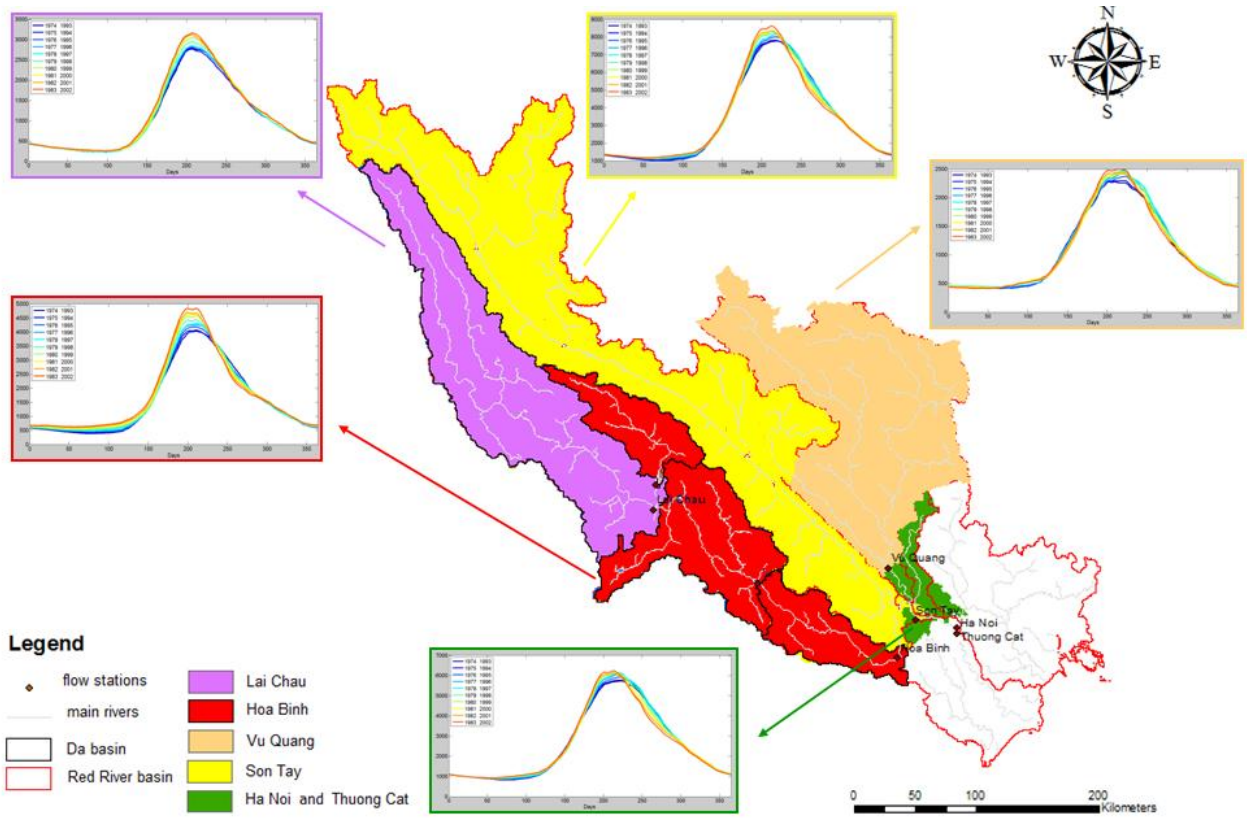

Figure 5.19: Moving plot in all the Red River basin on the period 1974-2002 (H=20 and f=10).

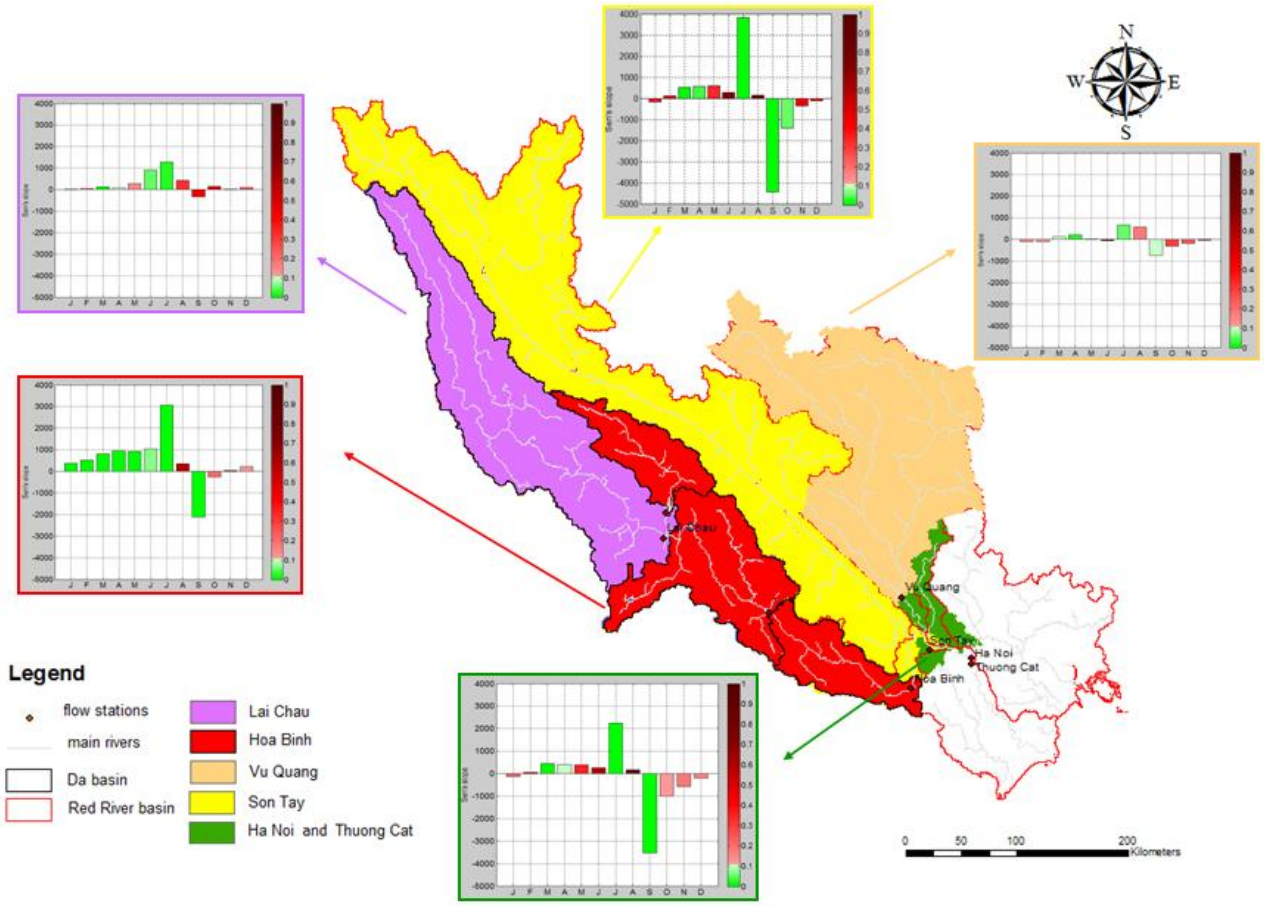

Figure 5.20: Results of Mann-Kendall's test and Sen' slope in all the Red River basin on the period 1974-2002.

As we said, the longest common period among streamflow stations is 1968-2011. Using this time horizon, the results are quite different compared to the ones of 1974-2002. In particular, the Mann-Kendall's test shows an increasing trend in the first part of the year like the presented analysis, but not in July (no station has trend during this month), and a decreasing trend in many stations in the second part of the year starting from August. So, September decreasing trend still occurs in the period 1968-2011 and more stations present it, if compared to 1974-2002.

5.6 Conclusions

With the results so far presented, we provide an overview of the hydrological regime changes in the Red River basin over the period between 1974 and 2002. Now we can compare the changes in patterns of each significant variable to the others.

Precipitation presents an increasing trend during July and a decreasing one during September in most stations. These changes probably have effects on streamflow because we observe the same evolution in almost the entire basin in the considered period. The situation is different for what concerns the months of the first part of the year. In fact, run-off always increases (see paragraph

5.4.2), while rainfall decreases during January and April (see paragraph 5.3.2), and has no trend in other months.

Concerning temperature data, they have different effects on evaporation which depend on the two typical monsoonal seasons. During dry season, higher temperature involves an increase in evaporation and consequently in precipitation and decrease in streamflow. During wet season, atmosphere is already rich of water vapour so it is closer to the saturation threshold, but atmosphere can hold a higher water vapour quantity with temperature increase. However, in the basin, we note a rising trend of annual mean temperature in many considered stations in the basin of the Da river and also mainly during January, April and December. In particular, these three months belong to the dry season, so we cannot expect a precipitation decreasing trend and a discharge increasing one. Moreover, the widespread increase of the annual mean temperature suggests that it is a regional effect, maybe caused by global warming, and not a local one, like on precipitation and streamflow.

From these considerations, it seems that something else which influences the hydrological regime has changed, but we have not considered it yet. One of the likely drivers can be land cover change. In fact, from literature, we find out that one of the deforestation effects is the base-flow increase, as well as a general rise of streamflow. Pettitt's test has detected break points in the time series between 80s and 90s, such as the strong deforestation period occurred in Vietnam. Moreover, with the spatial analysis done especially for precipitation, we see that stations which present trend in a specific month are sometimes in an area nearby. Hence, the next step is to analyse the possible contribute of land cover change on the hydrological regime of the basin.

Chapter 6

Hydrological modelling

6.1 Introduction

The second step of this thesis consists in better understand the role and the impacts of land cover change on the hydrological regime in monsoon dominated basins, studying the Red River one. Here, modelling helps us, dealing as an instrument which is able to tie land cover change to hydrological regime. We calibrate and validate the model to reproduce studied hydrological processes of the basin in the period from 1974 to 2002 and to make sensitivity analysis in comparison to the parameters corresponding to soil properties and land cover.

We use Topkapi-ETH, a spatially distributed and physically based model. We have not many available data and this model does not require a lot of input variables. Another one of its advantages is the possibility to work with large scale. Nevertheless, it cannot operate on the whole Red River basin with a reasonable resolution (we mean about 250 metres).

For our analysis, we focused on the little sub-basin of Nam Muc (with an area of about 2,880 km^2, see figure 6.1), in the Da basin, which hold most of characteristics we are looking for. It shows hydrological regime changes in the period between 1974-2002, particularly a discharge increasing trend and a precipitation decreasing one. Its streamflow is not influenced by the Chinese reservoirs. It is characterised by land cover change (figures 6.9 and 6.10).

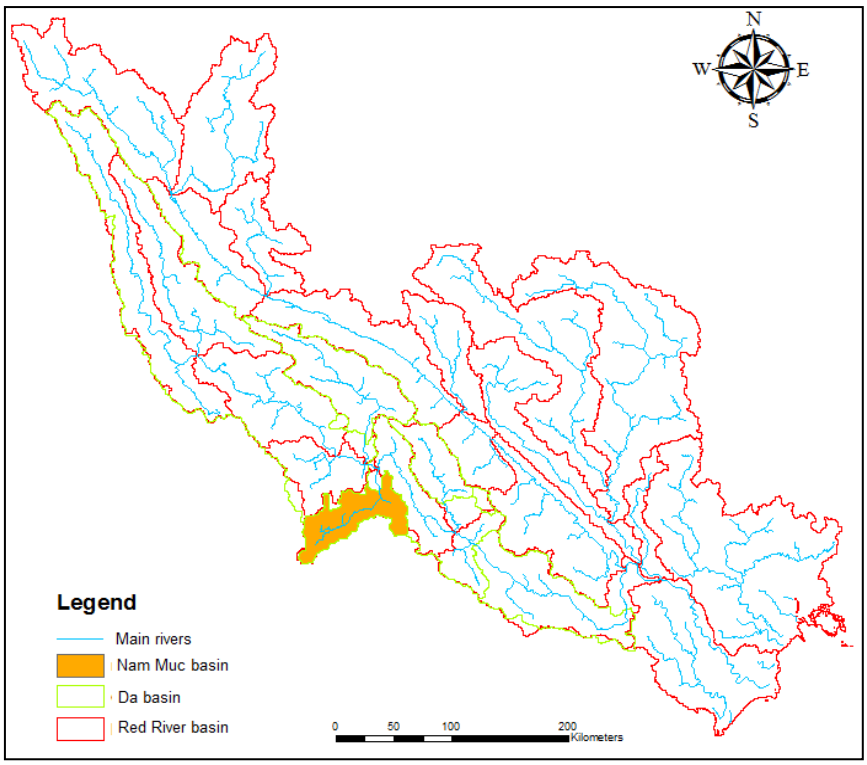

Figure 6.1: Position of Nam Muc sub-basin in the Red River area.

In the considered time horizon, Nam Muc basin outlet records an increasing streamflow volume all over the year (see figure 6.2) and using Pettitt's test with α=0.05, we detect a break point in each monthly volume between 1985 and 1993, except in May, August, September and October. We study this basin to understand if these changes are due to land cover change.

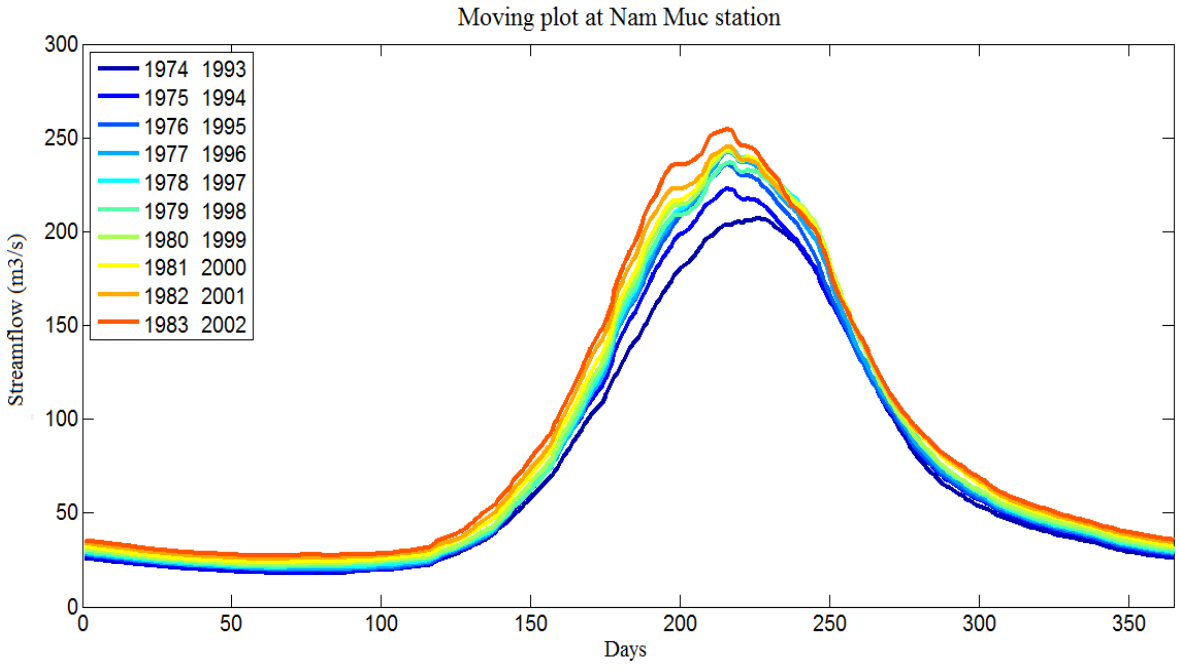

Figure 6.2: Streamflow moving plot at Nam Muc station in the period 1974-2002 with H=20 and f=20.

It is confirmed also by the comparison between the average flow duration curves for the first and the last decade of the considered period 1974-2002. In fact, figure 6.3 shows an average run-off increase both in peaks and in base-flow in the period 1993-2002 compared to 1974-1983.

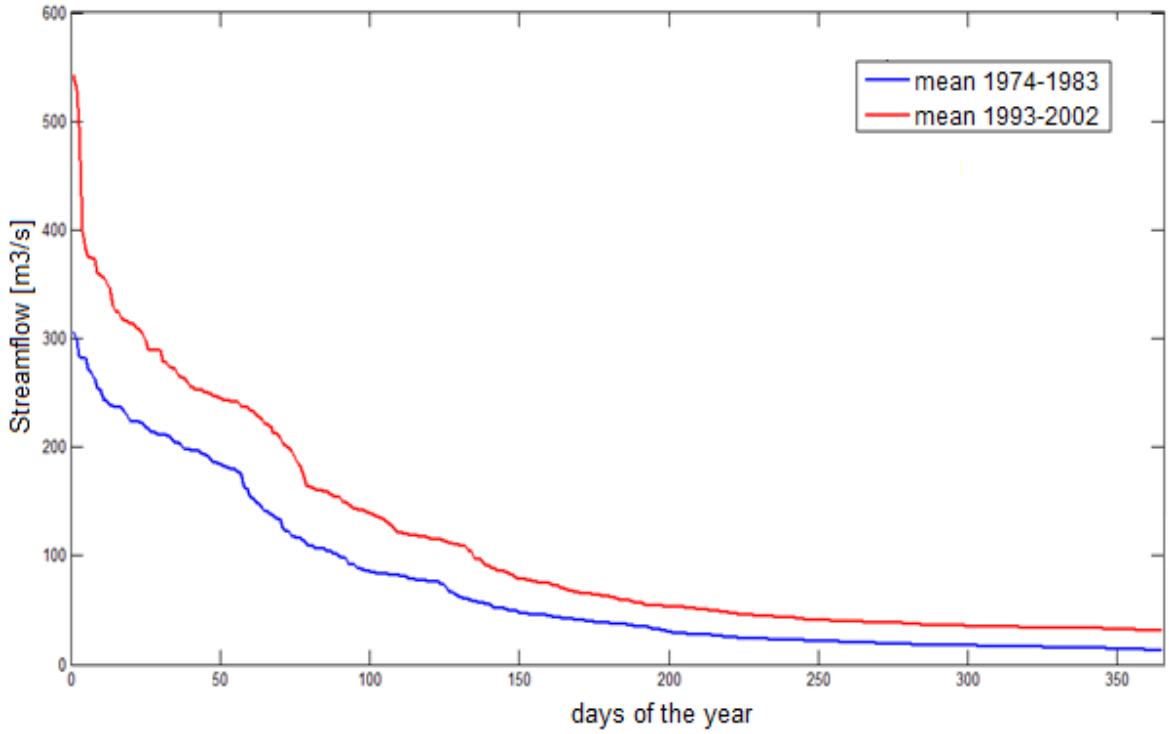

Figure 6.3: Average flow duration curves of the first and last decade of period 1974-2002 at Nam Muc station.

6.2 Topkapi-ETH model inputs

First, it is necessary to build a grid of the area to consider, which includes a bigger area than the chosen sub-basin to avoid boundary problems. So not all cells of the grid belong to drained area of Nam Muc and the model computes only the ones that it recognizes inside this area. We define a square grid cell size of 240 meters. Each upload map must have the same resolution and dimensions.

The input includes time series of temperature, precipitation and cloud transmissivity for the time horizon we want to simulate, that is 1974-2002. We have no available data about the last variable, so we use daily uniform value for the whole area and considered period. For the other two variables, we use daily observations of selected stations. Beside the time series, the model needs spatial information about station position and in addition it must know at which station each cell must be assigned. So we divide up the grid with Thiessen's polygons to define influence area of the

involved stations. The proximity of a station to the analysed area is not the only factor to take into consideration: it is important to check the station characteristics, such as elevation, to understand if they can reproduce basin ones.

For Nam Muc sub-basin, we choose four precipitation and two temperature stations, and analyzed the corresponding time series. Figure 6.4 shows an increasing precipitation volume in July at Dien Bien (top corner on the right) and Tuan Giao (down corner on the right) stations. A decreasing precipitation volume in January, February and August occurs in all four stations and also in September except at Dien Bien. Concerning temperature, Quynh Nhai and Lai Chau have an elevation, respectively, of 802 and 244 metres, but the daily mean temperature is not affected by this difference in level. In both temperature moving plots we can observe an average increase in January and December (figure 6.5). The final result of these operations for precipitation and temperature stations in Nam Muc basin is respectively illustrated in figures 6.6 and 6.7.

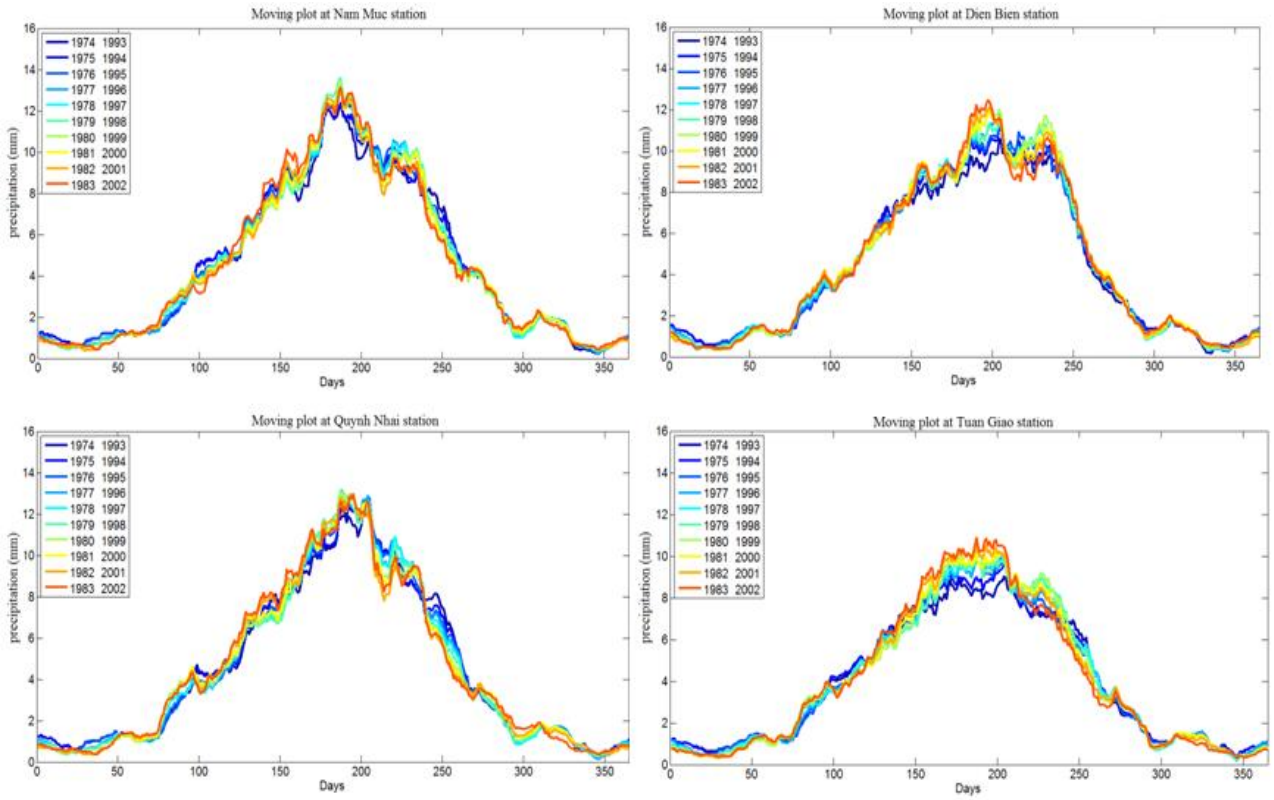

Figure 6.4: Precipitation volume moving plot in the period 1974-2002 for the stations of Nam Muc, Dien Bien, Quynh Nhai and Tuan Giao in the Nam Muc sub-basin (with H=20 and f=10).

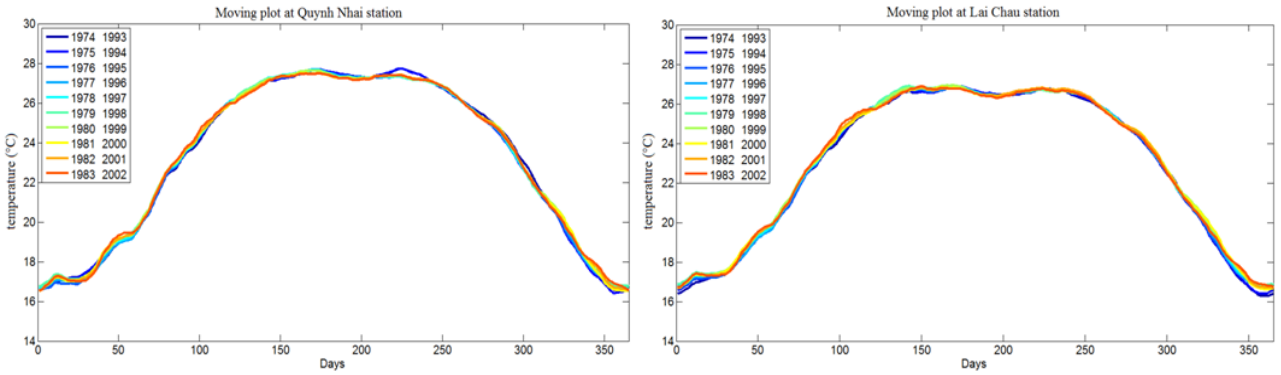

Figure 6.5: Average temperature moving plot in the period 1974-2002 for the stations of Nam Muc, Dien Bien, Quynh Nhai and Tuan Giao in the Nam Muc sub-basin (with H=20 and f=10).

The model also requires soil and land cover maps and we use the FAO ones. Figure 6.8 shows the soil map and, as we can observe, there are only two types of soil: chromic luvisol and mainly orthic acrisol. Luvisol soil is technically characterized by a strong accumulation of clay in the B-horizon and a high cation exchange capacity. Acrisol soil is associated with humid tropical climates and consists only of clays with low cation exchange capacity. The soil type classification does not change if a higher resolution grid is considered.

We have two land cover maps available; the first one is relative to 1981-1994 and the second one of 2000 (see figures 6.9 and 6.10 respectively). Considering that the model accepts only one classification for each grid cell category for the whole simulation time period; it means that we can use only one map, so we employ the first one, because it is more representative of the considered period being referred to central years.

We describe each grid cell of the catchment area with its spatial location and its characteristics. There are two main types of cell properties and both are necessary to the model. The first one is derived from the DEM of the area and consists, for example, of slope, aspect, surface normal vectors (x, y, z) using the gradient and maximum steepness methods, and flow direction through the order of cell processing. The second one depends, instead, only on the cell location and includes land cover and soil category number, precipitation and temperature station code; in this way, the model connects the classification id to its parameters.
The last input, that Topkapi-ETH needs, is the location of the considered basin outlet.

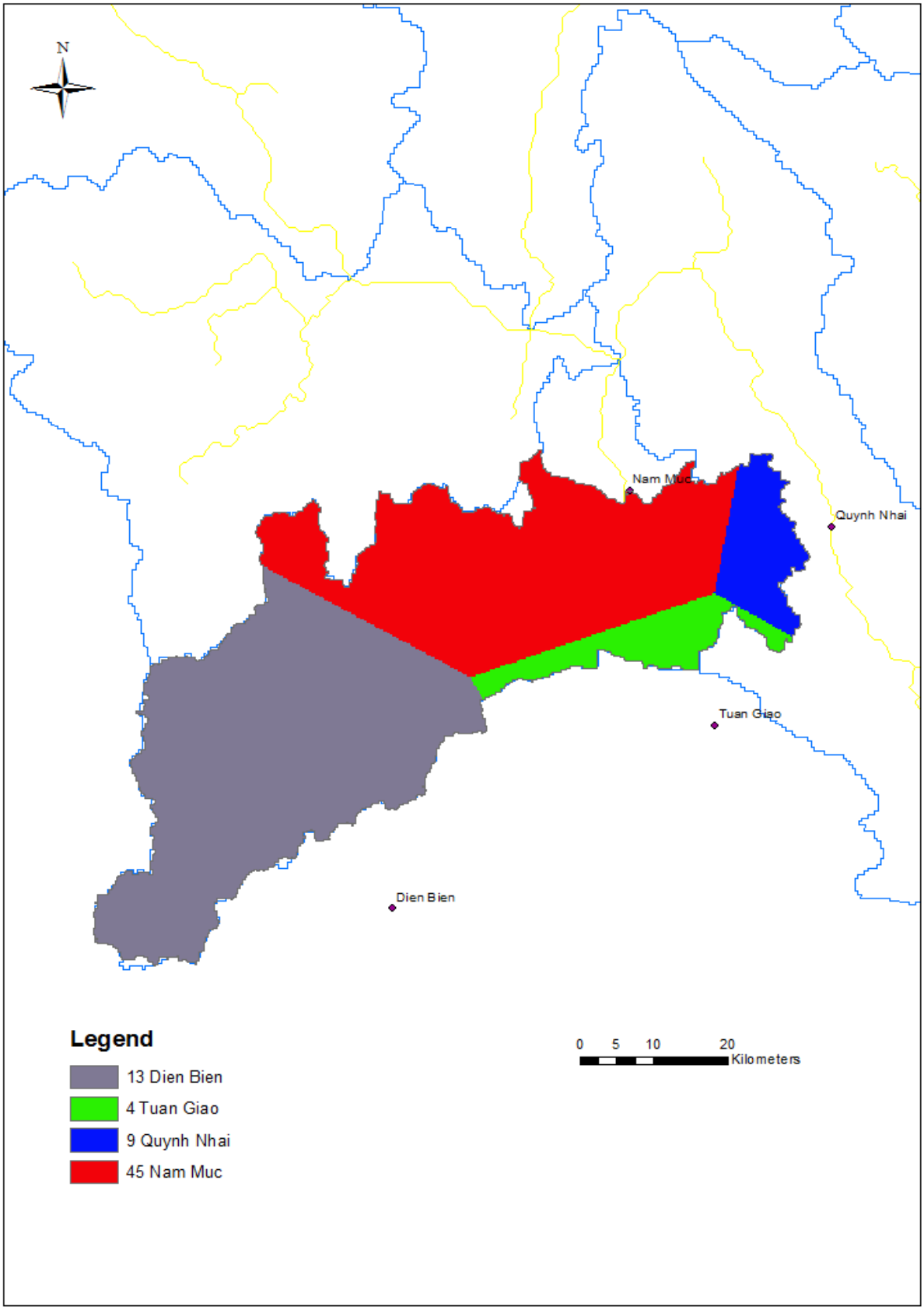

Figure 6.6: Thiessen's polygons of the precipitation stations considered in the Nam Muc basin.

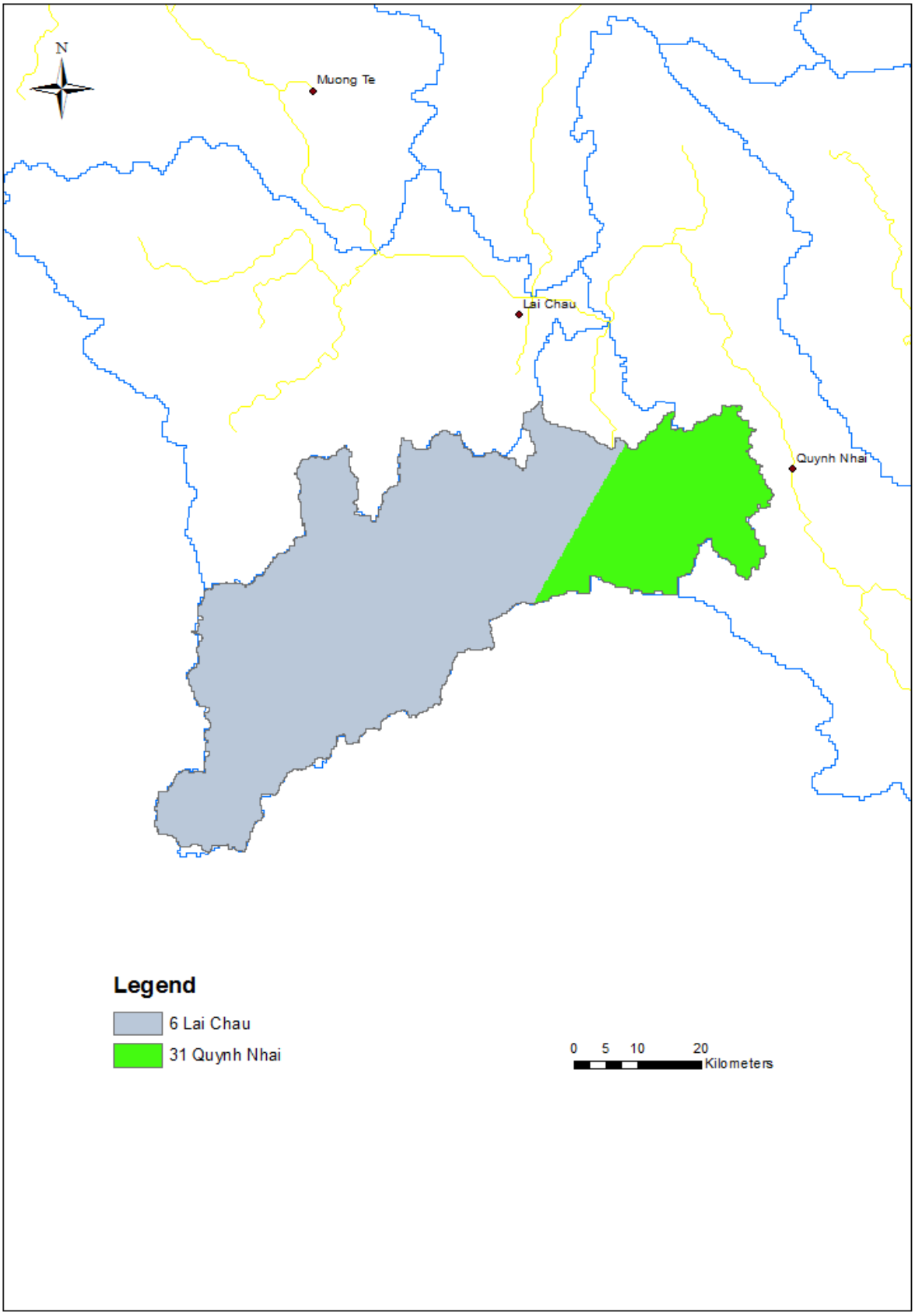

Figure 6.7: Thiessen's polygons of the temperature stations considered in the Nam Muc basin.

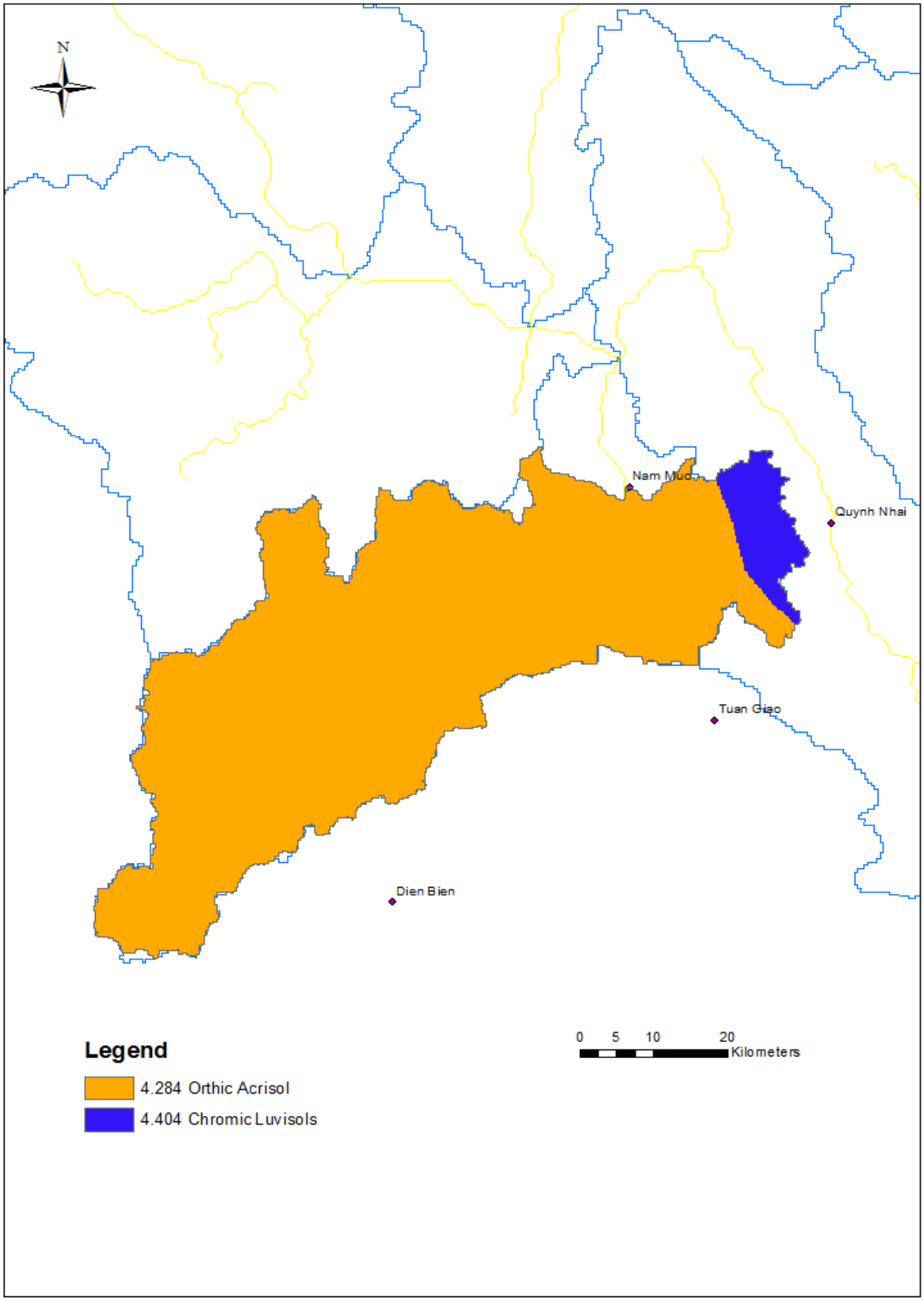

Figure 6.8: Soil map of the Nam Muc basin (source: FAO).

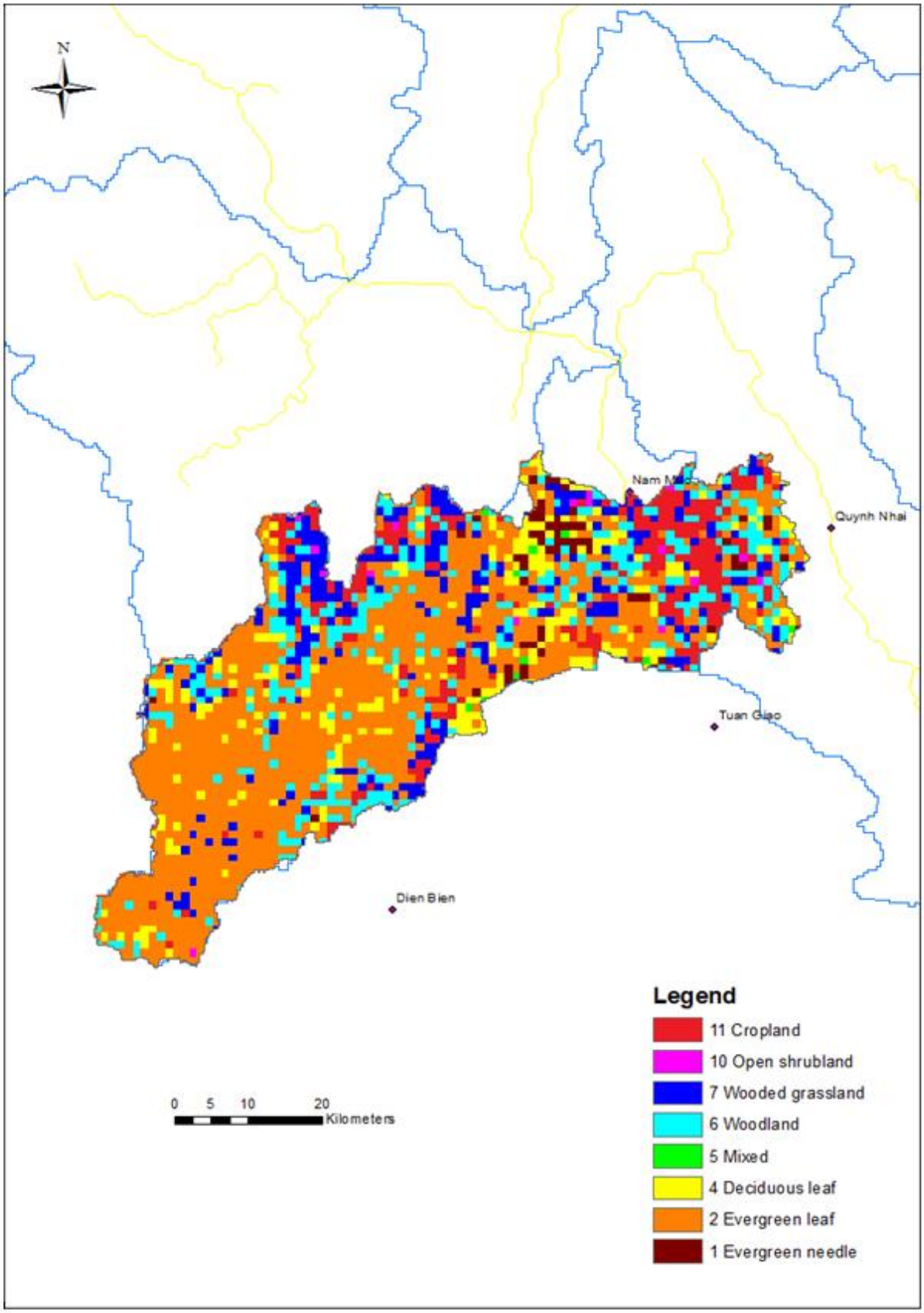

Figure 6.9: Land cover map dated 1981-1994 of the Nam Muc basin (source: FAO).

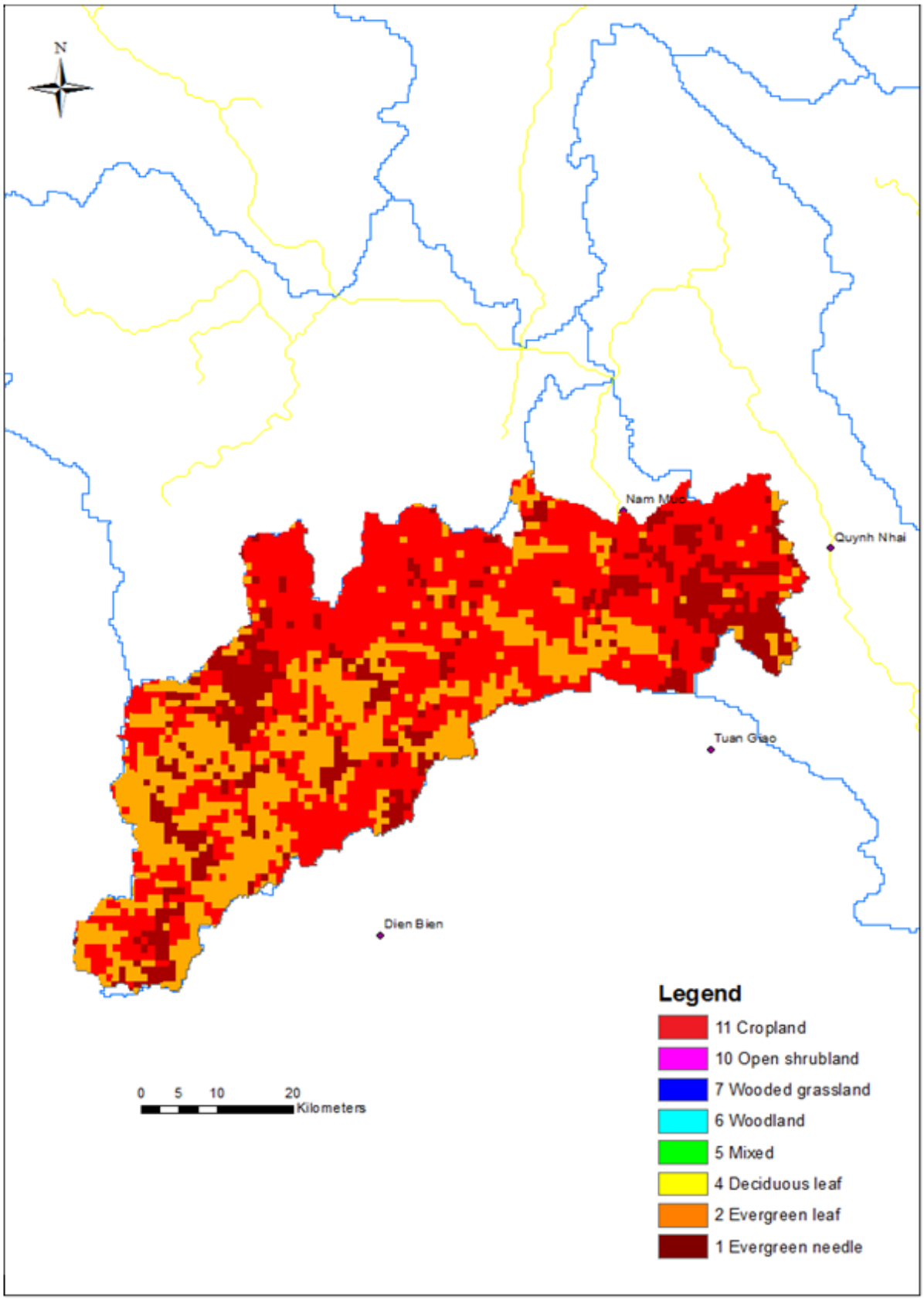

Figure 6.10: Land cover map dated 2000 of the Nam Muc basin (source: FAO).

6.3 Model calibration

Starting from reference values provided by FAO, we proceed with the model calibration. During this phase, we calibrate manually the parameters requested by Topkapi-ETH, in particular working on soil and vegetation cover. The parameters which represent these dynamic components are the following:

- Depth. It is the thickness of the layers for the soil type.

- Soil saturation. It is the water content ratio at saturation of two soil layers.

- Horizontal (KsH) and vertical (KsV) hydraulic conductivity at saturation of two soil layers. It is a measure of a saturated soil ability to transmit water when subjected to a hydraulic gradient. We can think about it as the ease with which saturated soil pores allow water movement in the two directions. Its value varies within a wide range of several orders of magnitude, depending on the soil material. Usually, clay soil has a lower hydraulic conductivity at saturation than sandy one.

- Monthly evapotranspiration coefficients (ETCF). They represent the evapotranspiration crop factors for each land cover type and respective month. These parameters are always positive. In the cool months (January, February, November and December), the ET value is low, whereas the warm season (May, June, July and August) is characterized by high values. The difference among seasonal values is lower in wet regions than dry ones. ET depends on land cover, in fact it is higher in forests than bare soils.

- Manning coefficient. It describes the roughness coefficient for the surface of the land use types. Roughness coefficient defines the resistance to flows in open channels. It depends on channel velocity, flow area and channel slope. In forested area, the major roughness is caused by trees and brushes.

In Topkapi-ETH, the run-off generation can be described through two mechanisms: infiltration and saturation excesses. We employ both of them. So, when the maximum infiltration rate is reached or when soil is saturated, we have lateral water fluxes.

Our objective is to obtain the parameterization which better represents the case study system. We evaluate every tried parameter combination with some indicators, such as NSE, R^2 and RMSE, to compare the simulated streamflow with the observed one at Nam Muc station.

Moving the first four parameters among the above explained ones, we obtain the baseline (see figures 6.11 and 6.12). It is the starting point for each following experiment.

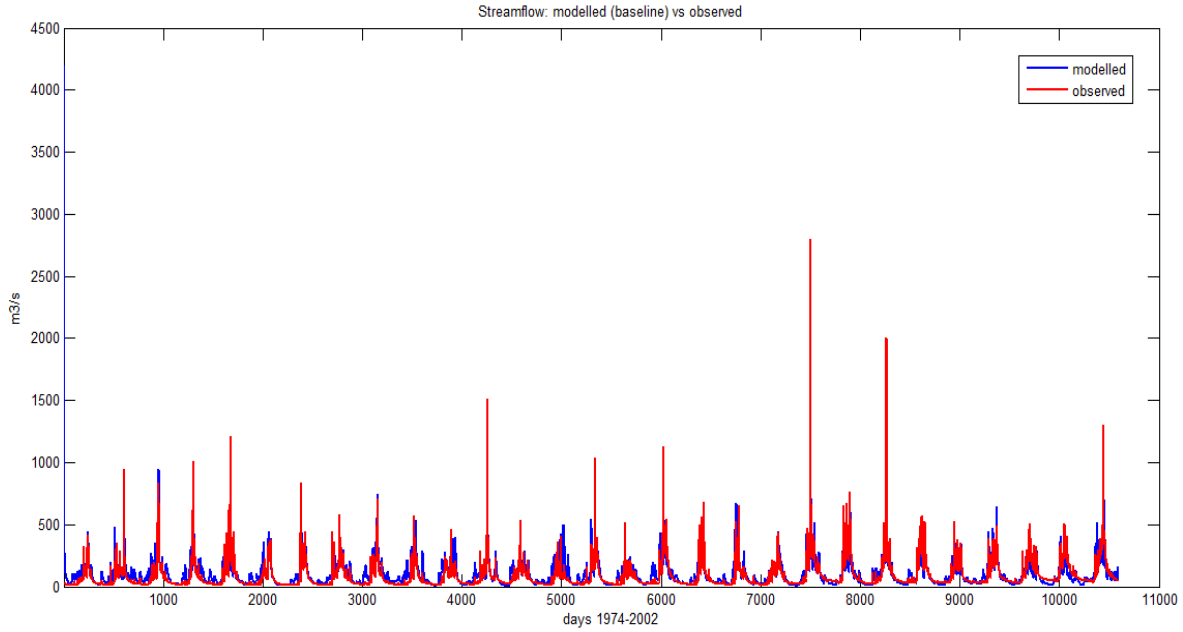

Figure 6.11: Streamflow comparison between the output of the best parameterization simulation and the observations for the period 1974-2002.

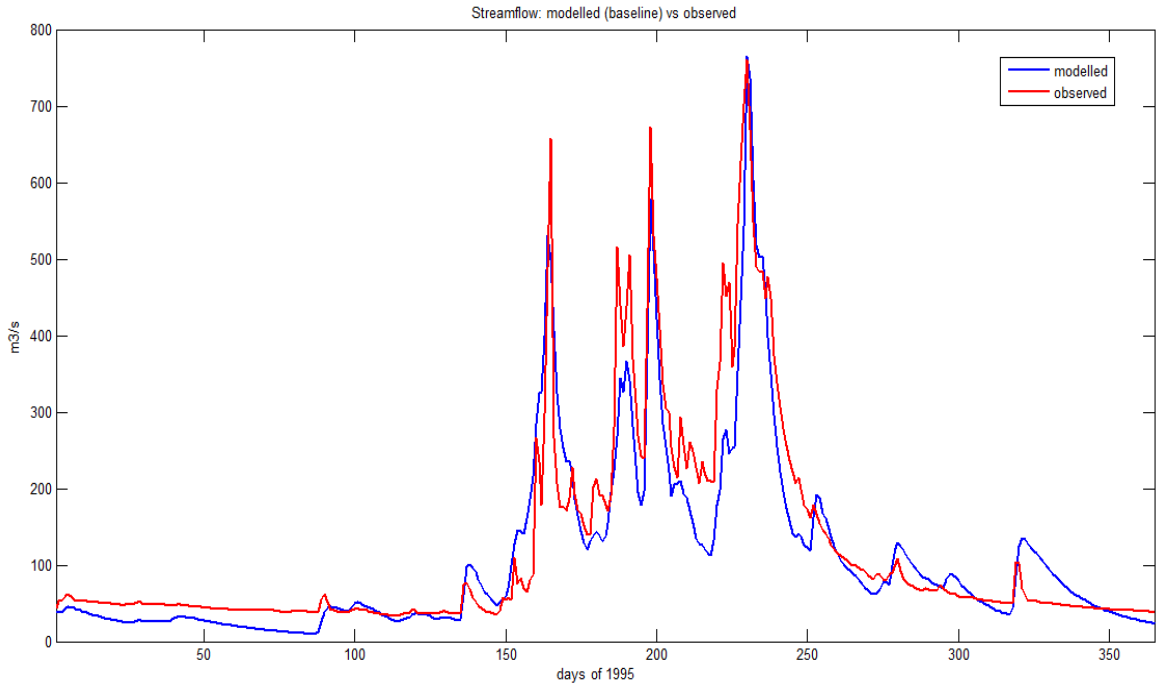

Figure 6.12: Streamflow comparison between the output of the best parameterization simulation and the observations for the period 1974-2002: zoom on one year (1995).

Excluding the first two years of model warm up, the indicator values for the baseline are: NSE= 0.6693, R^2=0.6878 and RMSE= 2.5303 mm/d.

6.4 Land cover scenarios

6.4.1 Experiment setting

To understand how much the model is sensitive to soil and land cover parameter changes, we compare the behaviour of three scenarios to a fixed and homogeneous land cover on the whole considered basin. One scenario represents afforestation, whereas the other two correspond to deforestation, with agricultural and bare soil use. Hence, we define as land cover respectively: evergreen leaf, cropland and bare soil.

At this level, the parameters which come into play are: the monthly evapotranspiration coefficients, Manning's coefficient and hydraulic conductivity at saturation of the two soil layers. From an applicative point of view, for evapotranspiration and Manning's coefficients, we associate to all classes the parameter value of the selected land cover. So, for instance, in the afforested scenario, all land cover types have ETRF and Manning's coefficients of evergreen leaf; we employ the same parameters of evergreen leaf used in the baseline.

About hydraulic conductivity at saturation, we have to talk about it separately. In fact, it is a soil property and it also depends on land cover, but this relationship is missing in the model. As we said in the paragraph 2.6, in literature there are many evidences for the decrease of hydraulic conductivity at saturation from a forested to a deforested land cover, but there is no information about the magnitude of this evolution. Change quantification of this parameter is complicated because it is not a measurable variable, it has indeed a wide range in which it varies even if the type of soil is the same. So, in deforested scenarios, we reduce the parameter of one order of magnitude, that is the minimum change to which model is sensitive.

Tables 6.1, 6.2 and 6.3 show the parameter values in the three scenarios, respectively the monthly evapotranspiration coefficients, Manning's coefficients, and horizontal and vertical hydraulic conductivity at saturation of the two soil layers. In particular, bare soil class is not presented in the baseline parameterization and its monthly evapotranspiration coefficients are wet climate reference values. Moreover, it is important to note that fields are not cultivated during January, June, November and December, and so cropland ETRF coefficients are the same of bare soil in these

months. This is due to the harvest times after the two Vietnamese seasonal crops (the winter-spring and summer-autumn ones) and field rest period.

ETRF	Evergreen leaf	Cropland	Bare soil
January	1.2375	0.1679	0.1679
February	1.32	1.1	0.1861
March	1.52625	1.21	0.2421
April	1.4625	0.525	0.2594
May	1.31625	0.6615	0.3004
June	1.4025	0.3215	0.3215
July	1.4025	0.7245	0.3355
August	1.4025	0.504	0.3261
September	1.4025	0.819	0.2893
October	1.7325	0.93	0.2389
November	1.65	0.2008	0.2008
December	1.2375	0.1872	0.1872

Table 6.1: Monthly evapotranspiration coefficients used in the three scenarios.

	Evergreen leaf	Cropland	Bare soil
Manning's coefficient	0.25	0.08	0.07

Table 6.2: Manning's coefficient values used in the three scenarios.

	Evergreen leaf	Cropland and Bare soil
KsH and KsH-low	10^-3	10^-4
KsV and KsV-low	10^-3	10^-4

Table 6.3: Order of magnitude of hydraulic conductivity at saturation for the two soil layers. The suffix 'low' is related to the bottom layer.

6.4.2 Results

Figures 6.13-6.18 show the simulated streamflow trajectories in the three scenarios compared with the baseline. We study them one by one in detail.

In figure 6.13, we compare the baseline to the afforested scenario in a representative year of the whole simulated period (1974-2002). In 1990 the recorded data are suitable, because it is not a particularly dry year and there are no occasional peaks. The different behaviour occurs in particular during the wet season, that is between day 110 and day 270 of the selected year. In fact, in this period, the simulated run-off is lower with evergreen leaf as only land cover of the basin, than with baseline configuration (which is reported in figures 6.11 and 6.12). During the dry season, we note less changes between the two settings, instead. This result does not come as a surprise, because the two parameterizations differ in evapotranspiration coefficients that are higher with trees land cover, in particular in the rainy season; it involves low flows in the channel and less intensity of the peaks. The effect of Manning's coefficient does not act on the peak magnitude, but on the curve slope after the peak, which it is attenuated by the roughness of trees in this scenario.

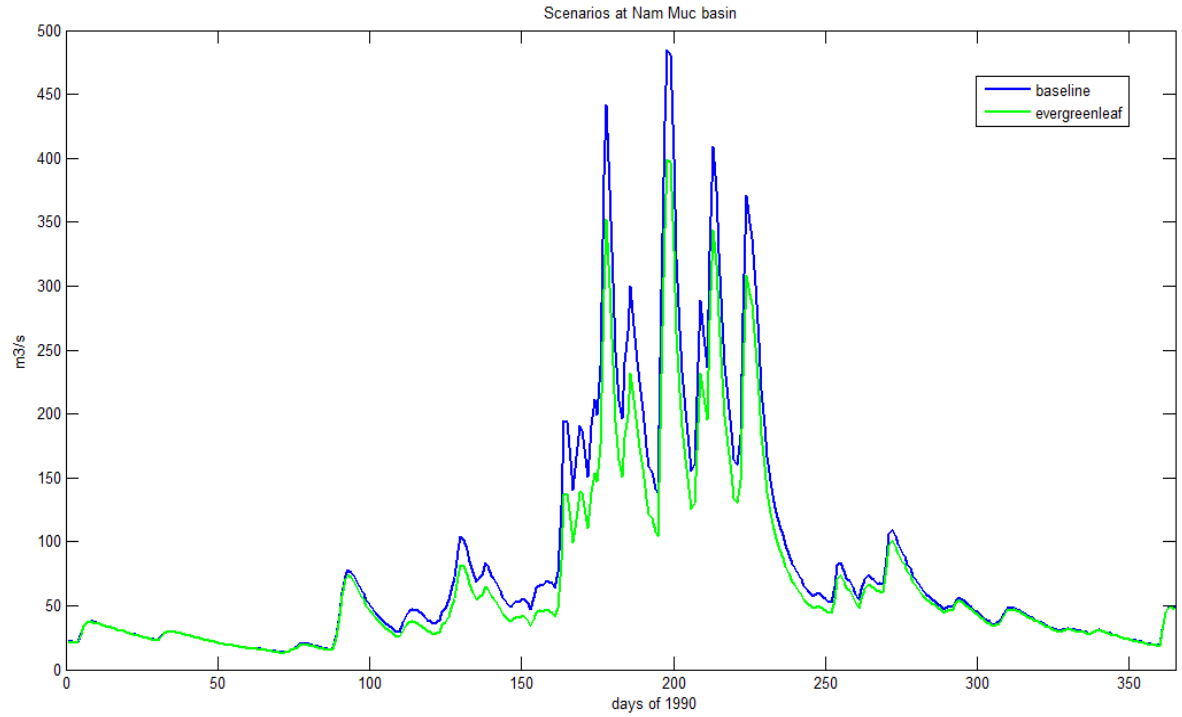

Figure 6.13: Afforested scenario compared to the baseline in 1990, a representative year of the period 1974-2002.

Figure 6.14 represents the mean for each day of the year on the entire considered period 1974-2002 for the two cases. On average, the afforested scenario and baseline almost overlap in the dry season (the difference is less than 10^{-1} m3/s), whereas the streamflow reduction caused by land cover change is in the order by 17% if compared to the baseline in the rainy months.

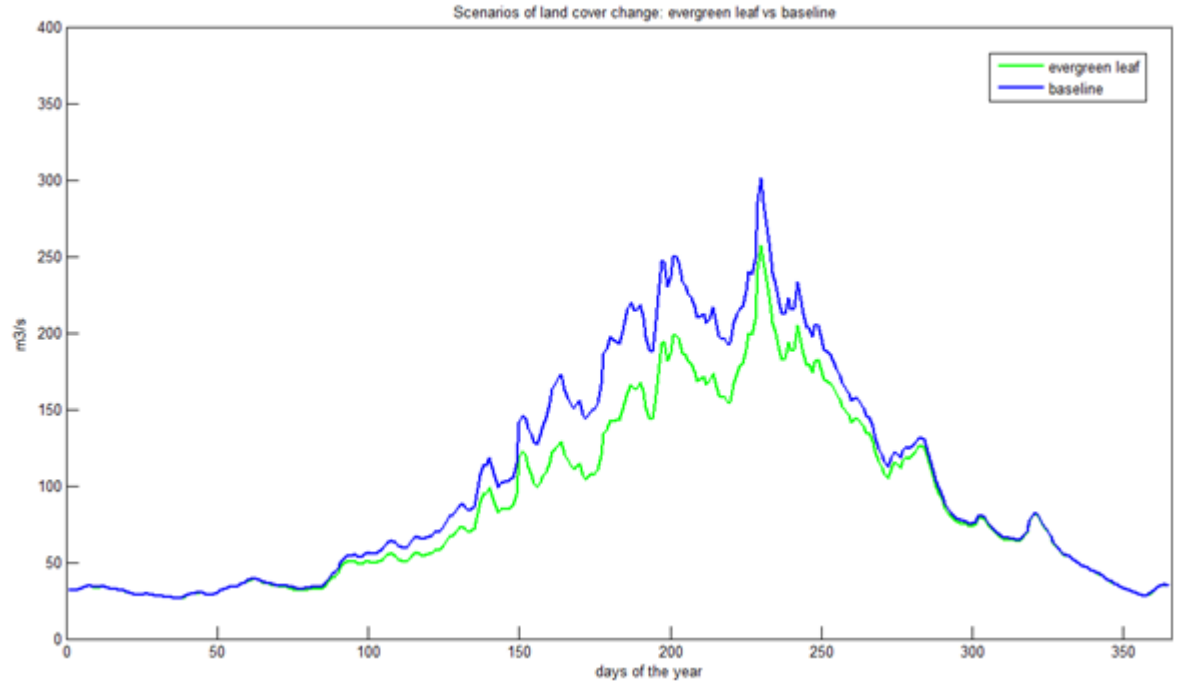

Figure 6.14: Average behaviour of the afforested scenario compared to the baseline during 1974-2002.

In both deforested scenarios, we have to remember that also the hydraulic conductivity at saturation for the two soil layers is changed. Figure 6.15 shows the parallelism between bare soil scenario and baseline in a typical year of the simulated period. The land cover change consequences are evident during the whole year. In fact, we can note a base-flow increase in the dry season (from day 1 to day 90 and from day 280 to day 365), and also a rising of peak magnitude in the wet one (from day 135 to day 280). These differences in the two settings are due both to evapotranspiration coefficients and hydraulic conductivity decrease. Moreover, here it is clear the Manning's coefficient decrease effect; in fact, the peaks are not smooth anymore, but are shaped.

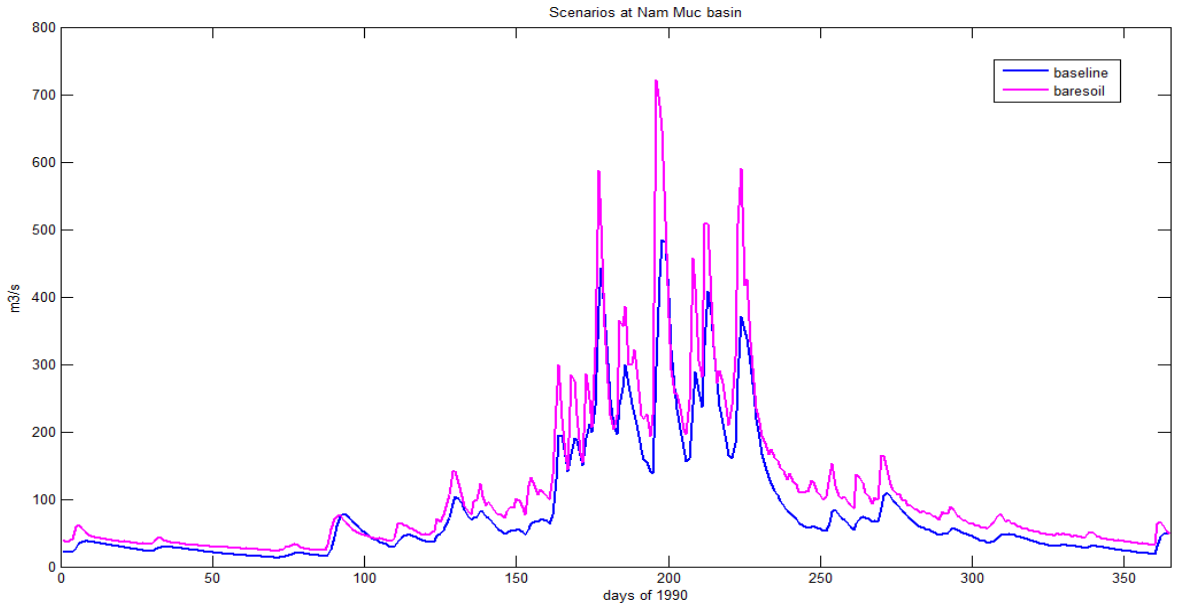

Figure 6.15: Bare soil scenario compares to the baseline in 1990, a representative year of the period 1974-2002.

On average, as confirmed by figure 6.16, with deforested scenario the run-off is always higher than the baseline.

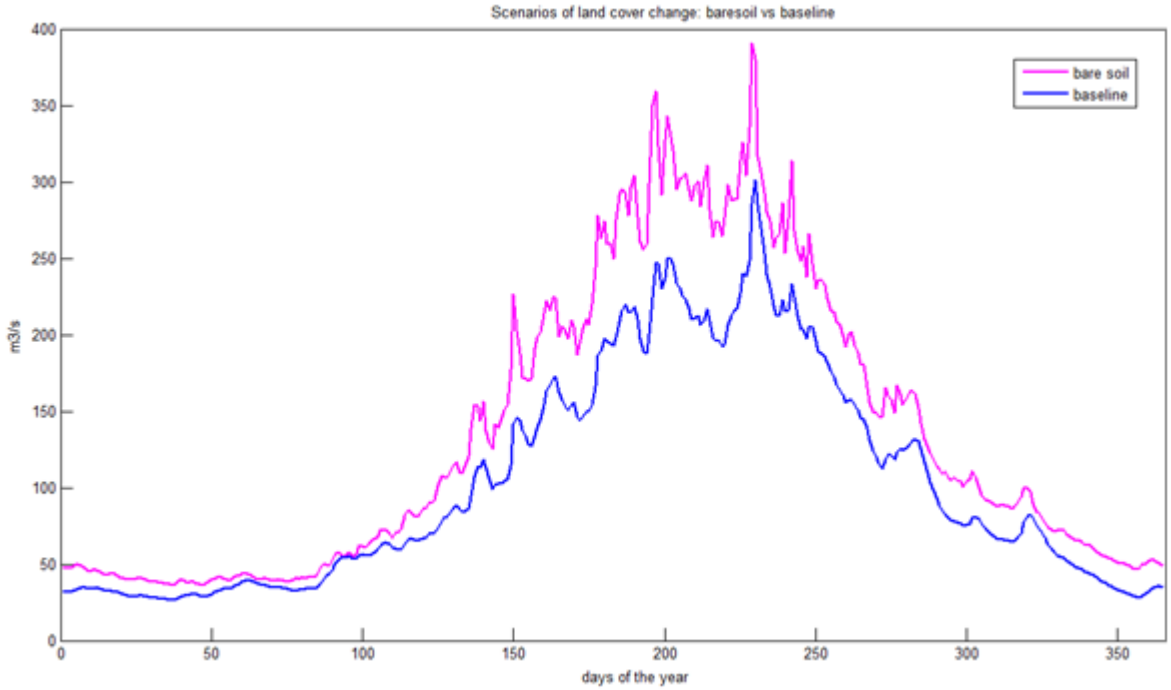

Figure 6.16: Average behaviour of the bare soil scenario compared to the baseline during 1974-2002.

Figure 6.17 describes the comparison between the agricultural scenario and the baseline in 1990. We can note an increase of base-flow in dry season (from day 1 to day 80 and from day 285 to day 365) and of peaks in wet one (from day 165 to day 285), such as bare soil scenario. Moreover, also the Manning's coefficient effect is very clear in the graph.

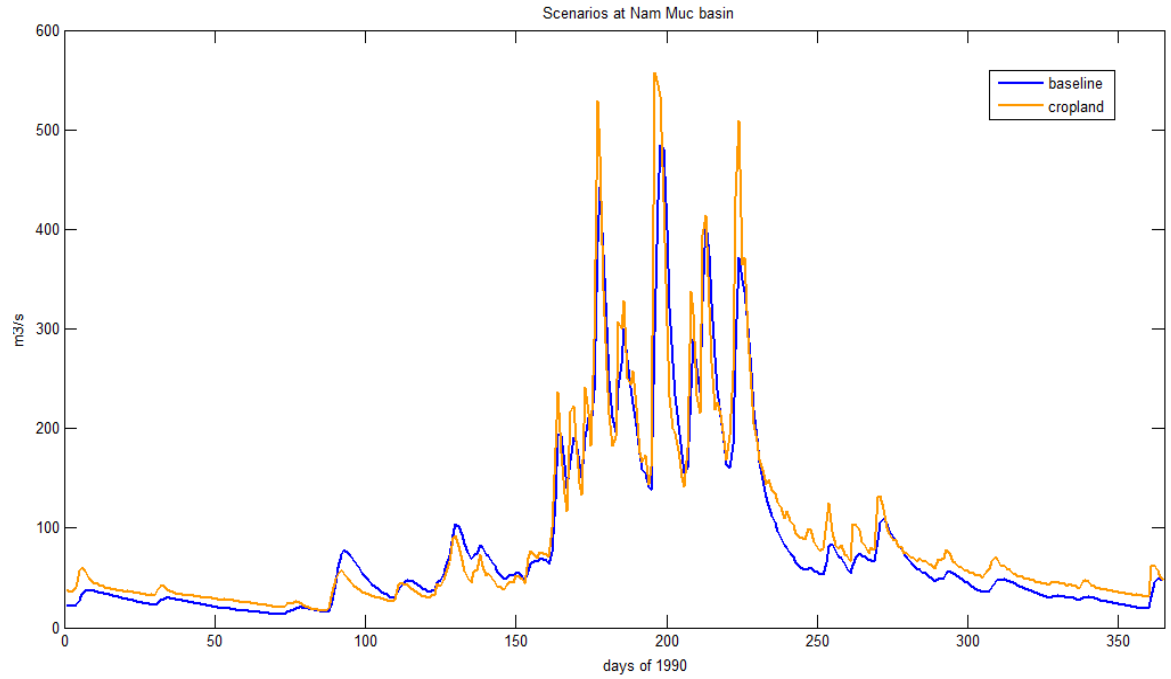

Figure 6.17: Agricultural scenario compares to the baseline in 1990, a representative year of the period 1974-2002.

On average, the behaviour of agricultural scenario is not easy like the other two cases (see figure 6.18). We note a streamflow decrease between the end of March and May. This happens because in these months the effect of hydraulic conductivity is still more powerful than the one of evapotranspiration coefficients. In fact, using the hydraulic conductivity of the baseline, we look at a higher run-off in cropland than evergreen leaf forest also in this season. We cannot ignore land cover change effect on soil properties, but hydraulic conductivity is a constant value for each soil layer in Topkapi-ETH. In the rest of the year, the discharge of agricultural scenario is higher than baseline, instead.

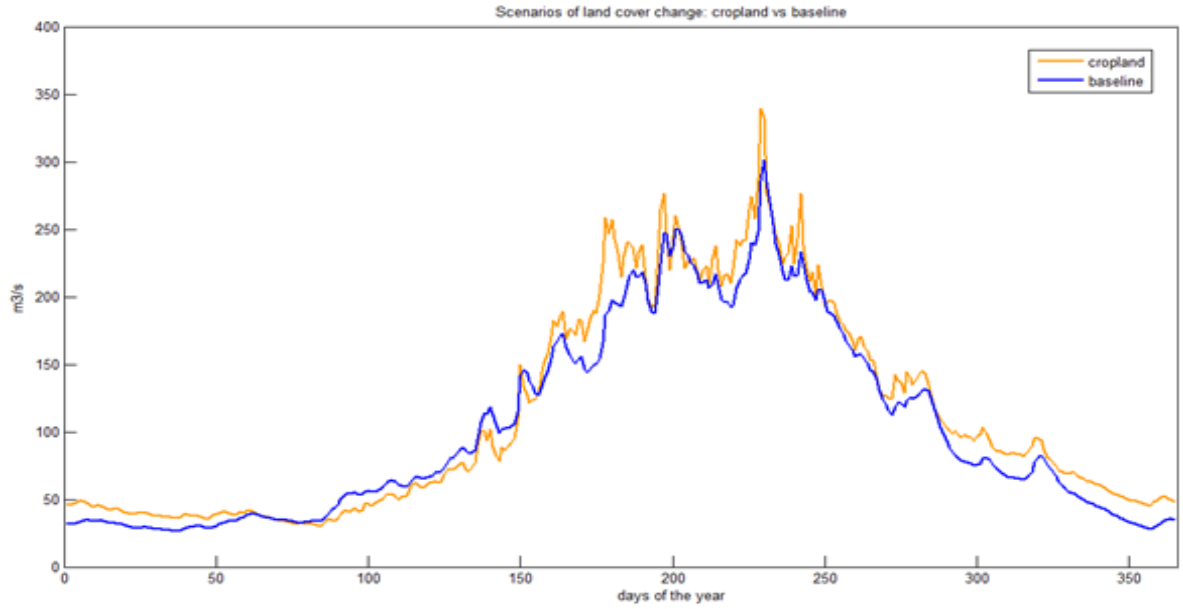

Figure 6.18: Average behaviour of the agricultural scenario compared to the baseline during 1974-2002.

To understand the magnitude of the decreasing or increasing tendency in the three scenarios, we comparatively analyse them. Figure 6.19 illustrates the average behaviour of the homogenous land cover scenarios during the simulated period (1974-2002). As we can observe, in the period from November to February the two deforested scenarios overlap, because they have the same evapotranspiration and hydraulic conductivity coefficients until January. In this period, their run-off is higher than in the afforested scenario. The main difference among the three land covers is in the wet season, when the run-off raises progressively from evergreen leaf to cropland scenario and from cropland to bare soil. The smaller increase of agricultural land use discharge than bare soil one is due to its higher evapotranspiration coefficients. The run-off of bare soil scenario is, on average, always higher than afforested and agricultural (except from November to January). Moreover, streamflow of evergreen leaf land cover is lower than the one of cropland, except for April. This is the result of the hydraulic conductivity effect, which we have explained in figure 6.18.

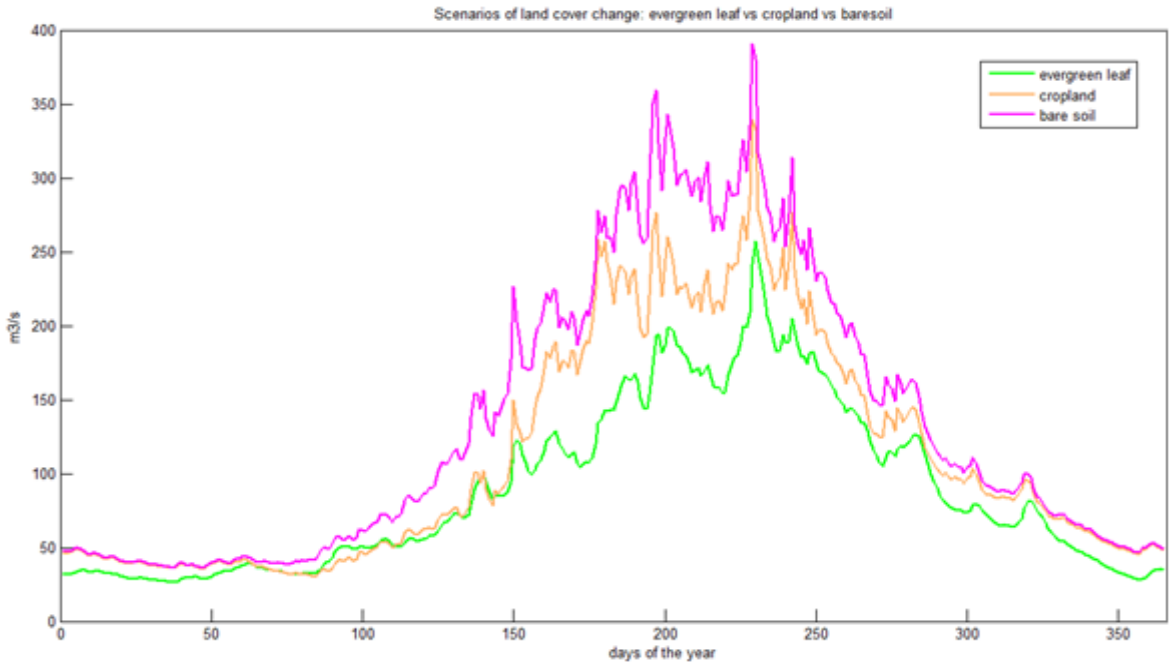

Figure 6.19: Average behaviour of the three land cover scenarios during the simulated period (1974-2002).

To study the land cover contribution to hydrological regime changes, whether the observed change in time series is due to land cover or to other factors, such as precipitation conditions. If the same tendency is present in both scenarios, it means that it does not depend on land cover change. Hence, using MASH, we analyse the similarities among the three scenarios in the whole considered period (1974-2002). Figures 6.20, 6.21 and 6.22 represent the moving plot of simulated streamflow respectively of afforested, agricultural and bare soil scenario.

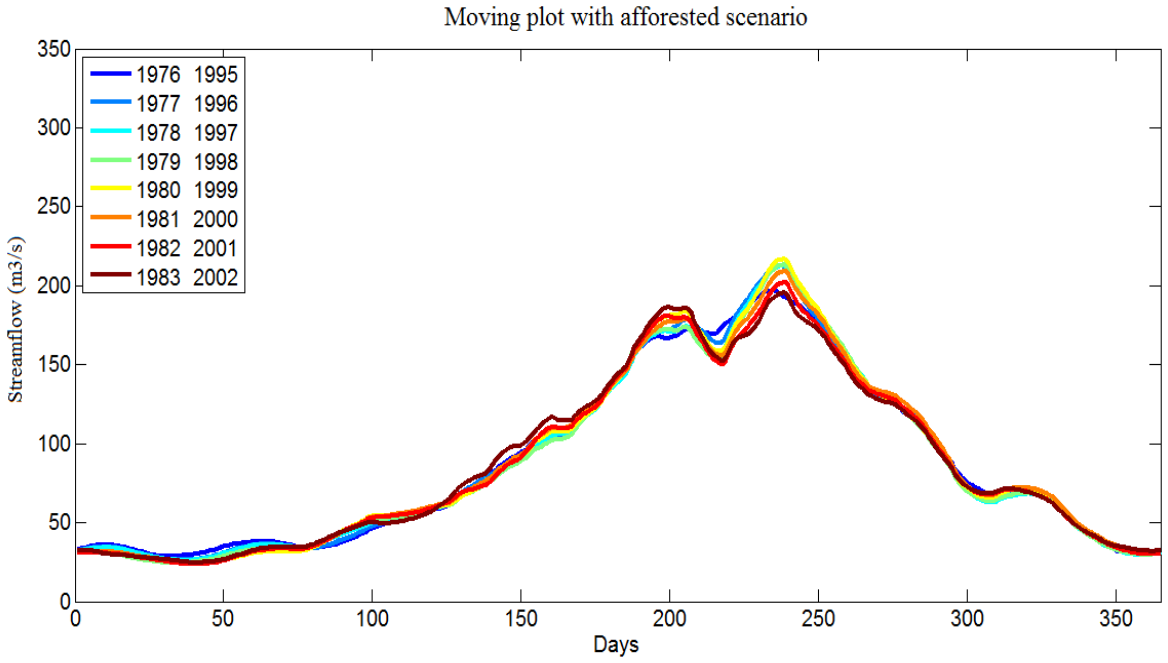

Figure 6.20: Streamflow volume moving plot at Nam Muc station with the afforested scenario in the period 1974-2002, using H=20 and f=10.

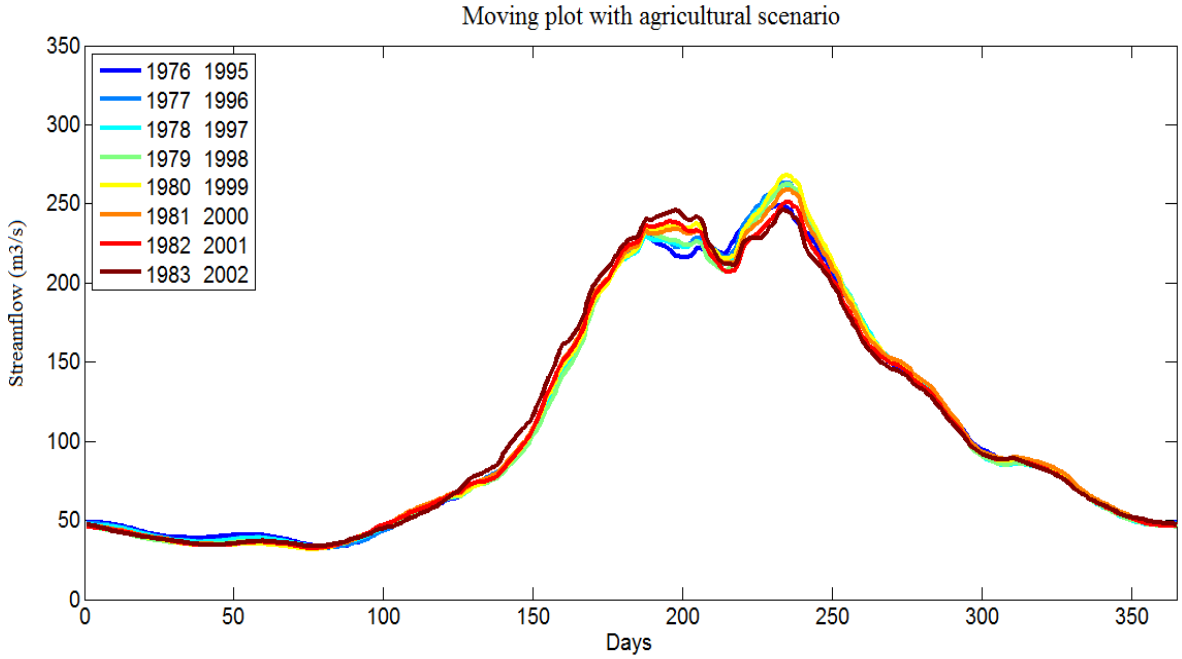

Figure 6.21: Streamflow volume moving plot at Nam Muc station with the agricultural scenario in the period 1974-2002, using H=20 and f=10.

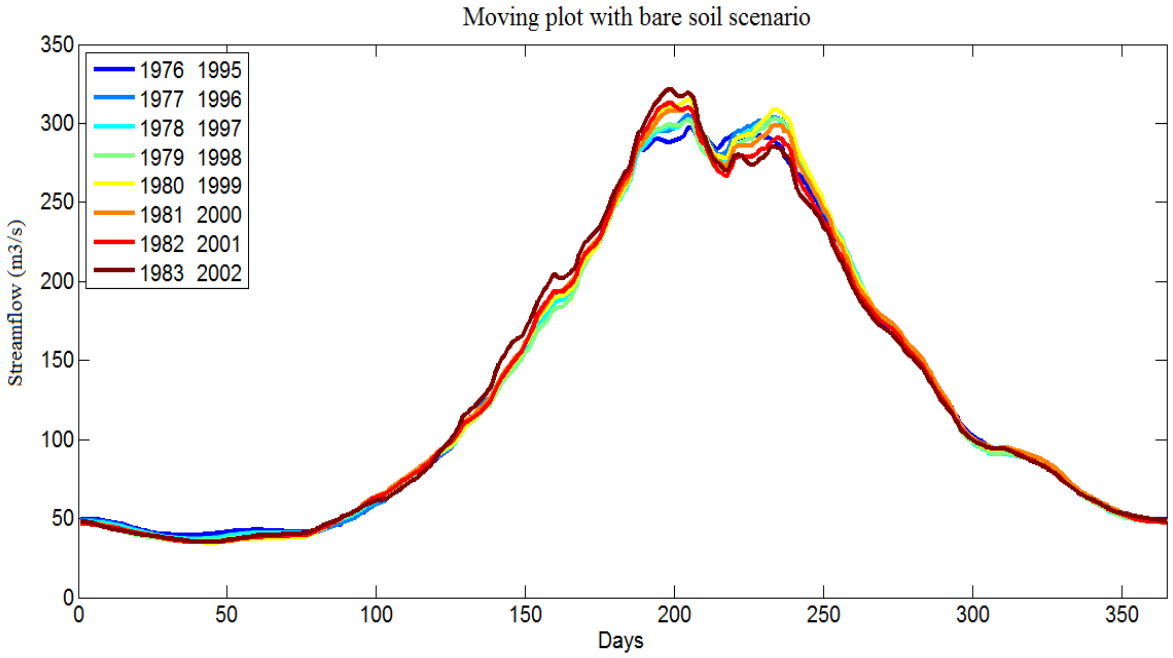

Figure 6.22: Streamflow volume moving plot at Nam Muc station with the bare soil scenario in the period 1974-2002, using H=20 and f=10.

In these three figures, we can note that each scenario presents a decreasing run-off in January and February, contrarily with what we have detected in observations. It happens also in September, but here this phenomenon could be caused by the decreasing tendency of precipitation time series used as inputs. In July, we observe a discharge increase, probably due to rainfall contribution. Moreover,

we have to pay attention to the period before the peak (about from 130th to 180th day of the year). In fact if we look at the dark red line, we note an increase of run-off, but this is the only curve which gives this impression, so probably this effect occurs only in the year 2002 which raises the mean in this period.

In conclusion, the increasing streamflow recorded at Nam Muc station in January-February and May-June in the period 1974-2002 could be due to deforestation. Moreover the land cover change could emphasize the increasing discharge occurred in July in the analysed time horizon.

6.5 Effects of land cover change from 1981-1994 to 2000

We have so far made experiments about unreal homogenous land cover scenarios in the Nam Muc sub-basin, to check the model sensitivity to soil and vegetation parameters changes. We now consider the model performance with the real basin land cover in the period 1974-2002. With this model it is not easy to represent dynamic and land cover evolution in this area, because, as said, Topkapi-ETH accepts only one classification for each model run. Hence, we compare two simulations on the period 1974-2002. The first one employs the land cover map of 1981-1994 (shown in figure 6.9), while the second one the land cover map of 2000 (see figure 6.10). Looking at figures, we can observe a lot of changes. On the one hand, the 'evergreen leaf' (deciduous) class decreases in the basin in favour of cropland one, which represents an example of deforestation. On the other hand, also afforestation occurs through the increase of 'evergreen needle' class. Moreover, the intermediate categories, like woodland, wooded grassland, open shrub-land and mixed, disappear.

The parameters of both simulations are the best obtained during the calibration phase. So, the model run with land cover map of 1981-1994 is the baseline. Figure 6.23 shows an average comparison between the two simulations in the period 1974-2002. The red line is always above the blue one, but with the net increasing from April to September. This is due to lower evapotranspiration coefficients of 'cropland' class than the ones of 'evergreen leaf' category; the coefficients of these two classes are different, in particular during the wet season. In fact, it is important to remember that the hydraulic conductivity does not change with land cover but only with the soil type. This is the reason why we cannot observe a discharge increase also at the beginning and at the end of the year.

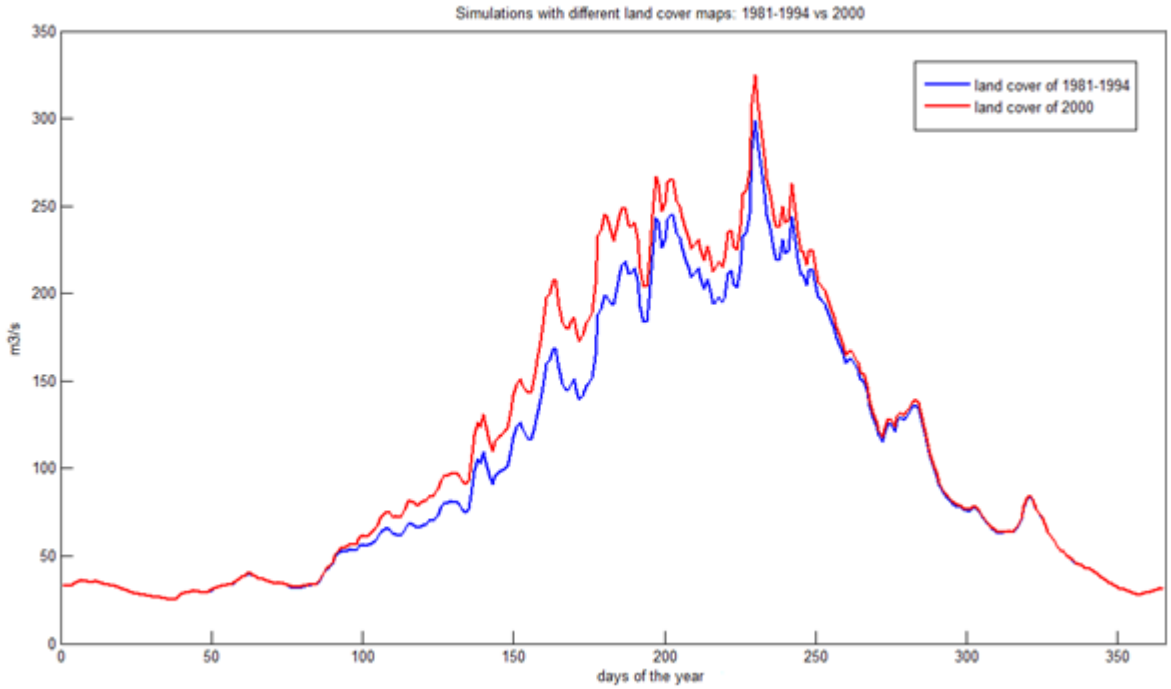

Figure 6.23: Average behaviour of streamflow in the period 1974-2002 with the land cover of 1981-1994 and 2000.

We have simulated the system on static conditions on the whole period 1974-2002, because with this model it is not possible switching between two land cover configurations in the same run, as we would like. Anyway, we have demonstrated that under the same temperature and precipitation conditions, land cover influences streamflow a lot. In figure 6.23, the main recorded effects due to evapotranspiration occur of course in the rainy season, but in previous paragraphs land cover consequences are evident also in the dry season, acting on soil hydraulic properties. So this increasing tendency on streamflow would confirm the observations.

Chapter 7

Discussion, conclusions and further research

The first two objectives of the thesis were to analyse changes on hydro-meteorological regime and investigate through a model the effects of land cover change on streamflow patterns of the Vietnamese part of the Red River basin. This area is in the North of Vietnam and it is characterized by subtropical and monsoon dominated climate, which presents two seasons: wet (from May to October) and dry (from November to April).

We first analysed time series of evaporation, temperature, precipitation and streamflow to assess if any changes have interested the basin during the period 1974-2002, which is the longest possible time horizon for all available variables. To reach this purpose, we used trend detection methods, including a novel tool, called MASH, and state-of-the-art tools, to further validate the results, such as the Mann-Kendall's test; we could not employ linear regression method because of the lack of a necessary condition, the data normal distribution. Finally, with the Pettitt's test we investigated the presence of break year/s in the time series to identify changes in variables behaviour.
We discarded evaporation dataset and we focused on the other three variables. All available temperature stations were in the Da river basin, the largest tributary of the Red River, which is located in the Western part of the whole considered area. Here, we observed an annual increasing mean temperature trend for many stations and also mainly during the months of January, April and December. The widespread increase of the annual mean temperature suggested that it could be a regional effect, maybe due to global warming, and not a local one. Precipitation and streamflow stations were, instead, homogeneously distributed in all the Red River. The first ones presented an increasing trend during July and a decreasing one during September, detected with both Mann-Kendall's test and MASH method. The same tendency was recognized also in run-off series in almost the entire basin in the considered period. Hence, it is likely that these precipitation changes had effects on streamflow. The situation is different for the months of the first part of the year, from

January to June: discharge always increases, while rainfall reduces during January and April, and has no trend in other months. In fact, we identify a rising trend also in annual run-off, but no trend in annual precipitation. The rainfall volume growth in July was probably balanced by the reduction in September, and this could be the reason why no annual trend in precipitation is detected.

One possible driver of these mechanisms could be land cover change. In literature many studies which confirm that deforestation involves a rising streamflow, particularly in the base-flow, as we recorded in the data. In fact, in the basin, rapid changes in land cover occurred mostly from the forties to the nineties to support the fast population growth and economic development. Lately, an afforestation process began in many zones. Both of these two types of human intrusion on land cover were visible looking at the difference between 1981-1994 and 2000 FAO maps. The most widespread change was the decrease of 'evergreen leaf' (deciduous) class in the basin in favour of cropland one. Another important gap was the increase of 'evergreen needle' category. Moreover, the intermediate classes, like woodland, wooded grassland, open shrub-land and mixed, disappeared.

In the second part of the work, we employed a spatially distributed and physically based model, Topkapi-ETH, to study how land cover change influenced the run-off, and to test the sensitivity of the model parameters associated to soil and vegetation cover, which represented the third objective of the thesis.

We analysed the behaviour of three scenarios with a fixed and homogeneous land cover on the Nam Muc area, a little sub-basin of the Red River. One scenario corresponded to afforestation (evergreen leaf), whereas the other two to the deforestation, with agricultural (cropland) and bare soil use. The differences among these scenarios are in evapotranspiration coefficients, hydraulic conductivity at saturation of soil and Manning's coefficient. The first two parameters are the most important ones and they are higher in afforested than deforested scenarios. On average, the discharge of bare soil scenario is higher than the one of evergreen leaf all over the year. Moreover, we observe that bare soil scenario has also a higher mean streamflow than cropland one, except from November to February, when it is the same. During wet season, the run-off raise progressively from evergreen leaf to cropland scenario and then to bare soil one. The lower increase of agricultural land use streamflow than bare soil one is due to its higher evapotranspiration coefficients. In the dry season the discharge of agricultural scenario is higher than afforested one, but not in April. This is the effect of lower hydraulic conductivity.

Furthermore, analysing the same tendencies among the three scenarios in the whole considered period (1974-2002) with MASH, we could understand which movements of run-off simulated

volume did not depend on land cover change. Each scenario presented a decreasing discharge in September and an increasing one in July, probably due to rainfall contribution. In January and February, instead, moving plot of scenarios showed a decrease in the period 1974-2002, contrarily to observation data. During May and June, we did observe no significance volume change. Hence, the increasing discharge recorded at Nam Muc basin outlet in January-February and May-June could be due to deforestation. Moreover the increasing streamflow, occurred in July in the analysed time horizon, could be supported by the land cover change. Therefore, on the one hand, even if there are models more sensitive than Topkapi-ETH, it shows anyway a good performance in land cover parameter susceptibility.

On the other hand, this model has some huge limits. The first one is that the evapotranspiration coefficients are the only monthly parameters, but this is not sufficient. In fact, it would be also important that soil properties depend on season and land cover too. The second limit is the absence of land cover dynamic. Considering the static land cover conditions of the system, we compared two simulations on the period 1974-2002 which employed the land cover map respectively of 1981-1994 and 2000. The greater presence of cropland class in the second map caused an increasing mean streamflow from April to September in its simulation than in the other one with the first map. It is caused to the lower evapotranspiration coefficients of 'cropland' which had replaced the 'evergreen leaf' category. In fact, the hydraulic conductivity did not contribute, because it was the same in both simulations, and so we could not observe a run-off increase both at the beginning and the end of the year.

In conclusion, recalling the initial research question, we have demonstrated that under the same temperature and precipitation conditions, the land cover change from afforested to deforested area supports the streamflow increase. The recorded effects due to evapotranspiration mechanisms occur mainly in the wet season, but land cover change consequences are also evident in the dry season thanks to the impacts on soil hydraulic properties.

Further research could include the use of a more sensitive model to land cover and soil changes or the enhancement of Topkapi-ETH to reduce its limits, in order to improve the knowledge about land cover changes in hydrological regime. Moreover, it would be important to have additional information on how land cover change influences soil properties, in particular the hydraulic conductivity at saturation.

Bibliography

[1] B. J. Abiodun et al. 2008. “Modelling the Impacts of Deforestation on Monsoon Rainfall in West Africa”.

[2] V. Andréassian, 2004. “Waters and forests: from historical controversy to scientific debate”. *Journal of Hydrology, vol. 291, 1-27.*

[3] D. Anghileri, F. Pianosi, R. Soncini-Sessa, 2013. “Detection of meteo-hydrological trends and water resources impacts at the basin scale”. *Politecnico di Milano, Dipartimento di Elettronica e Informazione, Italy*.

[4] Asian Development Bank TA No 2871-VIE Red River Basin Water Resources Management Project, 2000. “Final Report on Management Study on Land Use and Water Management”.

[5] G. Bloschl, 2007, “At what scales do climate variability and land cover change impact on flooding and low flows?”. *Hydrological processes, no.21, 1241-1247.*

[6] M. Bonell, 2010. “The impact of forest use and reforestation on soil hydraulic conductivity in the Western Ghats of India: Implications for surface and sub-surface hydrology”. *Journal of Hydrology, vol. 391, 47-62.*

[7] H. Bormann, K. Klaassen, 2008. “Seasonal and land use dependent variability of soil hydraulic and soil hydrological properties of two Northern German soils”. *Geoderma, vol. 145, 295-302.*

[8] J. A. C. Bradshaw, 2007. “Global evidence that deforestation amplifies flood risk and severity in the developing world”. *Global change biology, vol. 13, 2379-2395.*

[9] A. E. Brown et al., 2013, “Impact of forest cover changes on annual streamflow and flow duration curves”. *Journal of Hydrology, vol. 483, 39-50.*

[10] A.E. Brown et al., 2005. “A review of paired catchment studies for determining changes in water yield resulting from alterations in vegetation”. *Journal of Hydrology, vol. 310, 28-61.*

[11] Y. Casali, R. Rota, 2012. “Valutazione del trend di cambiamento climatico”. Bachelor thesis at Politecnico di Milano.

[12] A. Castelletti et al., 2012. “Assessing water reservoirs management and development in Northern Vietnam”. *Hydrology and Earth System Sciences, vol. 16, 189-199.*

[13] J. Charney et al., 1977. “A Comparative Study of the Effect of Albedo Change on Drought in Semi-Arid Region”. *J. Atmos Sci, vol. 34, 1366-1385.*

[14] N. Chattopadhyay, M. Hulme, 1997. “Evaporation and potential evapotranspiration in India under conditions of recent and future climate change”. *Agricultural and Forest Meteorology, vol. 87, 55-73.*

[15] G. S. Chen et al., 2012. “Simulated Local and Remote Biophysical Effects of Afforestation over the Southeast United States in Boreal Summer”. *Journal of Climate, vol. 25, 4511-4522.*

[16] T. H. Dang et al., 2010. “Long-term monitoring (1960–2008) of the river-sediment transport in the Red River Watershed (Vietnam): Temporal variability and dam-reservoir impact “. *Science of the Total Environment, vol. 408, 4654-4664.*

[17] S. W. Fleming, 2012. “Detection of long-term change in hydroelectric reservoir inflows: Bridging theory and practise”. *Journal of Hydrology, vol. 470-471, 36-54.*

[18] S. Frosini de Barros Ferraz, C. A. Vettorazzi, D. M. Theobald, 2009. “Using indicators of deforestation and land-use dynamics to support conservation strategies: A case study of central Rondonia, Brazil”. *Forest Ecology and Management, vol. 257, 1586-1595.*

[19] D. J. Gaffen, R. J. Ross, 1999. “Climatology and Trends of U.S. Surface Humidity and Temperature”. *Air Resources Laboratory, NOAA/Environmental Research Laboratories, Silver Spring, Maryland.*

[20] J. R. Garrat, 1978. “Flu Profile Relations above Tall Vegetation”. *Quart J. Roy. Met. Soc., vol. 104, 109-211.*

[21] R. K. Goyal, 2004. “Sensitivity of evapotranspiration to global warming: a case study of arid zone of Rajasthan (India)”. *Agricultural Water Management, vol. 69, 1-11.*

[22] L. J. Gordon et al., 2005. “Human modification of global water vapor flows from the land surface”. *PNAS, vol. 102, no. 21.*

[23] A.R. Hibbert, 1971. “Increases in streamflow after converting chaparral to grass”. *Water Resources Research, vol. 7, 71-80.*

[24] R. Johnson, 1998. “The forest cycle and low river flows: a review of UK and international studies”. *Forest Ecology and Management, vol.* 109, 1-7.

[25] S. Kanae, 2001. “Impact of Deforestation on Regional Precipitation over the Indochina Peninsula”. *Journal of hydrometeorology, vol.* 2, *51-71*.

[26] Z.W. Kundzewicz, A.J. Robson, 2004. “Change detection in hydrological records: a review of the methodology”. *Hydrol. Sci. J., vol. 49, 1-19.*

[27] P.N.J. Lane et al., 2005. “The response of flow duration curves to afforestation”. *Journal of Hydrology, vol. 310, 253-265.*

[28] T.P.Q. Le et al., 2007. “The changing flow regime and sediment load of the Red River, Viet Nam”. *Journal of Hydrology, vol. 334, 199-214.*

[29] X. Lee, 2011. “Observed increase in local cooling effect of deforestation at higher latitudes”. *Nature, vol. 479.*

[30] Z. Li et al., 2006. “Climate change and human impact on the Song Hong (Red River) Delta, Vietnam, during the Holocene”. *Quatern Int, vol. 144, 4-28.*

[31] Y. B. Liu et al., 2004. “Assessing land use impacts on flood processes in complex terrain by using GIS and modeling approach”. *Environmental Modeling and Assessment, vol. 9, 227-235.*

[32] A. Longobardi, P. Villani, 2009. “Trend analysis of annual and seasonal rainfall time series in the Mediterranean area”. *International Journal of climatology.*

[33] D. Ma et al., 2013. “Simulated impacts of afforestation in East China monsoon region as modulated by ocean variability”. *Clim Dyn, vol. 41, 2439-2450.*

[34] G. Mahe et al., 2005. “The impact of land use change on soil water holding capacity and river flow modelling in the Nakambe River, Burkina-Faso”. *Journal of Hydrology, vol. 300, 33-43.*

[35] J.L. McGuinness, L. Harrold, 1971. “Reforestation influences on small watershed streamflow”. *Water Resources Research, vol. 7, 845-852.*

[36] V. M. Meher-Homji, 1980. “Repercussions of Deforestation on Precipitation in Western Karnataka”. *Archiv. für Meteorol. Geophys. Biokl., vol. 28B, 385-400.*

[37] V. M. Meher-Homji, 1991. "Probable impact of deforestation on hydrological processes*". Climatic Change, vol. 19, 163-73.*

[38] W. Nie et al., 2011. "Assessing impacts of Landuse and Landcover changes on hydrology for the upper San Pedro watershed". *Journal of Hydrology, vol. 407, 105–114.*

[39] A. N. Pettitt, 1979. "A Non-Parametric Approach to the Change-Point Problem". *Journal of the Royal Statistical Society, vol. 28, 126-135.*

[40] L. T. P. Quynh et al., 2005. "Nutrient (N, P) budgets for the Red River basin (Vietnam and China)". *Global biogeochemical cycles, vol. 19.*

[41] V. Sahin, M. J. Hall, 1996. "The effects of afforestation and deforestation on water yields". *Journal of Hydrology, vol. 178, 293-309.*

[42] D.F. Scott, W. Lesch, 1997. "Streamflow responses to afforestation with Eucalyptus grandis and Pinus patula and to felling in the Mokobulaan e perimental catchments, South Africa". *Journal of Hydrology, vol. 199, 360-377.*

[43] P. Sonali, D. N. Kumar, 2013. "Review of trend detection methods and their application to detect temperature changes in India". *Journal of Hydrology , vol. 476, 212–227.*

[44] D. Spartà, 2013. "Impact of deforestation on local precipitation patterns over the Da River basin, Vietnam". Master thesis at Politecnico di Milano.

[45] D. V. Spracklen, S. R. Arnold, C. M. Taylor, 2012. "Observations of increased tropical rainfall preceded by air passage over forests". *Nature 11390.*

[46] Y. C. Sud et. al, 1988. "Influence of land surface roughness on atmospheric circulation and precipitation: A sensitivity study with a general circulation model". *J. Appl. Meteor., vol. 27, 1036-1054.*

[47] Y. C. Sud and W. E. Smith, 1985. "Influence of Local Land Surface Processes on the Indian Monsoon". *J. Climate & Applied Meteorol., vol. 24, 1015-1036.*

[48] G. Sun et al., 2006. "Potential water yield reduction due to forestation across China". *Journal of Hydrology, vol. 328, 548-558.*

[49] A. L. S. Swann et al., 2011. "Mid-latitude afforestation shifts general circulation and tropical precipitation". *PNAS, vol. 109 no. 3, 712-716.*

[50] J. Tu, 2009. “Combined impact of climate and land use changes on streamflow and water quality in eastern Massachusetts, USA”. *Journal of Hydrology, vol. 379, 268–283.*

[51] V. V. Tuan, 1993. “Evaluation of the impact of deforestation to inflow regime of the Hoa Binh Reservoir in Vietnam”. *Hydrology of Warm Humid Restons, no. 216.*

[52] J. X. L. Wang, D. J. Gaffen, 2001. “Late-Twentieth-Century Climatology and Trends of Surface Humidity and Temperature in China”. *Journal of climate, vol. 14, 2833-2045.*

[53] W. D. M. Warren, 1974. “A Study of Climate and Forests in the Ranchi Plateau. Pt. II”. *Indian For., vol. 100, 291-314.*

[54] K. M. Willett et al., 2007. “Attribution of observed surface humidity changes to human influence”. *Nature 06207.*

[55] B. Yan et al., 2012. “Impacts of land use change on watershed streamflow and sediment yield: An assessment using hydrologic modelling and partial least squares regression”. *Journal of Hydrology, vol. 484, 26-37.*

[56] H. Yin, C. Li, 2001. “Human impact on floods and flood disasters on the Yangtze River”. *Science, vol. 41, 105-109.*

[57] M. Zhang et al., 2012. “The effect of forest harvesting and climatic variability on runoff in a large watershed: The case study in the Upper Minjiang River of Yangtze River basin”. *Journal of hydrology, vol. 464-465, 1-11.*

[58] K. Zhang, 1986. “The Influence of Deforestaion of Tropical Rainforest on Local Climate and Disaster in Xishuangbanna Region in China”. *Climatological Notes, vol. 35, 223-236.*

[59] H. Zhang, A. Henderson-Sellers, K. McGuffie, 1996. “Impacts of tropical deforestation-Part I: process analysis of local climatic change”. *Journal of climate, vol. 9, 1497-1517.*

[60] H. Zhang, A. Henderson-Sellers, K. McGuffie, 1996. “Impacts of tropical deforestation-Part II: the role of large-scale dynamics”. *Journal of Climate, vol. 9, 2498-2521.*

[61] A. D. Ziegler et al., 2004. “Hydrological consequences of landscape fragmentation in mountainous northern Vietnam: evidence of accelerated overland flow generation”. *Journal of Hydrology, vol. 287, 124-146.*

Sitography

[1] ftp://asterweb.jpl.nasa.gov/Collections/SoutheastAsia/

[2] http://www2.jpl.nasa.gov/srtm/

[3] http://bioval.jrc.ec.europa.eu/products/glc2000/products.php

[4] http://www.diva-gis.org/gdata

[5] http://earthenginepartners.appspot.com/science-2013-global-forest/download.html

[6] http://earthexplorer.usgs.gov

[7] http://gdex.cr.usgs.gov/gdex/

[8] http://www.fao.org/geonetwork/srv/en/

[9] http://www.vietnamembassy.org.uk/climate.html